Alternative approaches for the characterisation of chromatographic separations from scale down experiments

Jayan Chathurika Senaratne

A thesis submitted for the degree of

Doctor of Engineering

of

University College London.

Department of Biochemical Engineering

University College London

15th November 2017

I, Jayan Chathurika Senaratne, confirm that the work presented in this thesis is my own. Where information has been derived from other sources, I confirm that this has been indicated in the work.

Abstract

Accurately characterising the design space of a process is critical for the development of robust and economic purification processes. However, this can require extensive experimentation which can be expensive and time consuming. Furthermore, this experimentation may require amounts of material that is not available during the early stages of process development, which can lead to delays in the development of the biopharmaceutical product.

An approach that can ease the burden of characterisation is the use of scale-down methods and devices. Scale-down experiments require significantly smaller amounts of material and can be automated to improve throughput. Unfortunately various issues associated with scale-down experimentation limit their usefulness.

One such issue is that various sources of variability can introduce noise into the results of these experiments. In this study Monte Carlo simulations were carried out in conjunction with a mechanistic general rate model of a typical ion exchange chromatographic purification to investigate the impact of variability on the results of these experiments. A comparison of alternative process modelling approaches was carried out to determine which was capable of producing the most accurate process models from noisy data. A Kriging algorithm was found to be the most capable technique.

There are also various scaling effects that cause the scale down experiments to not be representative of the large scale process. Two approaches were developed that augmented extensive scale down experimentation with a small number of large scale experiments to produce representative models of the large scale design space. One of the approaches used derived transformation functions to transform the scale-down data into the large scale design space and the other used a Cokriging algorithm. Using the

cation exchange chromatography purification of myoglobin from egg white proteins as a test platform it was shown that it was possible to produce accurate characterisations of the large scale process using only a fraction of the material that would be otherwise required for carrying out the experimentation at large scale.

These approaches were further tested using a purification sequence consisting of a heat treatment step followed by a cation exchange chromatography step for the purification of an antibody fragment from *E. coli* lysate. In this study fractionation diagrams were adapted to describe the elution profiles of the product and its various impurities to enable the multi-objective optimisation of the process. It was demonstrated that this approach could be used to produce detailed characterisations that revealed the relationships between the process variables and multiple responses across the whole process sequence.

Acknowledgements

I sincerely thank my project supervisor, Professor Nigel Titchener-Hooker, for his encouragement and patience. His guidance and advice made this project possible.

I greatly appreciate the insight of my industrial supervisor, Dr. Peter Levison.

Thank you to both the EPSRC and Pall Life Sciences for providing the funding for this project.

The members of the UCL Department of Biochemical Engineering were always ready to support me and give me helpful tips and hints. I learnt a lot from engaging with them, and I thank them for sharing their ideas with me.

Thank you to Dr. Spyros Gerontas for helping me set up the simulations that were essential for this project.

Joe Newton assisted me with the fermentations and provided me with feed material for my experiments. His generosity is greatly appreciated.

To my family and friends: thank you, so very wholeheartedly, for your unconditional love and support.

Contents

List of Figures

List of Tables

Chapter 1

Introduction

1.1 Process chromatography

1.1.1 Introduction to process chromatography

Chromatography is one of the most widely used separation processes in bioprocessing. Chromatography systems consist of a solid stationary phase and a fluid mobile phase. The molecules of the mixture which requires separation are dissolved in the mobile phase which flows past the stationary phase (Harrison et al., 2003). The molecules of the different components of the mixture will have varying levels of interaction with the stationary phase. This causes the individual components in the sample to migrate at different rates which provides the basis for their separation (Doran, 1995).

While some analytical applications of chromatography may use a gas mobile phase (gas chromatography), bioprocessing applications use liquid mobile phases (liquid chromatography) (Doran, 1995). For process scale separations the stationary phase normally takes the form of porous beads which are packed into a column packed. Other forms of stationary phase such as membranes and monoliths are also widely used. However, packed beds remain the dominant chromatographic process due to the selectivity, resolution and recovery that they achieve (Chhatre and Titchener-Hooker, 2009).

1.1.2 Role of chromatography in downstream processing

Downstream processing describes the processing scheme used for the recovery and purification of products from biochemical processes (Liddell, 1994). In addition to chromatography, downstream processes can include other unit processes such as centrifugation, depth filtration, precipitation and ultrafiltration. Figure 1.1 shows a typical downstream processing sequence for the purification of a monoclonal antibody produced in a mammalian cell culture.

In mammalian cell culture the product is expressed into the cell culture media. In other expression systems the product may be expressed into the intracellular space and it will necessary to disrupt the cells to release the product. Centrifugation or depth filtration or a combination of the two will be used to remove cells and cell debris and clarify the media. A Protein A or similar affinity chromatography step will then be used to capture the product. As this step is highly specific to the product it will serve to significantly improve the purity and will also act as a concentration step. Two further chromatography steps will be used as polishing steps to remove any remaining impurities. This steps may be ion exchange, hydrophobic interaction or mixed mode chromatography steps. Viral inactivation and viral filtrations steps will be included in the purification sequence to remove viruses. Finally, ultrafiltration/diafiltration will be used to concentrate the product and exchange it into the final formulation.

Chromatography is used in downstream processing to separate the product from its contaminants. Regulatory agencies such as the FDA require that the biopharmaceutical products be produced with a consistent purity and quality and be devoid of harmful contaminants. For the production of most biotherapeutics, chromatography is the only unit process that can meet these requirements (Guiochon, 2002). Therefore, most downstream processes will contain at least one chromatographic stage and typically will include three to five chromatography stages (Walsh, 2002).

A typical chromatography scheme for the purification of a protein product would include three stages. The first stage would be a capture step where the target protein is captured and most of the impurities flow through without adsorbing. After this stage the purity of target protein would be expected to be greater than 70%.

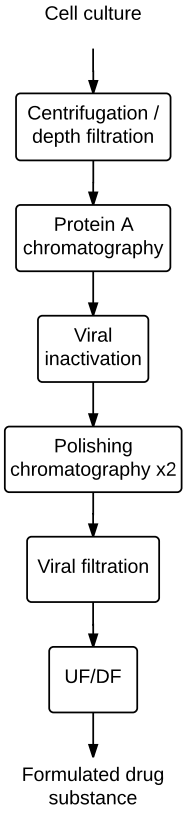

Figure 1.1: Typical platform process for the purification of a monoclonal antibody. The purification process Adapted from Shukla et al. (2007)

The second stage would be a purification step to remove most of the remaining impurities, bringing the purity of the target protein to around 99%. The third and final stage would then be a polishing step to remove any remaining trace impurities. The product is then at its required level of purity and is ready for formulation (Sofer and Hagel, 1997).

1.2 Types of chromatography

The types of chromatography differ from each other by the nature of interaction that occurs between the stationary phase and the molecules in the mobile phase. These can be categorised into two groups, adsorption chromatography and non-adsorption chromatography.

1.2.1 Adsorption chromatography

In the type of chromatography there are chemical interactions between the molecules in the mobile phase and the stationary phase. The strength of these interactions will be different for each component of the solute. This variation in the strength of interactions causes the components to migrate through the stationary phase at different rates. The differential migration of the components provides the basis for their separation (Doran, 1995). Differential migration causes the mixture to resolve into a series of bands, each containing a separate component. The component with the weakest interactions will appear first, while the component with the strongest will appear last. However, despite the formation of the bands there may not be complete resolution each component.

The types of adsorption chromatography include:

1. Ion exchange chromatography – Electrostatic interactions between the sample molecules and the ion exchange matrix
2. Hydrophobic interaction chromatography – Interactions between hydrophobic regions of the sample molecules and a hydrophobic stationary phase
3. Affinity chromatography – Interactions between the matrix and specific chemical groups on the molecules of the sample

1.2.1.1 Ion Exchange Chromatography

This is one of the most widely used and best understood types of chromatographic separation used for the separation of proteins. In ion exchange chromatography charged regions on the matrix or charged ligands grafted onto the surface of the matrix interact with surface charges on the solute molecules via electrostatic interactions (Shukla and Yigzaw, 2007).

Proteins are large amphoteric molecules containing both negatively charged amino groups and positively charged weak acid groups. Ion exchange matrices interact with these charged groups on the protein. According to the required separation a positively charged (anion exchanger) or negatively charged (cation exchanger) matrix can be used.

Typical ion exchange matrices consist of sulphonate or quaternary amine groups covalently bonded to the resin (Wheelwright, 1991).

Ion exchange chromatography can be controlled by varying the pH. As proteins contain both positively charged and negatively charged groups, changes in pH will affect the overall charge. The pH at which a protein has a net charge of zero is known as the isoelectric point (pI). At a pH below the isoelectric point, the net charge of the protein will be positive and it will bind to a cation matrix. Conversely, at a pH above the isoelectric point, the net charge of the protein will be negative and it will bind to an anion matrix. However, the strength of the interactions between the matrix and the protein do not depend entirely on the net charge of the protein. This is because there may be localised concentrations of a particular charged group which can lead to other interactions with the matrix (Shukla and Yigzaw, 2007; Wheelwright, 1991).

During the operation of these processes, the sample will be loaded at a pH which promotes the adsorption of the target protein. The elution of the target protein can be promoted through the selection of the salt concentration or the pH of the elution buffer. Changing the salt concentration to change the ionic strength of the buffer or changing the pH to change the charge of the pH will lead to the elution of the target protein (Wheelwright, 1991).

1.2.1.2 Hydrophobic interaction chromatography

Proteins contain a number of hydrophobic amino groups on their structure. In an aqueous environment the protein will fold itself so that the majority of these hydrophobic groups are buried within the structure to minimise free energy. However, some hydrophobic groups will remain exposed and these will be available for interactions with the hydrophobic groups on the chromatography matrix (Wheelwright, 1991).

The hydrophobic interactions can be promoted through the addition of salts, particularly lyotropic salts. The column will be loaded using a mobile phase with a high salt concentration . The concentration of the salt in the mobile phase will then be reduced to effect the elution of the adsorbed protein. The concentration can be reduced gradually to enable selective desorption and elution will be in order of hydrophobicity. Alternatively, a hydrophobic competitor can be used to displace the bound proteins. The salt

concentration must be carefully controlled to ensure that the hydrophobic proteins do not bind to each other and precipitate instead of adsorbing to the resin.

Although HIC does not rely on charged interactions, the pH may influence the retention and selectivity of the protein by causing structural changes.

1.2.1.3 Affinity chromatography

This type of chromatography can typically offer purities of >95% in one step. Affinity chromatography can achieve a very specific separation based on the presence and location of certain groups on the target molecules. These specific groups can be the binding sites on receptors and antibodies or the active sites on enzymes.

In this type of chromatography, the ligand which shows affinity to the target molecule (affinity ligand) is coupled to an inert matrix. When the feed is introduced to the column these ligands bind the target molecule and all the impurities pass through. This is followed by a wash step and the target molecule is then dissociated by changing the conditions of the mobile phase or by introducing an agent which displaces the target molecule from the affinity ligand.

An example of affinity chromatography is Protein A chromatography which is widely used for the manufacture of monoclonal antibodies. Industrial Protein A resins use a form of Protein A that has been engineered to be highly specific to the the Fc region on an antibody. Protein A will typically be used as a capture step and due to its specificity the only major impurities present in the eluate from this step will be aggregated and fragmented forms of the product.

1.2.1.4 Mixed Mode Chromatography

It is generally desirable to reduce the number of steps in a process. Fewer steps typically improves yield of the whole process and a shorter processing time can be beneficial to product quality. However, reducing the number of process steps may compromise the final purity of the product. For this reason the use of highly specific steps such as affinity chromatography is beneficial. Another type of chromatography that has the potential to deliver high specificity is mixed mode chromatography. Ideally this would

be used as the final step in a two step separation process.

Most chromatography media contain elements of other types of interaction in addition to the intended type. In the case of mixed mode chromatography, the media is engineered to combine a number of types of interaction to increase selectivity. For example, hydroxyapatite matrices contain calcium surface groups which provide affinity interactions, and phosphoryl surface groups which provide cation exchange interactions (Gagnon, 2009). On other mixed mode media the different groups on the ligands provide the different types of interactions. For example, the ligands on 2-mercaptoethyl (MEP) media have hydrophobic interactions at neutral pH. But as the pH decreases, a nitrogen atom on the ligand becomes charged, resulting in charged interactions (Gagnon, 2009).

A well characterised mixed mode mechanism is that of hydroxyapatite. As mentioned above hydroxyapatite matrices have calcium and phosphoryl surface groups that provide different types of interactions. A typical separation would involve the purification of immunoglobulin G (IgG). The IgG has a weak affinity to the calcium groups but has strong interactions with the phosphoryl groups. During the loading of the column, a low phosphate concentration will be set to suspend the weak calcium affinity interactions. This leaves the strong interactions with the phosphoryl groups intact. Elution is carried out using a sodium chloride gradient. The sodium chloride replaces the IgG at the phosphoryl sites. At higher sodium chloride concentrations the aggregate groups will be replaced at the phosphoryl sites and elute. Some of the contaminants show a strong affinity to the calcium groups and these will be removed by cleaning with concentrated phosphate (Gagnon, 2009).

1.2.2 Non-adsorption chromatography

Non-adsorption chromatography consists of size exclusion chromatography. Size exclusion chromatography (SEC), also known as gel filtration chromatography, separates the components of the solute based on the size of its molecules and there are no chemical interactions between the molecules and the stationary phase (Sofer and Hagel, 1997). In SEC the stationary phase consists of porous particles. The size of the solute molecules determines the extent to which each component will diffuse into the pores of

the particles. Smaller molecules will diffuse deeper into the pores while the diffusion of larger molecules will be restricted by the size of the pores. As the diffusion of the larger molecules is restricted, they will have a higher rate of migration through the stationary phase than the smaller molecules. The differential migration causes the resolution of the individual components into bands, with the component with the largest molecules appearing first.

1.3 Process chromatography operation

1.3.1 Forms of stationary phase

There are several forms of stationary phase in use at a process scale including resins, membranes and monoliths.

Resins are the most common form of stationary phase. Resin particles can be solid, porous, or gel and range in diameter between 2 - 100 μm. Polymer and silica are the two basic resin materials used for the formation of these particles. The resin provides the high surface area required for the interactions with the solute molecules and this area is generally 100 - 1500 m^2/g (Harrison et al., 2003). In some resins the resin surface can be chemically modified according to the required separation. For example, in affinity chromatography, antibody ligands can be bound to the surface for the separation of proteins. In other resins, the resin itself will contribute to the interactions with the molecules, e.g. hydroxyapatite and size exclusion chromatography.

While resins are the most common form in use, there are instances where other forms of chromatography may be more appropriate. For example, larger fusion proteins and viruses may not diffuse into the small pores of the particles in the packed bed. For these separations involving larger proteins, membrane chromatography and monolith chromatography might be more suitable (Ghosh, 2002).

It all the forms of stationary phase it is important that the base matrix has the following characteristics:

1. It should not have unintentional interactions with any of the components in the feed.

2. It should have a strong structure to provide uniform and rapid flow conditions.

3. It should be resistant to chemical and microbial degradation.

4. It should not restrict the mass transfer of the proteins to the binding sites.

1.3.2 Modes of operation

Chromatography steps are usually operated as a batch process consisting of two key steps (Wheelwright, 1991). The first step is to load the feed material onto the column while promoting the desired interactions between the solute and the matrix. During the second step, elution, the solute is resolved into its components and is eluted as fractions. Depending on the process there may be additional steps such as wash steps or columns regeneration steps.

There are three distinct modes of operating chromatographic separations (Cramer and Jayaraman, 1993); elution, frontal and displacement.

1.3.2.1 Elution Chromatography

Elution chromatography is the most widely used operating mode for process scale chromatography. In elution chromatography, desorption of the proteins off the matrix occurs due to the action of a modifying agent in the elution buffer. For example, in Protein A chromatography, reducing pH of the mobile phase changes the conformation of the Protein A binding site, causing the desorption of the bound protein. Elution chromatography can be divided according to the method used to introduce the modifying agent (Cramer and Jayaraman, 1993).

1. Isocratic elution

2. Gradient elution

3. Step elution

In isocratic elution there is no change in buffer composition during the elution phase of the process (Wheelwright, 1991). This mode of elution will only be used where only

the pure material has bound to the column and the only requirement of the elution phase is to recover as much of the bound material as possible.

For other applications, a change in the composition of the buffer is required to resolve the bound proteins from one another. For example, in hydrophobic interaction chromatography, a decreasing salt concentration in the mobile phase may be used to achieve the desired resolution. These changes can be either continuous where there are gradual changes in the elution buffer or stepwise where there are discontinuous changes from one buffer composition to another. A gradual change in the composition is known as gradient elution while a stepwise change is step elution. Gradient elution results in an improved resolution of the components compared to that achieved with step elution. However, for process chromatography, step elution is the preferred mode of elution as consistent gradients are difficult to reproduce at large scale (Sofer and Hagel, 1997).

1.3.2.2 Displacement Chromatography

Displacement elution is similar to elution chromatography and involves a change in composition of the buffer to effect the desorption of the proteins (Cramer and Jayaraman, 1993). In elution chromatography the elution buffer causes a change in the interactions between the protein and the chromatography matrix which results in the desorption of the proteins. In displacement chromatography, the elution buffer contains a substance that has a higher affinity to the matrix and displaces the protein on the matrix. An example of this is the use of elution buffers with high salt concentrations in ion exchange chromatography. In this situation the salt ions will have an higher affinity for the ion exchange resin and displace the bound proteins.

As with elution chromatography, displacement chromatography can be operated using isocratic, gradient or step elution.

1.3.2.3 Frontal Chromatography

Unlike elution and displacement chromatography which load the feedstock into column and then use an elution buffer to elute the proteins, frontal chromatography uses a continuous feed stream for the duration of the batch. As the material is fed to the column, molecules with a higher affinity for the matrix will displace lower affinity

molecules. This results in the component with the lowest affinity appearing out of the column first at a high purity. The components will continue to appear in order of ascending affinity strength. These components will have a decreasing purity as they are mixed with the continuously introduced feed stream. Eventually the matrix will be saturated with the strongest affinity component and the column effluent will have the same composition as the feed. The remaining component can then be eluted in its pure form after washing the column (Sofer and Hagel, 1997).

This mode of operation is typically used where there is an impurity which has a higher affinity for the resin relative to the product, and makes up a small proportion of the feed material. The column is loaded to a high capacity, leading to any bound protein being displaced by the impurity. Eventually the column will be saturated with the impurity and the recovery of the pure product high. This mode is also called flow-through mode.

1.4 Development of a chromatography process

1.4.1 Process development

Developing a chromatographic process involves defining a number of parameters including the type of resin, buffer composition, the conditions of the separation (pH, salt concentration, etc.), elution gradient type, height of the packed bed, feed flow rate (Rathore et al., 2003).

A typical process development scheme begins with the determining the type of chromatography step to develop, e.g. affinity chromatography, cation exchange chromatography, etc. This selection can be made based on prior experience with similar molecules or based on an understanding of the properties of the product and its impurities (Rathore and Velayudhan, 2003). Several matrices of the selected type of chromatography will then be screened to identify their suitability for the application. As an example, for a capture step, a high binding capacity for the product will be desired while for a polishing step, the resolution between the product and the impurities will be of greater importance. At the end of this stage the matrices are narrowed down to a very small number of candidates.

A process can then be developed in detail for the identified candidate(s). For bind and elute separations this involves optimising the binding conditions to maximise the binding capacity and then optimising the elution conditions to improve the resolution between the product and the impurities. The development of flow-through steps is simpler as the flow-through conditions will dictate both the capacity and the resolution of the separation.

Optimisation of the binding conditions is carried out by loading the column at different conditions until the product breaks-through to determine the dynamic binding capacity of the column. The elution conditions can then be optimised by running test gradients at different conditions to test which provides the greatest resolution between the product and the impurities. Decoupling the optimisation like this can simplify development and reduce the required experimentation. But caution must be exercised as there may be interactions between the various process variables. For example, optimum binding conditions may cause the resolution during elution to be poor while weaker binding conditions may provide an adequate binding capacity and not adversely affect the resolution.

After optimisation, the robustness of the process is investigated. This is carried out to ensure that deviations that can be expected in the manufacturing process will not adversely affect the quality of the product. Finally the consistency of the process will be tested by scaling up the process to an intermediate scale that is larger than the development scale but smaller than the production scale. This is carried out to ensure that the process is not susceptible deviations in performance during scale up.

As detailed above, a large amount of experimentation is required to develop a chromatography process. To reduce the burden of this experimentation these experiments are carried out at the smallest feasible scale. This reduces the amount of material that is required and these experiments can be easily automated. These scale-down techniques are discussed in further detail in Section 1.4.3.

A further tool for reducing the experimental burden is the use of design-of-experiments methods. These methods allow the identification of a subset of experiments that can provide a thorough understanding of the design space instead of carrying out experi-

ments at every permutation of the process variables. These methods are discussed in further detail in Section 1.5.3.

An alternative to the experimental exploration of the design space is the use of mathematical models. This approach involves building a mechanistic model that accurately describes the process. It may be necessary to carry out a small number of experiments to calibrate the model. The model can then be used to explore and optimise the process. The use of these models is discussed in Section 1.5.4

Platform approaches have also been introduced for simplifying process development. These approaches develop a process strategy for a particular group of biological products. The platform contains guidance about the overall process scheme and windows for the operating conditions. Therefore, when developing a process for a product belonging to that category, the guidance in the platform narrows down the scope of experimentation required for process development (Shukla and Yigzaw, 2007).

1.4.2 Scaling up chromatography processes

1.4.2.1 Introduction

After the initial process development the chromatographic separation is scaled up to the required process scale. This is conventionally carried out in stages, e.g. from lab scale to pilot scale and from pilot scale to production scale. Lab scale chromatography columns have packed bed volumes which range from 1 10 mL. The separation will then be scaled up to the pilot scale. The pilot scale is typically around a tenth of the final production scale. The pilot scale runs provide indications of how the process will perform at its full scale and its reproducibility. Additionally, the pilot scale operation may be used to produce material for clinical trials and therefore needs to meet the same GMP criteria as the production scale process. After the pilot scale runs, the process will be scaled up to the production scale. The size of the production scale column varies according to the product. This could be up to 100 times the initial lab scale (Aldington and Bonnerjea, 2007).

As the scale increases, factors such as improper column packing, poor distribution, channelling, dispersion problems in the column and dispersion in auxiliary apparatus

Table 1.1: Guidelines for linear scale up of chromatographic separations (Sofer and Hagel, 1997)

Increase	Maintain
Column diameter	Column bed height
Sample volume in proportion to column cross sectional area	Eluent velocity
Volumetric flow rate in proportion to column cross sectional area	Sample concentration
Chromatography media volume	Ratio of sample volume to bed volume

can cause deviations from the expected performance of the column (Lode et al., 1998; Ghosh, 2002). Re-optimisation of the process is required if these deviations occur to ensure that the process continues to provide the required purity and yield. A re-optimisation of the process may be considered a process change which then requires further revalidation of the process. For these reasons, integrating scalability and validation into a process helps to avoid regulatory and production delays during development (Sofer and Hagel, 1997).

1.4.2.2 Conventional scale up

The standard method for scale up in industry is to increase the diameter of the column while maintaining the bed height. Under this approach the bed height of the column is fixed during the early stages of process development, taking into account the pressure-flow characteristics of the matrix. The process development and optimisation work will then be carried out on columns with this bed height. The guidelines in Table 1.1 will then be used to scale up the defined process.

In chromatographic separations the mass transfer in the columns is closely related to the residence time in the column. This approach to scale up maintains the residence time by maintaining the bed height and the velocity of the eluent through the column. Scale up is achieved by increasing the column diameter and proportionally increasing the volumetric flow rate.

1.4.2.3 Alternative approaches to scale up

A number of alternative methods have been put forward for scaling chromatographic separations.

Keeping resolution constant

Yamamoto et al. (1987) developed a relationship for the resolution of the chromatographic bands during gradient elution.

$$Resolution \propto \left(\frac{D_m L}{g(V - V_0) u d_p^2} \right)^{\frac{1}{2}} \tag{1.1}$$

where D_m is the molecular diffusivity, L is the column length, g is the slope of the gradient, V is the column volume, V_0 is the column void volume, u is the interstitial fluid velocity and d_p is the particle diameter. This relationship shows that the resolution can be maintained during scale up by increasing the length of the column in proportion to the product of the eluent velocity and the gradient slope.

Maintaining the residence time

Al-Jibbouri (2006) proposed a similar method related to the residence time and based on a derivation of the van Deemter equation. The van Deemter equation (van Deemter et al., 1956) can be simplified as follows.

$$H = A_h + \frac{B_h}{v} + C_h v \tag{1.2}$$

where H is the height equivalent to a theoretical plate, A_h is the contribution due to axial diffusion, B_h is the contribution due to longitudinal diffusion (perpendicular to the flow of fluid), C_h is the contribution due to mass transfer and v is the interstitial velocity. Hansen and Mollerup (2005) assumed that the longitudinal diffusion was negligible and simplified the van Deemter equation to the following.

$$H = A_h + C_h v \tag{1.3}$$

The residence time is given by the following equation.

$$t = \frac{l}{v} \tag{1.4}$$

where t is the residence time and l is the length of the column. By combining this relationship with the simplified van Deemter equation, the following relationship for the number of plates N can be obtained.

$$N = \frac{l}{H} = \frac{1}{\frac{A_h}{l} + \frac{C_h}{t}} \tag{1.5}$$

This relationship can then be used to scale up by changing the residence time and the length of the column and maintaining the number of plates.

The two methods described above allow for changes in bed height during scale up. This means that the process development can be carried out on columns with a smaller bed height, which requires less feed material. The column can then be scaled up by increasing both the bed height and the diameter of the column. However, these methods have not gained widespread use in industry. This is because at very small scales various scaling effects can cause deviations which are not present in larger columns. For example, for a very small column, the extra-column volume of the experimental system can be very large, causing peak broadening which will not be seen in large columns (Kaltenbrunner et al., 1997). This makes the use of these scale up methods infeasible as they will not account for such effects.

1.4.3 Scale down methods

1.4.3.1 Advantages of using scale-down methods

As discussed above, the prevalent linear scale up approach dictates that the process development is carried out on columns which have the same bed height as the final process. With typical bed heights being 10 — 30 cm and the smallest bench scale columns having a diameter of 0.5 cm, this results in minimum column volumes of 2 — 6 mL. Even at this scale, screening all the process variables can require a relatively large amount of material. This had led to the development of scale down methods

that provide an alternative platform for process development that uses a significantly smaller amount of material per experiment.

These methods also enable process development activities to be carried out at an earlier stage of development when material is scarce. These early experiments can provide an insight into the manufacturability of the product. Additionally these methods tend to be easier to automate. This helps to reduce further the cost and effort associated with the process development activities.

These techniques also enable a Quality by Design (QbD) design approach at later stages of development. QbD approaches require further exploration of the design space to understand the relationships between the numerous process variables and the quality attributes of the product. The capability of microscale techniques to rapidly carry out a large number of experiments using a very small amount material enables this exploration (Chhatre and Titchener-Hooker, 2009).

To benefit from the above advantages scale down methods have been developed for downstream bioprocesses such as microfiltration (Rayat et al., 2014), centrifugation (Chatel et al., 2014), ultrafiltration (Kazemi and Latulippe, 2014), depth filtration (Noyes et al., 2015), homogenisation (Li et al., 2013), precipitation (Yoshimoto et al., 2013), flocculation (Espuny Garcia Del Real et al., 2014), virus filtration (Wieser et al., 2015). These methods can be divided into two categories; methods that use devices which are direct mimics of the large scale process (Rayat et al., 2014; Noyes et al., 2015; Yoshimoto et al., 2013; Espuny Garcia Del Real et al., 2014; Wieser et al., 2015) and methods that use devices that mimic a key effect of the large scale process (Chatel et al., 2014; Kazemi and Latulippe, 2014; Li et al., 2013). These methods are largely capable of predicting trends in the large scale process and are therefore useful for identifying potential windows of operation and optimising the process. However, these methods are not all capable of accurately predicting the actual performance of the large scale process. This may be more pronounced in methods that mimic only a key effect of the large scale process as further modelling may be required to relate the scale down results to the large scale process. For example Li et al. (2013) used focussed acoustics to mimic the protein release that occurs during a homogenisation process. The rate of protein release was measured using focussed acoustics which was then related to the

rate of release in the pilot scale homogenisation process.

1.4.3.2 Scaled down chromatographic devices

Microscale methods include microlitre batch incubation in microwell plates, micropipette chromatography tips, and miniature packed columns. These devices are typically used in conjunction with an automated liquid handler which helps to accelerate the throughput of the experiments. These methods can be used to investigate variables such as resin type, binding capacity, buffer composition, flow rate range and feed loading level. While these devices can be representative of the large scale process and provide valuable information, they are not geometrically similar to large scale columns. Therefore, they cannot be used to predict the actual performance of the scaled up process (Lacki, 2014). In order to obtain scaling predictions, models are required to transform the outputs (Chhatre and Titchener-Hooker, 2009; Hutchinson et al., 2009). Despite not being able to provide a direct prediction of the large scale process, these devices have been used to identify trends in the design space and narrow down potential windows of operation (Rege et al., 2006; Coffman et al., 2008; Toueille et al., 2011; Bhambure and Rathore, 2013).

The smallest scale down technique involves batch experiments carried out in microwell filter plates. Each well in the plate contains a microlitre quantity of resin slurry. The feed material is added to the wells and the plate is incubated for the required amount of time. At the end of the incubation the mobile phase can be removed from the wells using a centrifuge or vacuum manifold. This process can be repeated using other mobile phases to mimic other phases of a chromatographic process (Chhatre and Titchener-Hooker, 2009). While this approach can be used to gain an understanding of the adsorption/desorption of a process, gaining an understanding of the entire process can be difficult as this format does not share the same dynamics as a chromatography column. For example these batch experiments can be used to determine the static binding capacity of resin at various conditions but the dynamic binding capacity of a column with the same resin cannot be determined directly. However through the use of suitable models it is possible to estimate the dynamic binding capacity (Carta, 2012), investigate the effect of ligand density on yield and impurity clearance (Fogle et al., 2012),

and virus clearance (Connell-Crowley et al., 2013). Additionally these microwell plate experiments can be used to determine isotherm parameters for building mechanistic models that describe the chromatographic separation (Nfor et al., 2012; Traylor et al., 2014). With further development the mechanistic models can be used to gain a detailed understanding of the process.

Another device that contains resin at the microlitre scale is the packed micropipette tip. This typically consists of 10 µL pipette tips which are packed with the chromatography resin of interest. The tips are loaded by aspirating and dispensing the feed material. The actual process can be approximated by setting the aspiration/dispensation flow rate to maintain the same flow rate as the final process.

The scale down device with the greatest similarity to the actual process is the miniature column (Lacki, 2012). These are small columns which have packed beds in the range of 0.05 - 5 mL. Smaller versions of these miniature columns, such as the Robocolumn, which has a column volume of 0.05 - 0.6 mL are used with automated liquid handling systems. The tips of the liquid handler are used to dispense the feed material or buffer into the top of the column and the eluate is collected from the bottom of the column. As the fluid dynamics of these columns are similar to an actual chromatography column this serves as a closer approximation of the real process. Equivalence between the miniature columns and the actual process is achieved by maintaining a constant residence time. However, studies have shown that the performance of these columns are not directly comparable to larger packed bed columns and can only be used to produce a semi-quantitative prediction of the large scale design space (Sanaie et al., 2012; Welsh et al., 2014). This is because parameters such as the dispersion factor, wall effects and flow distribution are drastically different between these devices and large scale packed bed columns. Therefore these columns cannot be used to replace lab scale columns in process development (Sanaie et al., 2012). Further scale down of packed bed has been achieved by packing chromatography resin into lengths of PEEK tubing. This has allowed for packed beds as small as 5 μL (Lee et al., 2015).

1.4.3.3 Scale up from scaled down devices

It would be an advantage to be able to scale up directly from these scaled down devices as this would eliminate the requirement for the intermediate scaling stages, reducing cost and experimental effort. Despite providing the large amount of information required for screening, these devices cannot provide information regarding the exact performance of the large scale chromatography process. The exact large scale chromatogram cannot be inferred directly from the scaled down chromatogram due to factors such as changes in the dispersion and retention, different flow distribution, wall effects and relatively large extra-column volumes (Chhatre and Titchener-Hooker, 2009; Sanaie et al., 2012). The use of liquid handling platforms can introduce further error such as those in the dispensing of small volumes of protein solutions and resin slurries (Treier et al., 2012; Li et al., 2012). Therefore, further manipulation of the data would be required to produce predictions of the large scale chromatogram.

1.4.4 Validating scaled up processes

Validation generally refers to the use of documented evidence to prove that a process performs as it claims it should and produces a product with a consistent quality (Food and Drug Administration, 2011). A chromatographic process will typically be validated twice; at the pilot scale during the production for clinical trials, and at the final commercial manufacturing scale. This requires demonstrating that the performance of the process is consistent across the increasing scales. Thus validation of the process is made simpler if scalability is built into the process and if the process is thoroughly understood (Sofer and Hagel, 1997). Any change in the process requires an evaluation of the change and validation of the modified process. Scaling up is considered a change in the batch size and re-validation can be required. However, if scalability is built into the process, the potential for deviations will be reduced, easing validation(Sofer and Hagel, 1997).

1.5 Process characterisation

1.5.1 Quality by design

Regulatory bodies now mandate a quality by design approach to process development (Food and Drug Administration, 2009). This approach involves first identifying the critical quality attributes (CQA) of the product. As the name suggests, the CQAs are the attributes of the final product that are critical to its quality. The CQAs will be related characteristics of the product such as the purity and strength. The process parameters that have an impact on the CQAs can then be determined. These process parameters are known as the critical process parameters (CPP) can be identified through risk assessment followed by experimental confirmation.

Before the introduction of QbD, manufacturing process were defined at fixed process conditions. Any deviation from the set point of the process could lead to a failure of the batch. Under the quality by design approach, a multidimensional design space is defined within which any change in the CPPs will not have an adverse effect on the CQAs (Rathore, 2014). Defining the design space requires a thorough understanding of the interactions between the CPPs and the CQAs. In addition to ensuring the quality of the product, this approach has the benefit of adding flexibility to the manufacturing process. A change within the design space is not considered a process deviation which results in fewer failed manufacturing batches.

1.5.2 Responses from chromatography processes

1.5.2.1 Yield and purity

The critical quality attribute (CQA) that is affected the most by a chromatography step is the purity of the product. The yield of the process is also of importance. While the yield will not be a CQA, this can have a great effect on the feasibility of the process. For a chromatographic process the yield is defined as the ratio of the mass of material recovered in the eluate to the mass of material loaded on to the column. Similarly the purity can be defined as the ratio of the mass of eluted product to the total mass of protein eluted (Belter et al., 1988).

$$Y = \frac{M_E}{M_L} \times 100\% \tag{1.6}$$

where Y is the yield, M_E is the mass of material in the eluate, and M_L is the mass of material in the load.

$$P = \frac{M_P}{M_T} \times 100\% \tag{1.7}$$

where P is the purity of the product, M_P is the mass of product in the eluate and M_T is the total mass of protein in the eluate.

Chromatographic processes can reach a purity of around 99% and some pharmaceutical processes are in operation with purities which exceed 99.99% (Sofer and Hagel, 1997).

Depending on the upstream process used to produce the material some impurities may be considered important enough to defined as CQAs individually. Examples of this are host cell proteins and DNA which must cleared from the product to prevent adverse reactions in the patient.

1.5.2.2 Fractionation diagrams and maximum purification factor vs. Yield diagram

The typical output from a chromatography run is its chromatogram which provides a real-time illustration of the separation in progress. For protein chromatography this is produced by passing the eluate through a UV flow cell. The chromatogram is then the absorbance of the eluate as a function of time. Offline chromatograms can also be constructed by fractionating the eluate and determining the concentration of the individual components or other characteristics (e.g. pH, conductivity) against time. While the chromatograms provide a detailed image of the process they do not provide a characterisation of the process in terms of the outputs that are of importance from a process design perspective such as purity and yield.

The maximum purification factor vs. yield diagram provides a method of characterising the chromatographic process as a function of its purity and yield. Richardson et al.

(1990) developed this method for the optimisation of fractional precipitation processes. This method was adapted for chromatography to analyse the trade-offs between yield and purity (Ngiam et al., 2001, 2003). This method was also used to identify operating windows in multistage chromatography in order to optimise a chromatographic stage without compromising the following stages (Salisbury et al., 2006).

The maximum purification factor (PF) vs. yield diagram is derived from the fractionation diagram of the process. The fractionation diagram plots the fractional elution of the product protein against the fractional elution of the total amount of material introduced to the process. The points at which product collection begins and ends can be identified on the fractionation diagram. A tie line between these points will characterise the separation achieved for that particular selection. The height of this tie line (the difference between the y-coordinates) is the yield of the separation while the gradient of the tie line is the purification factor.

By systematically plotting these tie lines it is possible to create a diagram of purification factor vs. yield. At each given yield there are likely to be a number of purification factor points. A curve plotted through the maximum purification factors will characterise the process as a function of maximum achievable purity and yield. Figure 1.2 illustrates the procedure to generate the fractionation diagram and the maximum PF vs. yield diagram.

1.5.3 Design-of-experiments

As mentioned above, the defining a design space requires understanding the functional relationships between the critical process parameters (CPP) and the critical quality attributes (CQA). The design spaces for these processes can be made up of a large number of CPPs. Additionally the CPPs may may interact together to affect the CQAs. Characterising these effects using one-factor-at-a-time approaches can lead to an inordinate number of experiments (Hanke and Ottens, 2014).

Design of experiments approaches provide a systematic approach to reducing the amount of experimentation that is required for characterising these processes. In design of experiments the input variables that affect the process are known as the factors and the output characteristics of the process that are affected are known as the responses.

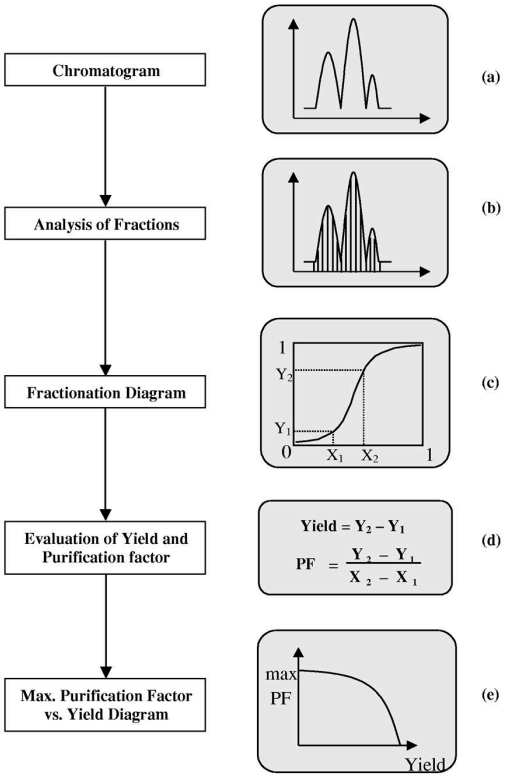

Figure 1.2: Schematic illustration of the procedure to generate the fractionation diagram and the corresponding maximum purification vs. yield diagram from an elution chromatogram. X and Y represent the cumulative fraction of total material and target product respectively (Ngiam et al., 2001).

With regards to biopharmaceutical development the factors are then the CPPs and the CQAs are the responses. A number of different experimental designs have found use in process development and these designs can be broadly divided into two categories (Kumar et al., 2014). These designs differ from one another based on the number of experiments that they require and the amount of process information that can be gleaned from the results.

The first are screening designs. These are used at the start of the process development process when there are a large number of potential process variables. They use the fewest runs to identify the factors that have grestest effect on the responses. In order to reduce the number of runs some effects will be confounded and thus these designs cannot be used to accurately model the process.

The other type of experimental design is used to optimise the process and test robustness. These designs are capable of estimating each effect and will require a larger number of runs. Therefore these will be carried out on the previously identified signifi-

cant effects only. The process can then be modelled by fitting a response surface to the resulting data which can in turn be used to define a robust design space for the process.

1.5.4 Mathematical models

An alternative to the experimental approach to process characterisation is to use mathematical models to simulate the performance of large scale column. These models have been shown to provide accurate predictions of the performance of chromatographic separations provided that the appropriate thermodynamic and kinetic information is provided (Guiochon, 2002).

A number of models have been derived which predict the performance and behaviour of chromatographic processes. Modelling linear chromatography (chromatography which is governed by a linear distribution isotherm) is relatively simple as this does not require complex numerical calculations. Non-linear chromatography is more complicated to model, especially for complex separations, as it is a very dynamic process and there are a number of interactions between the process variables. Unfortunately most process scale separation are non-linear in order to maximise the utilisation of the chromatography resin. Further, some experimental effort will still be required in order to gather the data required to calibrate the model. The experimental effort can be reduced by using miniature columns in conjunction with automated liquid handling platforms but errors introduced by the liquid handling platform can affect the accuracy of the models (Osberghaus et al., 2012). Nevertheless, developing accurate mathematical models enables the rapid investigation of various design and operating alternatives with minimal effort (Guiochon, 2002; Orellana et al., 2009; Sorensen et al., 2008).

The mathematical models can be divided into microscopic and macroscopic models. Microscopic models, also called stochastic models, model chromatography at a molecular level. Macroscopic models are those which consider the coarse grain features of the process such as relative rates of uptake, kinetics of transport and rate of depletion with considering the structural features of the individual molecules (Lipkowitz, 1995).

1.5.4.1 Microscopic Models

These models are statistical models which derive a statistical distribution for each molecule in the column to model the system. For example, the Giddings and Byring model assumes that there is random migration of the molecules through the column and that the molecules perform a random number of adsorptions and desorptions. The chromatographic process is therefore treated as a Poisson distribution to describe the migration of the molecules down the column (Giddings and Byring, 1955). It is difficult to extend this model to real separations as accounting for the interactions between the molecules of the different components and their competition for adsorption is complicated (Guiochon, 2002).

1.5.4.2 Macroscopic Models

Macroscopic models can be divided into two categories; plate models and rate models.

Plate models

Plate models divide the column into a series of equilibrium stages or plates. It is assumed that the mobile phase reaches equilibrium with the stationary phase before moving to the next plate. However, the division of the column into plates is arbitrary and therefore these models are empirical and cannot provide and predictive information without first determining the parameters of the particular column (Guiochon, 2002).

Rate models

The rate models model chromatography by finding the solution to a set of partial differential equations that describe the chromatographic process. This category of models includes the ideal model, the equilibrium-dispersive model and the general rate model. The complexity and effectiveness of these models varies depending on the assumptions made in their derivation. For example the ideal model assumes that the column is infinitely efficient (no peak dispersion) while the general rate model attempts to account for all the mass transfer kinetics that occur in the system. The complexity of the general rate model means that the derivation of a model is required for each individual system.

A number of separations have been scaled using rate models. One example of this approach was the use of a general rate model to scale up a simple two component separation from 1mL columns to large scale columns (Gerontas et al., 2010). In this case the 1mL column was used to obtain information about the adsorption/desorption kinetic parameters and effective diffusivity. This information was used to model the chromatogram of the large scale column. Heuer et al. (1996) used an equilibrium dispersive model to predict the chromatographic profiles of the large scale column. Small scale columns were used to obtain the adsorption isotherms for the separation of two isomers of a steroid compound. While the simulated chromatograms followed the general trend of the experimental chromatograms, there were deviations.

1.5.5 Testing and validating process models

As described above in Section 1.4.4, validation in a biopharmaceutical manufacturing context typically refers to the approach taken to establish that the manufacturing process produces product of a consistent quality. However, in a process modelling context validation refers to the testing that is performed to ensure that the process models provide accurate representations of the large scale process. Published research detailing methods for scaling chromatography typically validate the method through the comparison of the predicted results with experimentally obtained results (Gerontas et al., 2010; Heuer et al., 1996; Mollerup et al., 2007; Li et al., 1998; Osberghaus et al., 2012).

Chapter 2

Thesis objectives

The overall objective of this thesis was to identify and establish alternative approaches for characterising chromatographic separations from scale down experiments. The importance of producing accurate characterisations for satisfying regulatory authorities as well as optimising processes was detailed in Chapter 1. However this typically requires extensive experimentation which can be prohibitively expensive and time consuming if performed at large scale. Scale down experimental techniques can be used to alleviate this experimental burden but these techniques suffer from issues such as being susceptible to variability and not being adequately representative of the large scale process. Alternative modelling approaches for producing process models from scale down experimentation were examined in this thesis to reduce the effects of these issues.

Chapter 3: ***The feasibility of using mechanistic models to replace experimentation during the development of chromatographic separations***

The aim of this chapter was to explore the feasibility of using mechanistic models to aid the development and characterisation of chromatographic separations.

Mechanistic models can be a powerful tool as they provide a detailed understanding of the modelled process but their construction can require significant effort. In this chapter the amount of effort required was investigated by establishing a mechanistic model for the separation of three model proteins using ion exchange chromatography. This was used to examine the suitability of using mechanistic models instead of physical experimentation during the development of chromatographic separations.

Chapter 4: ***The use of maximum purification factor vs. yield diagrams as the basis for characterising and modelling chromatographic separations***

The aim of this chapter was to demonstrate how maximum purification factor vs. yield (PFY) diagrams could be used as the basis for modelling chromatographic separations.

The usual output from a chromatography experiment is the chromatogram which displays the online traces of UV absorbance, conductivity, pH, etc. of the eluate from the column. The chromatogram may be later augmented with concentration traces for individual components if the eluate is fractionated and analysed. However, due to their complexity, chromatograms are not the most convenient easiest basis for modelling chromatography processes.

PFY diagrams reduce chromatograms to a simple curve which shows the trade off between purity and yield for a given separation and in this chapter the use of these diagrams as the basis for modelling chromatographic purifications was explored.

Chapter 5: ***The initial development of Kriging approaches for the characterisation of chromatographic separations***

The aim of this chapter was to establish the use of Kriging and cokriging for use in characterising chromatographic separations.

The typical approach for deriving empirical models from design-of-experiments studies for chromatographic processes uses response surface methodology (RSM). RSM creates these models by regressing a parametric model onto the available data. The accuracy of the resulting model may be limited if there are complex non-linear relationships between the process variables and the response.

Kriging and cokriging are nonparametric modelling approaches that produce predictions of unknown points using the weighted sum of known points. Therefore they have potential to produce more accurate models of the process and this was explored in this chapter.

Chapter 6: ***A comparison of modelling approaches for producing accurate process models from high throughput experiments which have high variability***

The aim of this chapter was to establish the most suitable approach for producing process models from high throughput experimentation.

High throughput experimentation is widely employed to reduce the burden of process development. However, this experimentation is susceptible to various sources of variability. Therefore the approach used to model the process should be capable of minimising the effects of this variability on the accuracy of the process model.

In this chapter Monte Carlo simulations were carried out using a simulated ion exchange chromatography system to test the susceptibility of response surface methods, Kriging and partial least squares regression to variability.

Chapter 7: ***A comparison of approaches for using scale down experimentation to develop chromatographic separations***

The aim of this chapter was to develop a methodology for using data from scale-down experiments to aid the development of chromatographic separations.

Scale-down chromatography devices are widely used for process development. However, differences in the format and geometry of these devices may result in scaling effects which prevent the scale-down experimental data being used for characterising the large scale purification.

Two methodologies were established in this chapter for bridging the data from scale-down experiments into the design space of the final process using cokriging and transformation functions. The potential to use these approaches to minimise the number of large scale experiments required for process characterisation was tested.

Chapter 8: ***Extending the scale-down characterisation methodology to enable the optimisation of a two step purification process with multiple responses***

The aim of this chapter was to test further and extend the methodologies established in Chapter 7.

In the previous chapter the bridging methodologies were established for a relatively simple system consisting of a single response and therefore each chromatography experiment could be reduced to a single data point.

In this chapter a design space spanning two unit operations, the heat treatment of *E. coli* fermentation broth to reduce impurities and the subsequent cation exchange chromatography capture of an antibody fragment, was characterised. The objective of this two step process was to optimise the yield, the overall purity and the clearance of HCP and DNA impurities. The bridging methodologies were used to enable the optimisation of this process by modelling curves representing the elution of the product, total protein, DNA and host cell proteins using the minimum amount of large scale experimentation.

Chapter 3

The feasibility of using mechanistic models to replace experimentation during the development of chromatographic separations

3.1 Introduction

During the development of a novel biopharmaceutical product extensive process development studies are needed to satisfy the requirements of the various regulatory agencies. The ICH guideline on pharmaceutical development (ICH, 2009) states the following. "The aim of pharmaceutical development is to design a quality product and its manufacturing process to consistently deliver the intended performance of the product. The information and knowledge gained from pharmaceutical development studies and manufacturing experience provide scientific understanding to support the establishment of the design space, specifications, and manufacturing controls". An added benefit results from the process development studies often being used to optimise the process and improve its economics.

Process development studies typically involve performing physical experiments across the design space at a representative scale. For a chromatography process this typically means carrying out experiments on columns with the same bed height but smaller di-

ameter than the manufacturing scale column. This can be expensive, time consuming and require a large amount of feed material. For the development of some unit operations a promising alternative is to use a mechanistic model to predict the performance of the process. For many bioprocess unit operations our limited level of understanding precludes such an approach. However, mechanistic models of varying complexity have been sucessfully used to model and understand chromatographic processes. These include predicting the effects of scaling up a column (Gerontas et al., 2010), exploring the robustness of a chromatographic separation (Close et al., 2014), identifying optimal pooling strategies (Kumar et al., 2015) and minimising the cost of the process (Orellana et al., 2009).

The likelihood of failure for a biopharmaceutical product is high during the early stages of development. Therefore the goal during process development is to reduce the associated time and cost to minimise any potential losses. There is a potential to achieve this goal through the use of mechanistic models. In this chapter the feasiblity of such an approach was explored by recreating the comprehensive general rate model established by Orellana et al. (2009) for the separation of three model proteins (α-lactalbumin, bovine serum albumin, and conalbumin) using ion exchange chromatography.

As mentioned above, performing process development studies for chromatographic processes are associated with a high experimental burden and the aim of this thesis was to identify approaches for reducing this experimental burden. If it could be shown that mechanistic models could be used to produce accurate characterisations of the process with ease and little or no physical experimentation, then these models could be used as the basis for the rest of this research. Therefore, in this study, particular attention was given to the ease with which the mechanistic model could be established and the quality of the data that could be gathered.

3.2 General rate model

The general rate model was used to explore the use of mechanistic approach for characterising chromatographic separations. The general rate model is considered a comprehensive model for simulating chromatographic processes as it describes all of the

mass transfer effects found in the process. These are:

1. The convective mass transfer of the solutes in the bulk phase of the chromatography column.
2. The diffusive mass transfer of the solutes in the film surrounding the beads.
3. The diffusive mass transfer of the solutes in the pores of the beads.
4. The adsorption and desorption of the proteins on the surface within the pores of the beads.

Other mechanistic models may lump two or more of these mass transfer effects to simplify the model and its numerical solution. However, in some cases these simplifications can lead to inaccuracies (Antos et al., 2003). Therefore, they may need to be treated with caution and tested further to verify the model.

The general rate model makes the following assumptions (Gu et al., 1992):

1. The column is isothermal.
2. The beads are spherical and have the same size.
3. Diffusion in the radial direction is negligible.
4. There is no convective flow inside the pores of the bead.
5. The beads are uniformly packed in the column.
6. The mass transfer and kinetic parameters are constant.

These assumptions help to simplify the model by eliminating the need to model additional phenomena but it is important to establish the validity of these assumptions for each modelled process. For examples assumption 1 is often valid as chromatography processes are usually operated in a controlled environment to satisfy good manufacturing practice. However, assumption 5 may be frequently invalid as achieving a uniform pack in large manufacturing scale columns can be difficult (Siu et al., 2014).

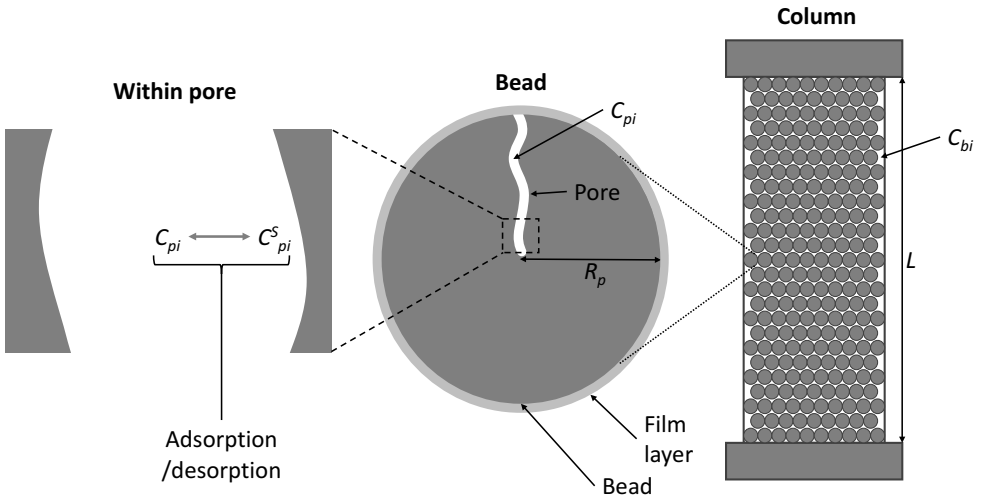

Figure 3.1: Schematic of a chromatography column illustrating some of the definitions used in the general rate model. C_{bi}, C_{pi}, and C^{S}_{pi} are the concentrations of i in the bulk phase, in the pore, and on the surface of the chromatography media respectively.

3.2.1 Mass transfer in the bulk phase of the column

Equation 3.1 represents the mass transfer of the proteins in the bulk phase of the column. The left hand side of this equation represents the convective and dispersive mass transfer effects of the proteins in the bulk of the column while the right hand side represents the mass transfer of the proteins to the surface of the beads through the film surrounding the bead.

$$\frac{\delta C_{bi}}{\delta t} + v_{int}\frac{\delta C_{bi}}{\delta Z} - D_{ax,i}\frac{\delta^2 C_{bi}}{\delta Z^2} = -\frac{3k_i(1-\varepsilon_b)}{\varepsilon_b R_p}(C_{bi} - C_{pi,r=R_p}) \tag{3.1}$$

where C_{bi} is the concentration of component i in the bulk phase of the column, t is the time, v_{int} is the interstitial velocity, Z is the axial coordinate, $D_{ax,i}$ is the dispersion coefficient, k_i is the film mass transfer coefficient, ε_b is the bed void fraction, R_p is the average bead radius, and $C_{pi,r=R_p}$ is the concentration of component i at the surface of the bead.

Equations 3.2, 3.3, 3.4, and 3.5 are the boundary conditions for equations 3.1.

At the inlet of the column:

$$Z = 0 \tag{3.2}$$

$$\frac{\delta C_{bi}}{\delta Z} = \frac{v_{int}}{D_{ax}}(C_{bi} - C_{bi,inlet}) \tag{3.3}$$

At the outlet of the column:

$$Z = L \tag{3.4}$$

$$\frac{\delta C_{bi}}{\delta Z} = 0 \tag{3.5}$$

3.2.2 Mass transfer in pores of the beads

Equation 3.6 represents the mass transfer of the proteins in the pores of the beads. Due to the very small diameter of the pores, it is assumed that protein mass transfer in the pores is by diffusion and there is no convective flow. The right hand side of the equation represents the protein diffusion through the pores of the beads while the left hand side accounts for the adsorption and desorption of the proteins on to the beads.

$$(1-\varepsilon_p)\frac{\delta C^S_{pi}}{\delta t} = -\varepsilon_p \frac{\delta C_{pi}}{\delta t} + \varepsilon_p D_{pi}\left(\frac{1}{R^2}\frac{\delta}{\delta R}\left(R^2\frac{\delta C_{pi}}{\delta R}\right)\right) \tag{3.6}$$

where ε_p is the bead void fraction, C_{pi} is the concentration of component i in the liquid phase inside the pores of the beads, C^S_{pi} is the concentration of component i on the surface of the beads, D_{pi} is the diffusivity of the proteins in the pores of the beads and R is the radial coordinate.

Equations 3.7, 3.8, 3.9, and 3.10 are the boundary conditions for equations 3.6.

At the surface of the bead:

$$R = R_p \tag{3.7}$$

$$\frac{\delta C_{pi}}{\delta R} = \frac{k_i}{\varepsilon_p D_{pi}}(C_{bi} - C_{pi,r=R_p}) \tag{3.8}$$

At the centre of the bead:

$$R = 0 \tag{3.9}$$

$$\frac{\delta C_{pi}}{\delta R} = 0 \tag{3.10}$$

3.2.3 Adsorption and desorption of the proteins

There are a number of approaches for describing the adsorption and desorption of the proteins on to the stationary phase. These can be selected and tailored to suit the chemistry of the stationary phase and the nature of its interactions with the proteins.

Equation 3.11 represents one such approach to describing the adsorption and desorption of proteins onto the stationary phase where there is competition between multiple proteins. This could be applied to ion exchange chromatography and hydrophobic interaction chromatography where multiple proteins can be expected to bind to the stationary phase. In this relationship the adsorption of the proteins is represented by second order kinetics as it is a function of both the concentration of the protein in the pore, and the concentration of available binding sites on the stationary phase. The desorption of the proteins is represented by first order kinetics as it is only a function of the concentration of the protein on the stationary phase.

$$\frac{\delta C^S_{pi}}{\delta t} = k_{ads,i} C_{pi} \left(C^{\infty} - \sum_{j=1}^{N_S} b_j C_{pj} \right) - k_{des,i} C^S_{pi} \tag{3.11}$$

where $k_{ads,i}$ is the rate of adsorption of component i, $k_{des,i}$ is the rate of desorption of component i, and C^{∞} is maximum concentration of component i on the stationary phase of the bead.

If the rates of adsorption and desorption are high, equilibrium can be assumed and Equation 3.11 can be reduced to the multicomponent Langmuir isotherm in Equation 3.12.

$$C^S_{pi} = \frac{a_i C_{pi}}{1 + \sum_{j=1}^{N_S} b_j C_{pj}} \tag{3.12}$$

where:

$$a_i = b_i C^{\infty} \tag{3.13}$$

Table 3.1: Parameters required for fitting the general rate model to specific separation

Column parameters	Mass transfer parameters	Adsorption/desorption parameters
• Linear velocity (v_{int}) • Bead radius (R_p) • Bed height (L) • Bed void fraction (ε_b) • Bead void fraction (ε_p)	• Dispersion coefficient (D_{ax}) • Film mass transfer coefficient (k) • Intraparticle diffusivity (D_p)	• Maximum conc. on the stationary phase (C^{∞}) • Rate of adsorption (k_{ads}) • Rate of desorption (k_{des})

and:

$$b_i = \frac{k_{ads,i}}{k_{des,i}} \tag{3.14}$$

3.2.4 Modulator relationship

In order to separate proteins on a chromatography column it will typically be required to control the conditions of the stationary phase. As an example, for the ion exchange chromatography process explored in this chapter, NaCl is used as a modulator. Different proteins will elute from the column at different modulator concentrations.

It is necessary to describe the effects of the modulator within the mechanistic model. For cases such as that described above, the effect of the modulator concentration on the adsorption/desorption kinetics can be modelled using equation 3.15 (Gu et al., 1992).

$$\log b_i = \alpha_i - \beta_i \log C_{p,N_s} \tag{3.15}$$

where C_{p,N_s} is the salt concentration.

3.3 Fitting the general rate model

Fitting the model described above to a particular separation requires quantifying a number of parameters. As detailed in 3.1, these parameters relate to the column, the mass

transfer of the proteins in the mobile phase, and their adsorption/desorption on to and from the stationary phase. Possible approaches for determining these parameters are detailed below.

3.3.1 Column parameters

Defining the linear velocity and the bed height will not typically present a problem. These parameters primarily affect the residence of the feed in the chromatography column. These parameters are typically optimised to maximise the adsorption of the product but minimise the duration of the process. However, pressure considerations will restrict the range of velocities and bed heights that can be used. In some cases prior experience will be used to set the values for these parameters. In other cases they may be kept as variables to be optimised during the development of the process.

The bead radius, bead voidage and bed voidage are physical characteristics which are particular to each resin. While the bead radius for a resin is typically found in the manufacturer's literature, the bed and bead voidage will usually have to be determined experimentally. A further complication is that the bed voidage can be affected by the quality of the column pack. Therefore these parameters may change from column to column. Furthermore, as the resin can settle during the course of a run, these parameters may change from one run to another.

The experimental determination of the bead voidage and bed voidage typically involves measuring the retention time in the column of two non-binding components. One of the components should be one small enough to enter the entire porous space of the bead, e.g. NaCl, while the other should be too large to enter the porous space, e.g. a large polymer such as blue dextran. The bead voidage and bed voidage can then be calculated from these values as shown by Gu et al. (2013).

Correlations such as those determined by Mohammad et al. (1992), Stickel and Fotopoulos (2001) and Perez-Almodovar and Carta (2009) do exist for calculating the total voidage of packed beds. However, these correlations are specific to the resin or resin type characterised in those studies. Furthermore the total voidage calculated in these correlations is only suitable for use in less comprehensive models where the bed voidage and bead voidage are lumped into a single parameter.

3.3.2 Mass transfer parameters

Mass transfer in a packed bed is well understood as it is common to a number of industrial unit operations. Correlations for estimating these parameters have been derived which eliminates the need for their experimental determination. Gu et al. (2013) have reviewed the available correlations in greater detail. The parameter estimation approach used by Orellana et al. (2009), which uses some of these correlations, was used in this study and is detailed below.

The axial dispersion (D_{ax}), film mass transfer coefficient (k) and the intraparticle diffusivity (D_p) were estimated using equations 3.16, 3.17 and 3.18 .

$$D_{ax} = \frac{v_{int} L}{Pe} \tag{3.16}$$

$$k = 1.165 v_{int}^{1/3} \left(\frac{1-\varepsilon_b}{\varepsilon_b} \right)^{1/3} \left(\frac{D_m}{R_p} \right)^{2/3} \tag{3.17}$$

$$D_p = \frac{D_m}{\tau_{tor}} \left(1 - 2.104\lambda + 2.09\lambda^3 - 0.95\lambda^5 \right) \tag{3.18}$$

where Pe is the Peclet number, D_m is the molecular diffusivity of the molecule, τ_{tor} is the particle tortuosity factor, and λ is the ratio of the molecular diameter to the pore diameter.

The estimation of D_{ax} required the Peclet number (Pe) which was estimated using Equation 3.19 (Gu et al., 2003) which in turn required the Reynolds number (Re) which is calculated using equation 3.20.

$$Pe = \frac{0.1L}{R_p \varepsilon_b} \tag{3.19}$$

$$Re = \frac{2R_p \rho v_{int} \varepsilon_b}{\mu} \tag{3.20}$$

where ρ is the density of the mobile phase and μ is the viscosity of the mobile phase.

It was assumed that the mobile phase had the same density and viscosity as water.

The correlations for the k and the D_p required the value of the molecular diffusivity (D_m) of the protein which was calculated using equation 3.21.

$$D_m = 2.74 \times 10^{-5} MW^{-\frac{1}{3}} \tag{3.21}$$

3.3.3 Adsorption/desorption parameters

The parameters that require fitting will depend on the isotherm that has been selected for describing the adsorption/desorption behaviour of the molecules on to the stationary phase of the column.

For the multicomponent Langmuir isotherm used in this study, the maximum concentration on the stationary phase and the rates of adsorption and desorption for each component are required. A modulator relationship was also included in the model to describe the effects of the mobile phase salt concentration on the rates of adsorption and desorption. Therefore, the parameters in the modulator relationship will also need to be determined.

Orellana et al. (2009) determined these parameters by performing experiments which involved loading a chromatography column with each component in its pure form. In each experiment the protein was eluted using a salt gradient and the model parameters were adjusted until the simulated results fit the experimental results.

3.3.4 Inverse fitting the general rate model

An alternative approach to fitting the general rate model is the inverse fitting approach. This is similar to the approach that was described above for estimating the isotherm parameters. However in this case rather than determining or estimating the parameters individually, the model is calibrated using a set of experimental results. The experiments will be designed to capture the effects of the process parameters and the number of required experiments will be depend on the complexity of the model. An optimisation routine is then used to calibrate the model parameters by minimising the error between the simulated results and the experimental results.

Table 3.2: Parameters for the modelled chromatography column

Column diameter (cm)	d_b	0.5
Particle diameter (cm)	d_p	0.009
Bed height (cm)	L	5.2
Interstitial velocity (cm/min)	v_{int}	14.15
Bed voidage	ε_b	0.36
Particle voidage	ε_p	0.79

Table 3.3: Estimated parameters for each component in the modelled chromatography system

Parameter	Conalbumin	Lactalbumin	BSA	NaCl
Axial dispersion coefficient, $D_{ax,i}$ $(cm^2 s^{-1})$	0.229	0.229	0.229	0.229
Film mass transfer coefficient, k_i (cm/min)	0.1395	0.2081	0.148	1.157
Intraparticle diffusivity, $D_{p,i}$ $(cm^2 s^{-1})$	1.43×10^{-5}	2.96×10^{-5}	1.61×10^{-5}	3.51×10^{-4}
Rate of desorption, $k_{des,i}$ (cm/min)	0.6803	1.088	0.8163	-
α	5.10	5.00	5.60	-
β	40.00	22.55	15.50	-

3.4 Simulated chromatographic separation

The general rate model described above was used to simulate the separation of conalbumin, lactalbumin and bovine serum albumin using the anion exchange resin Q Sepharose FF. This simulation was originally described by Orellana et al. (2009) and was adopted in this study to test the feasibility of using this approach for developing chromatographic separations. This simulation was suitable for this purpose since it mimicked a typical preparative chromatography system with a feed consisting of multiple proteins. Tables 3.2 and 3.3 detail the parameters of the column and the each component used to model this system.

Each simulation began with a column that had been equilibrated to the pH and ionic strength of the feedstock. The feedstock was then injected onto the column which was

followed by the elution phase of the process. The elution buffer was the equilibration buffer with added salt to increase the ionic strength and elute the bound protein.

The system of equations that made up this model was solved using COMSOL Multiphysics 4.1 (COMSOL Ltd., Cambridge, UK). The finite element method was used to discretise the partial differential equations with 27 axial elements and 27 radial elements being used. Increasing the number of elements beyond this number did not change the results of the simulation, indicating that the model had converged. The model was solved on a PC with an Intel Core i7 M620/2.67 GHz processor and 4 GB of memory and each simulation was solved in less than 2 minutes.

3.5 Discussion

3.5.1 Results of the simulated chromatography separation

Using a mechanistic model to simulate a chromatographic process is usually significantly quicker than carrying out physical experiments. Therefore it is possible to investigate the effects of the process variables in a significantly shorter amount of time than would be required experimentally. Furthermore, as there is no requirement for expensive feedstock, chromatography resin and other material, the development costs are significantly lower. However, it will not be possible to completely eliminate the need for physical experimentation as it will be necessary to verify the model and establish that the simulated results match the real process.

The ease with which the process could be simulated was demonstrated by investigating the effect of elution salt concentration on the chromatographic separation of conalbumin, lactalbumin and bovine serum albumin (BSA). The model was solved at different elution salt concentrations between 0.08 M and 0.16 M in 0.01 M intervals.

Figure 3.2 shows the chromatograms at elution salt concentrations of 0.08 M, 0.12 M and 0.16 M). These chromatograms show how changing the elution salt concentration can affect the separation of the three proteins. At an elution salt concentration of 0.08 M there is some resolution between the conalbumin and the lactalbumin, while the BSA is mostly retained on the column. As the elution salt concentration increases, the

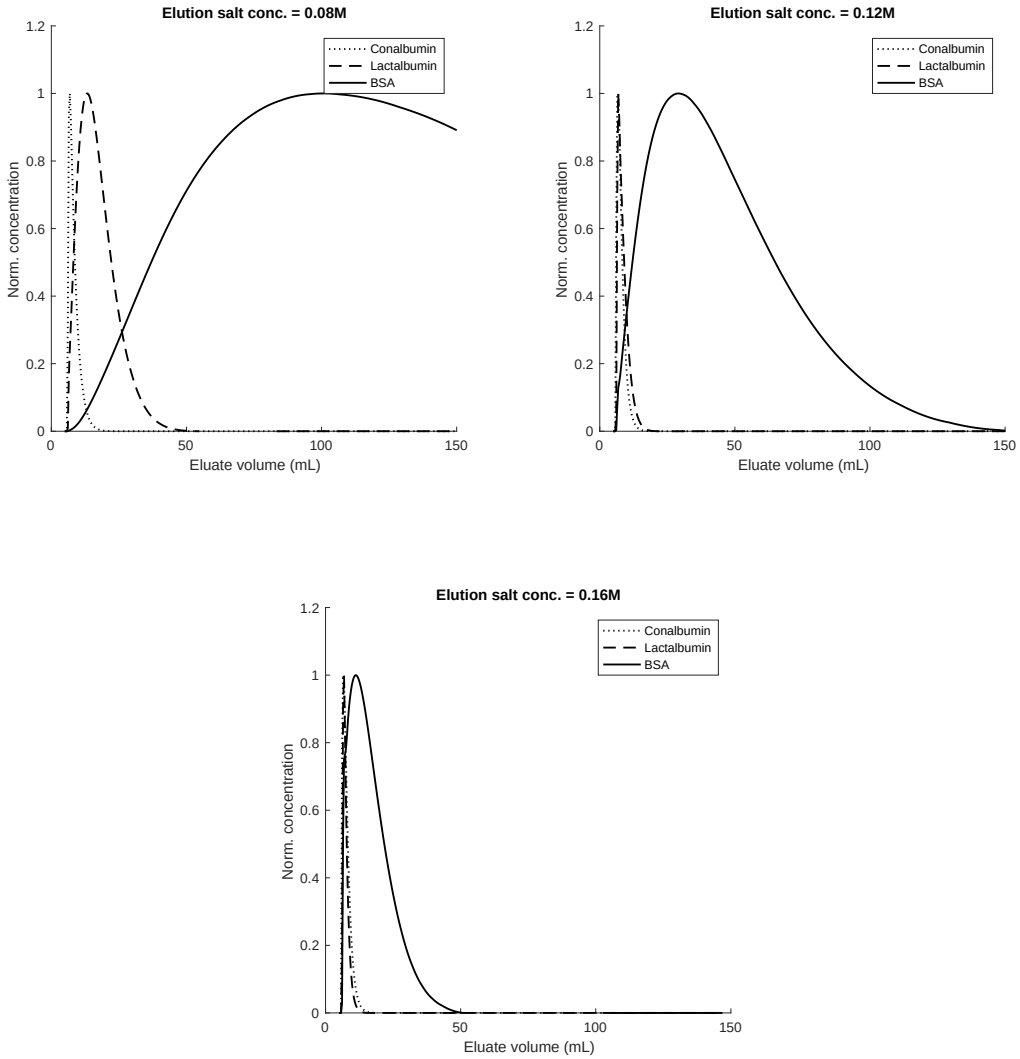

Figure 3.2: The simulated chromatograms for the separation of the conalbumin, lactalbumin and bovine serum albumin using anion exchange chromatography. The chromatograms are for the elution salt concentrations of 0.08 M, 0.12 M, and 0.16 M. The concentration trace for each protein is normalised by its maximum to highlight the relative location of each peak.

separation between the conalbumin and the lactalbumin disappears and elution of the BSA is also observed.

The calculation of these chromatograms highlighted the benefits of using mechanistic models during process development. A typical experimental approach would involve carrying out experiments at two or three points for a given process variable. But, as the limitations associated with feed material and time do not exist for the simulated process, it is possible to carry out a larger number of experiments to gain a deeper understanding of the process design space. This capability also enables the thorough optimisation of the process.

Using the mechanistic modelling approach it was possible to produce the well defined concentration profiles shown in the simulated chromatograms. To produce similar concentration profiles from physical experiments would require collecting and analysing a large number of fractions which would result in an unacceptable experimental burden.

3.5.2 Feasibility of using mechanistic modelling during process development

Using a mechanistic model during process development can have clear benefits. By using this approach the effects of the process variables can be rapidly and cheaply investigated. However, through building this model a number of shortcomings were identified which are discussed below.

3.5.2.1 Model creation

It is necessary to make various assumptions about the process during the construction of the model. This may be to reduce the complexity of the model to ease its numerical solution or to reduce the number of parameters that require determination. For example, it is necessary to select from a number of model formulations which have varying levels of complexity. While this study used the comprehensive general rate model, a simpler model with lumped parameters may have produced results with a similar level of accuracy. Using a model with fewer parameters will ease the creation of the model but if the model is oversimplified the simulated results will be a poor representation of the process. Similarly, it is necessary to select an isotherm model to describe the

interactions between the proteins and the stationary phase. This requires making assumptions about the types of interactions and will result in inaccurate results if done incorrectly.

Further assumptions may also need to be made beyond model selection. For example, in the model described in this study, Orellana et al. (2009) found that the saturation capacities of the three proteins were different. But to simplify the model they assumed that the saturation capacities of all three proteins were the same and equal to the protein with the greatest capacity. Other assumptions may be made to reduce the burden of experimentally determining the model parameters. An example of this is the determination of the particle voidage. This is used to describe the amount of the stationary phase that can be accessed by the components in the mobile phase. However, instead of determining this for each individual component, a single small molecule is used. While the effects of this assumption may be negligible, for purifications which consist of proteins with a large range of sizes, the error may become significant.

Making correct assumptions is complicated by the scarcity of understanding about the process during early stages of development. An instance of this can be seen in the study by Gerontas et al. (2010). This work modelled the scale up of the chromatographic separation of bovine serum albumin (BSA) and lactoferrin. However, the model failed to predict the presence of a tail in the BSA peak. This was later assumed to be due to the presence of an unknown impurity such as a protein aggregate but was not captured during the model development.

3.5.2.2 Parameter estimation

The step after creating the model involves setting the values of the model parameters. While some of these parameters will be typically known at the start of process development, e.g. the diameter of the stationary phase particles, a large number will be unknown, e.g. the mass transfer parameters of each feed component, especially when the separations are occuring in the presence of other competing species.

Some of the phenomena found in chromatography processes are found in other process and are well understood. Therefore the unknown parameters related to these phenomena can be estimated using correlations widely found in engineering literature. But this

in turn can increase the amount of initial information that is required. For example, the correlation used in this study to estimate the intraparticle diffusivity require the molecular diffusivity, molecular diameter, pore diameter and tortuosity factor for each component. While further correlations can be used to estimate the molecular diffusivity and molecular diameter from the molecular weight, the pore diameter and tortuosity factor are particular to the resin and are not commonly found in literature. Therefore some experimentation will be required to determine these parameters.

Other parameters such as the rates of adsorption and desorption that cannot be estimated will require experimental determination. Simple small scale batch experiments may be used to determine the isotherm parameters (Gu et al., 2013; Close et al., 2014). Alternatively the results from the bench experiments can be used to perform inverse fitting. This approach was used by Gerontas et al. (2010) to model the scale up of a two component separation, Borg et al. (2014) to model the separation of a antibody monomer from its dimer and other oligomers and Kumar et al. (2015) to model the separation of charged isoforms. For both approaches the number of required experiments will depend on the complexity of the model and the number of components in the feed, potentially resulting in a significant amount of experimentation.

The parameter determination experiments are usually performed using the feedstock components in their pure form. If this approach is taken further experiments will be required to isolate the components. In some cases the components may be present in very low concentrations and additional experiments may be needed to produce the impurities. For example, Borg et al. (2014) had to incubate product at low pH to create aggregated protein and then separated it from the remaining product using size exclusion chromatography.

Another complication can arise from modelling impurities which are made up of a number of proteins. The constituent proteins will not have the same properties and will therefore be difficult to model. This is particularly the case for residual impurities such as host cell proteins and DNA. These impurities tend to be made up of multiple molecules and often at low concentrations which further complicates their characterisation.

3.6 Conclusion

Mechanistic models can be used to rapidly and cheaply explore the design spaces of chromatography processes. However, the creation of a mechanistic model during the early stages of process development may prove to be difficult as the process will not be well understood and therefore the appropriate modelling approach will be less obvious. Furthermore, a significant amount of experimentation will still be required to create a mechanistic model regardless of model complexity and parameter determination approach.

Therefore, during the early stages of process development, the alternative approach of using small scale high throughput experimentation combined with rapid analytical techniques and statistical modelling might be more suitable.

Mechanistic modelling may be a tool more suited to the later stages of process development where an initial understanding of the process is already available. Very detailed characterisations of the process are required by the regulatory agencies during the later stages of development and mechanistic modelling can be used to avoid the large amount of experimentation that would otherwise be required.

Chapter 4

The use of maximum purification factor vs. yield diagrams as the basis for characterising and modelling chromatographic separations

4.1 Introduction

In this chapter the use of maximum purification factor vs. yield (PFY) diagrams as the basis for characterising and modelling chromatographic separations was evaluated.

In Chapter 3 the use of mechanistic models as a tool for developing chromatographic separations was reviewed and it was concluded that a more suitable approach for characterising chromatography processes would be to use physical experiments combined with statistical modelling.

These physical experiments are typically carried out using preparative chromatography systems such as AKTA Avants (GE Life Sciences). These systems include sensors to monitor characteristics such as the UV absorbance, pH and conductivity of the eluate from the column. Proteins typically absorb UV light with the measurements usually taken at around 280 nm to determine the concentration of the protein (Aitken and Learmonth, 1996). Therefore the UV absorbance of the eluate can be used to monitor the elution of proteins from the column. A plot of the UV absorbance of the eluate against

time is known as the chromatogram and is the typical output from a chromatography experiment. However, for preparative chromatography, it is usually not possible to directly quantify the performance of the process from its chromatogram. This is because it will typically not be possible to identify the concentrations of individual proteins on the chromatograms and therefore further analysis will be required to quantify the performance of the process.

In analytical chromatography the column is often loaded to a low level relative to the number of binding sites on the column. In these situations the majority of the binding sites on the chromatography media are unoccupied which allows the components to migrate at different rates through the column and resolve from one another. The identity of the components and their concentrations can then be deduced from the residence times and areas of the peaks on the chromatogram. On the other hand in preparative chromatography it is necessary to maximise the loading of the column to reduce the required column size and minimise the cost of goods for the process. In these situations it is unlikely that the components will resolve fully from one another and therefore it will not be possible to determine the identity and purity of the proteins directly from the chromatogram. An example of this is shown in Figure 4.1a. To quantify the performance of such a process, the eluate will need to be separated into appropriate fractions and the fractions subsequently analysed to determine the concentrations of the product and impurities. The determined concentrations can then be used to construct concentration profiles for each component as shown in 4.1b.

Chromatograms showing concentration profiles for each component can be complex and difficult to use as the basis for modelling the process. Such an approach was created by Edwards-Parton et al. (2008) which involved fitting curves to the peaks in the chromatogram. The fitted peak parameters were then used as the basis for modelling the process. However, this procedure required several preprocessing steps and made the assumption that the peaks took the form of an ideal Gaussian distribution, both of which are potential sources of error. Hutchinson et al. (2009) created an approach for predicting large scale elution profiles from small scale elution profiles by applying correction factors which correct the dispersion and retention effects. However, this was only demonstrated for the elution of a single component and may not be valid for

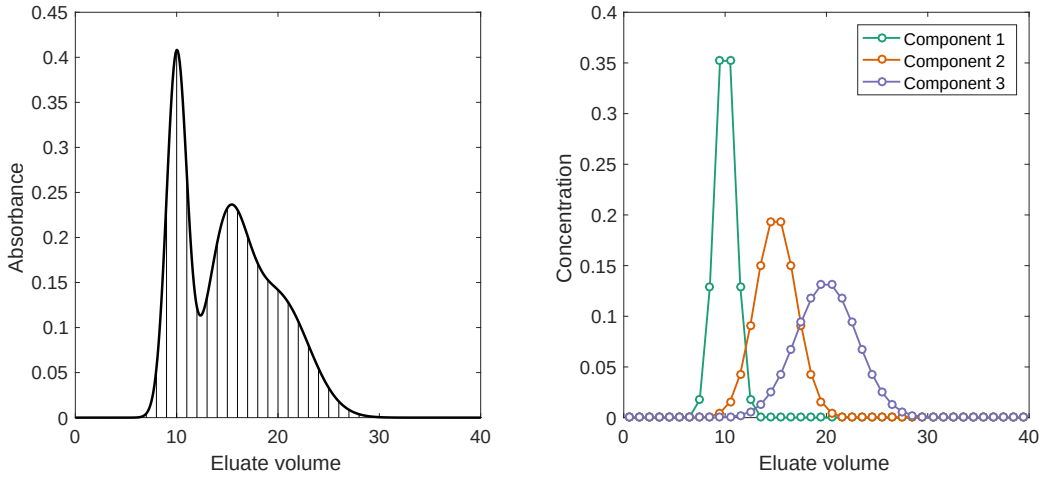

(a) **(b)**

Figure 4.1: Procedure for producing concentration profiles for each component for a chromatography experiment. 4.1a shows a mock chromatogram for a preparative chromatography run with three overlapping components. This figure also shows the eluate fractions that were taken in order to analyse for each component. 4.1b shows the concentration profiles that were produced for each component by fractionating and analysing the eluate.

multiple components. Furthermore, using the concentration profiles will not give an immediate quantitative indication of the process performance and it may be difficult to discern how a change to the process has affected the performance. An approach for reducing the complexity of this output and producing a quantitative output is to calculate the max. purification factor vs. yield (PFY) diagram from the concentration profiles.

PFY diagrams were originally derived for optimising fractional precipitation processes. These diagrams were then adapted for chromatography by Ngiam et al. (2001) to analyse the trade off between yield and purity. For a chromatographic separation the PFY diagram represents the trade off between the purity and the yield using a single continuous curve. The PFY diagrams were also used by Salisbury et al. (2006) to define windows of operation for process sequences consisting of two chromatography steps.

As mentioned above, in preparative chromatography the product is rarely well resolved from the impurities and will overlap each other in the eluate. Peak cuts therefore need to be applied to the eluate to maximise the collection of the product and minimise the collection of the impurities. Changing the cuts to improve the yield will result in more impurities being collected resulting in a lower purity and vice versa. Therefore a single

set of cuts cannot be found to maximise both the yield and purity. The PFY diagram illustrates the trade off between the yield and purity by evaluting all possible peak cutting scenarios and plotting the maximum purification factor that can be achieved at each yield value.

The PFY diagram is a simple curve that is a quantitative representation of the process performance in terms of the purity and yield. There is the potential to use these diagrams as the basis for modelling the design space of chromatographic separations and this was explored in this chapter. The simulated separation of conalbumin, lactalbumin and bovine serum albumin using anion exchange chromatography was used as platform for testing this approach. A number of chromatography experiments were simulated across a range of elution salt concentrations. The PFY diagrams were calculated for each of the experiments and used to produce a characterisation of the experimental space.

4.2 Methods

4.2.1 Chromatograms

The general rate model established by Orellana et al. (2009) and recreated in Chapter 3 was used to simulate a chromatgraphic separation at a number of points across its experimental space. This general rate model described the separation of 3 proteins - conalbumin, lactalbumin and bovine serum albumin using anion exchange chromatography. The experimental space consisted of one process parameter; the elution salt concentration. Simulations were carried out at elution salt concentrations between 0.06 M and 0.16 M in 0.01 M increments. Figure 4.2 shows the simulated chromatogram for an elution salt concentration of 0.08 M.

4.2.2 Fractionation diagrams

Calculating the fractionation diagram is the first step towards producing the max. purification factor vs. yield diagram. The fractionation diagram is a plot of y vs. x where x represents the fractional elution of the total protein and y represents the fractional elution of the product as defined in Equations 4.1 and 4.2.

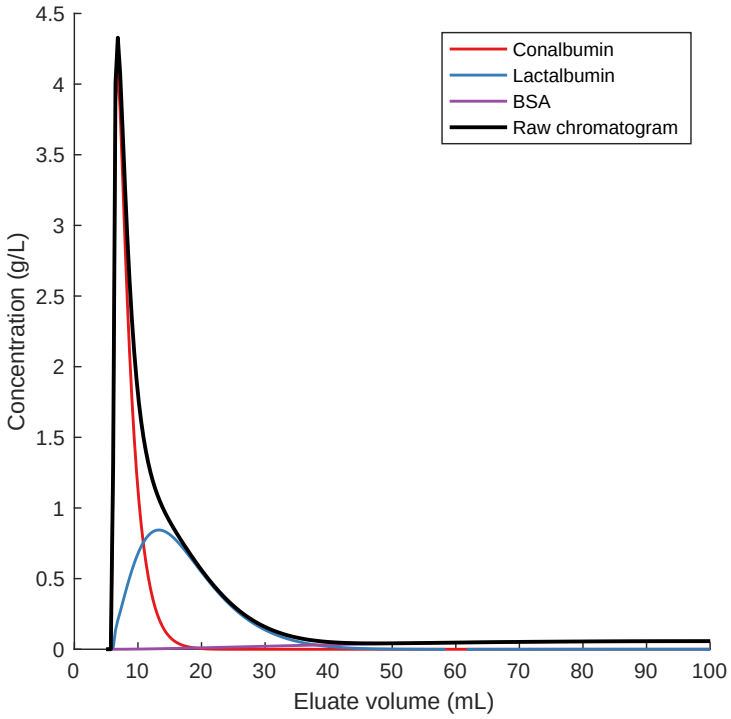

Figure 4.2: Simulated chromatogram for the separation of conalbumin, lactalbumin and bovine serum albumin using anion exchange chromatography at an elution salt concentration of 0.08 M.

$$x = \frac{\sum_{i=0}^{i} M_{T,i}}{\sum_{i=0}^{N} M_{T,i}} \tag{4.1}$$

where the eluate is divided into $i = 1,2,3 \cdots N$ fractions and $M_{T,i}$ is the mass of total protein in fraction i.

$$y = \frac{\sum_{i=0}^{i} M_{P,i}}{\sum_{i=0}^{N} M_{P,i}} \tag{4.2}$$

where $M_{P,i}$ is the mass of product in fraction i.

The fractionation diagram reduces the complex chromatogram with multiple peaks to

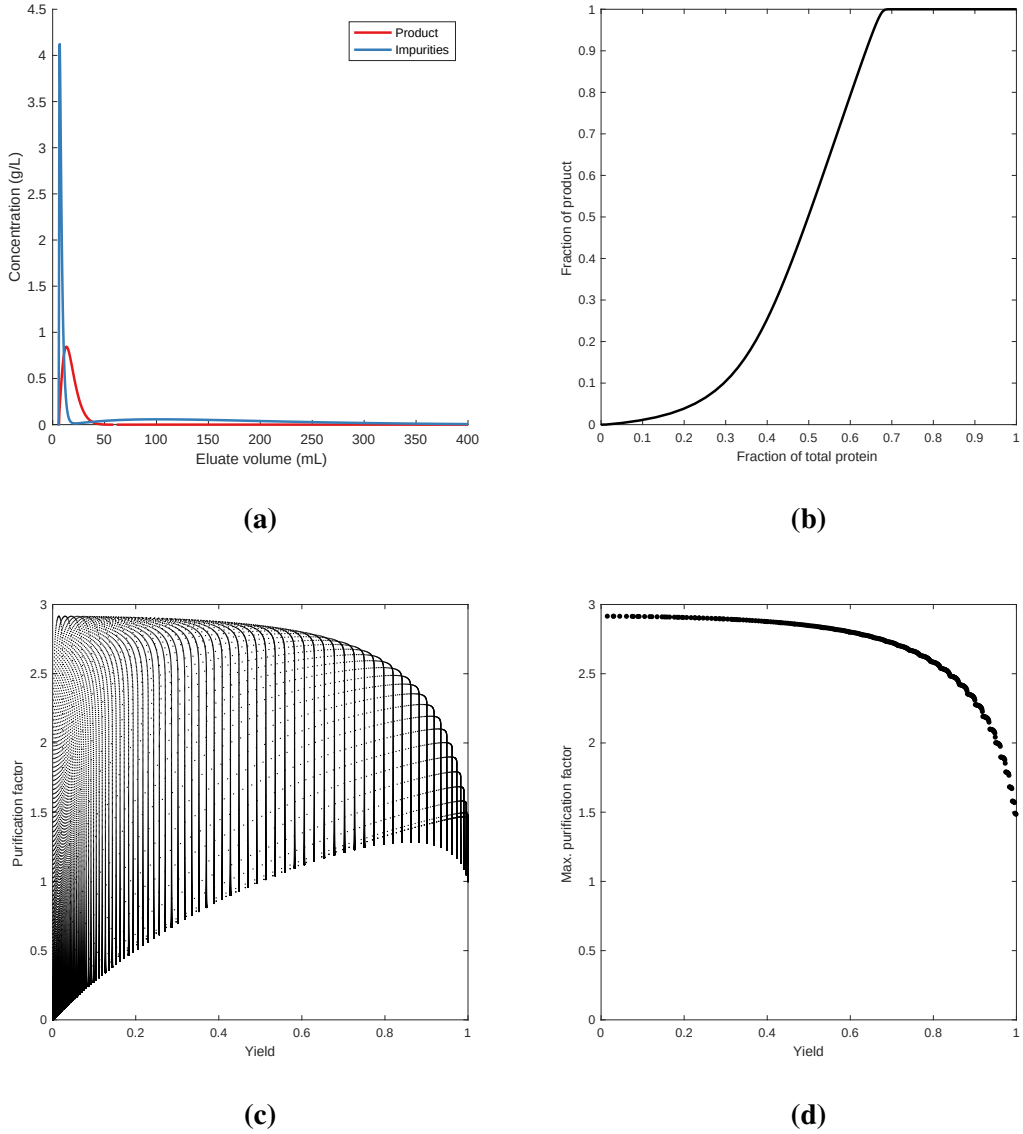

Figure 4.3: The procedure for calculating the maximum purification factor vs. yield diagram. First the fractionation diagram (4.3b) is calculated for the given chromatogram (4.3a). The set of purification factors and their corresponding yields (4.3c) are then calculated from the fractionation diagram. Finally, the max. purification factor is identified at each yield to produce the max. PF vs. yield diagram (Figure 4.3d)

.

a single curve which illustrates the relative elution of the product and the impurities. In this study the lactalbumin was considered to be the product and the conalbumin and BSA were treated as the impurities. This is shown in modified chromatogram in Figure 4.3a where the sum of the conalbumin and BSA profiles is shown as the impurity profile and the lactalbumin is shown as the product profile. Figure 4.3b is the fractionation diagram calculated for the chromatogram in Figure 4.3a.

4.2.3 Calculation of the purification factors and yields

During a chromatography process a fraction or series of fractions of the eluate from the column will be collected to recover the pure product. The start and end points of the collected fraction will be chosen to maximise the recovery of the product while minimising the collection of the impurities. The aim of this is to maximise the purity of the product but subject to a given minimum yield.

The start and end points of the fraction are known as the collection cuts. For a pair of collection cuts the fractionation diagram can be used to calculate the purification factor and the yield of the collected eluate using Equations 4.3 and 4.4. The purification factor is the factor by which product purity has increased and the yield is the fraction of product that was recovered. On the fractionation diagram these correspond to the gradient between the two points and the difference in y coordinates respectively.

$$PF = \frac{y_2 - y_1}{x_2 - x_1} \tag{4.3}$$

$$Y = y_2 - y_1 \tag{4.4}$$

where PF is the purification factor and Y is the yield and y_1, y_2, x_1 and x_2 are the coordinates of the two cuts on the fractionation diagram.

By calculating the purification factor and yield for each combination of collection cuts a set of purification factors and yields can be created which represents the possible performance of the chromatography process. Figure 4.3c shows the set of purification factors and yields that were calculated for the fractionation diagram in Figure 4.3b.

4.2.4 Maximum purification factor vs. yield diagrams

The fractionation diagram in Figure 4.3c shows the potential performance of the separation in terms of the purification factor and the yield. However, the majority of these points are sub-optimal as it would be possible to get a higher purification factor for the same yield. Therefore, by selecting the maximum purification factor at each value of

yield it is possible to derive a curve that represents the optimal performance of the separation. An example of this is shown in Figure 4.3d which is the maximum purification factor vs. yield diagram for the set of purification factors and yields in Figure 4.3c.

MATLAB scripts were written to obtain the maximum purification factor at each yield and produce the max. PF vs. yield diagram.

4.3 Results and discussion

Simulated chromatograms were produced for elution salt concentrations between 0.06 M and 0.16 M in 0.01 M intervals. Fractionation diagrams and maximum purification factor vs. yield (PFY) diagrams were calculated for each of these chromatograms.

Figure 4.4 shows the chromatograms for the elution salt concentrations of 0.08 M and 0.12 M and their corresponding max. PF vs. yield diagrams. The chromatograms show that as the elution salt concentration increases, the resolution between the product and its leading and trailing impurities reduces. The corresponding PFY diagrams highlight this behaviour but also allow for the direct quantification of the impact of the elution salt concentration on the product purity. As the elution salt concentration increases from 0.08 M to 0.12 M, the maximum possible purification factor drops from approximately 3 to 2.

Furthermore, as the separation is represented by a single curve it easily lends itself as an input to statistical modelling and visualisation. Figure 4.5a is a contour plot that visualises the entire simulated experimental space in terms of the elution salt concentration, yield and max. purification factor. This figure highlights how the characterisation of the process based on the PFY plots can be easily used to define a window of operation. For example, the highlighted region in Figure 4.5b shows the operating window where a purification factor of greater than 2.5 and a fractional yield of greater than 0.75 can be achieved.

4.4 Conclusions

In this chapter it was established that chromatograms may not be the most suitable basis for modelling chromatographic separations and PFY diagrams were evaluated

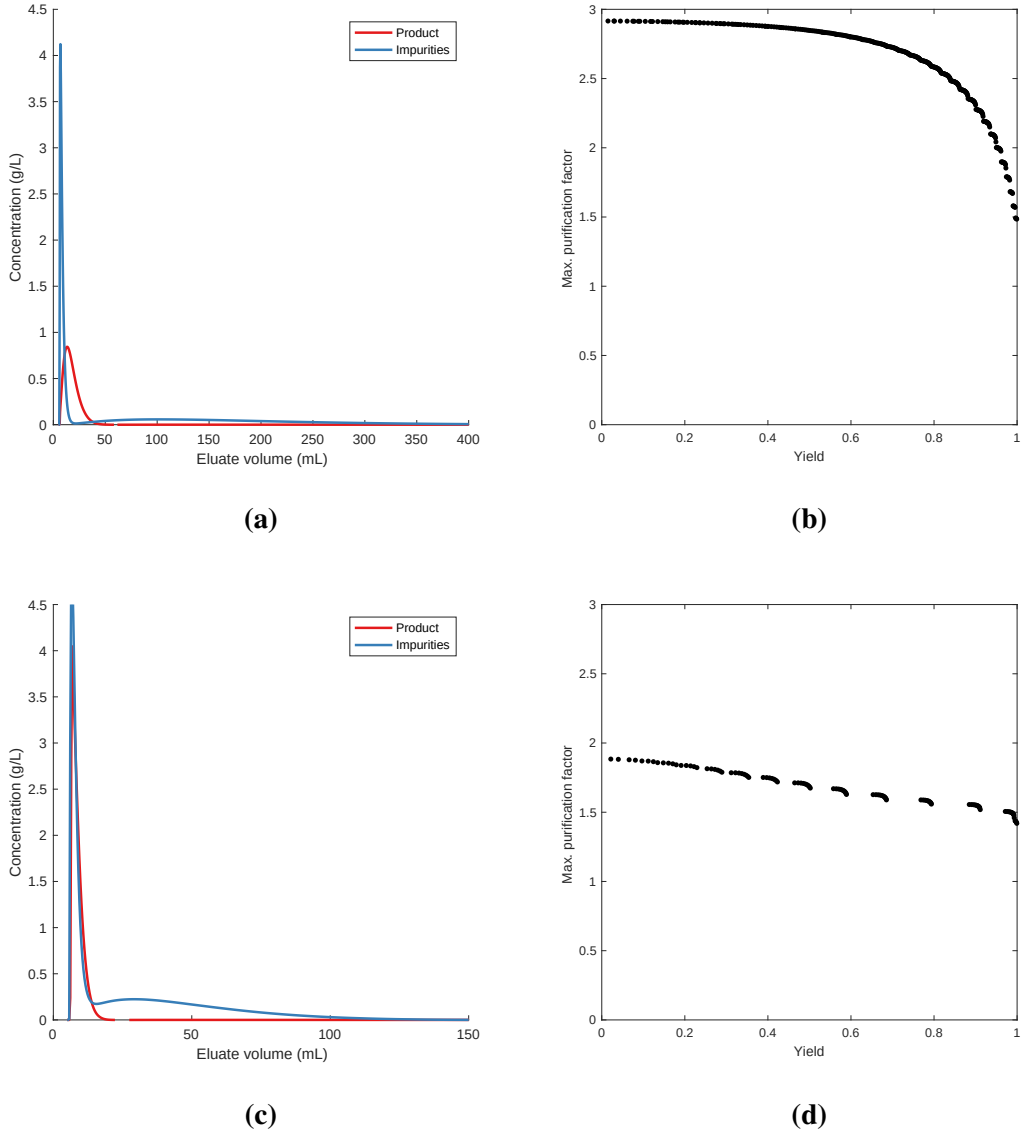

Figure 4.4: The simulated chromatograms and their corresponding maximum purification factor vs. yield diagrams for the purification of lactalbumin from a feed also containing conalbumin and bovine serum albumin using anion exchange chromatography. 4.4a and 4.4b correspond to an elution salt concentration 0.08 M while 4.4d and 4.4d correspond to an elution salt concentration 0.12 M

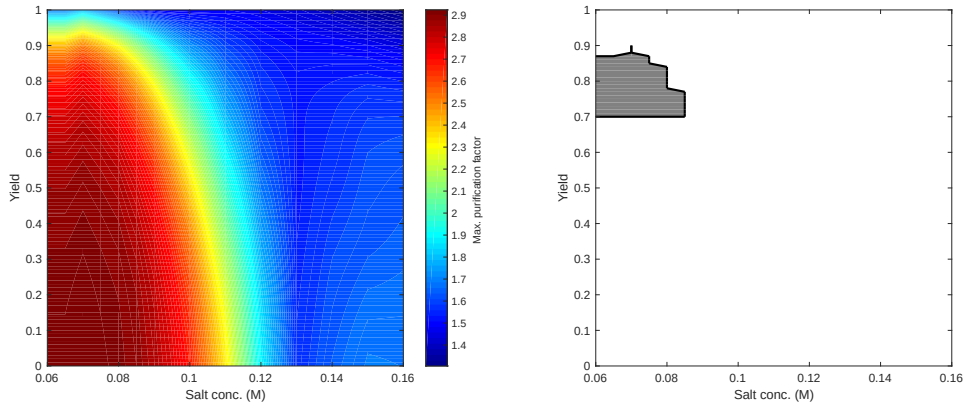

(a) **(b)**

Figure 4.5: 4.5a Contour plot characterising the effects of elution salt concentration on the yield and maximum purification factor for the separation of lactalbumin from conalbumin and bovine serum albumin. 4.5b Operating window within which a purification factor greater than 2.5 and a yield greater than 0.75 can be achieved.

as a possible alternative. It was demonstrated that the PFY diagrams were capable of highlighting and quantifying the effects of the process variables on the purification performance. It was also shown that PFY diagrams could be used as the basis for producing characterisations of the experimental space.

Chapter 5

The initial development of Kriging approaches for the characterisation of chromatographic separations

5.1 Introduction

In this chapter the use of Kriging and Cokriging as alternative approaches to the current methods of characterising chromatographic processes will be explored.

In Chapter 3 the importance of producing characterisations of chromatography processes was highlighted for both understanding and optimising the process, and also defining windows of operation. It was concluded that the best approach to achieve this would be to combine physical experimentation with statistical modelling to produce the required characterisations. Maximum purification factor vs. yield diagrams were then explored in Chapter 4 as a suitable basis for producing these characterisations as these had the ability to reduce the complex chromatograms consisting of multiple concentration profiles to a single curve which highlighted the trade off between yield and purity for each experiment.

Another issue with characterising chromatographic processes is that a prohibitively large number of experiments would be required to collect data across the whole experimental space. The experimental space for a chromatographic process will typically be made up of a large number of process variables, as high as 100 - 200 (Rathore,

2009) and each process variable can span a wide range. Therefore to perform experiments across the whole experimental space would require a large number of experiments which would be expensive and time consuming.

A further complication during the early phases of process development is that feed material is often scarce and therefore extensive experimentation may not be possible. This is exacerbated by the requirement to perform the experiments at a representative scale where results will be equivalent to the final process (Breece et al., 2002). For chromatography this typically means performing the experiments on a column with the same bed height which restricts the potential for scaling down the process and minimising the required amount of feed. Finally, as a large number of biopharmaceutical products fail during the course of development, there is an added incentive to minimise the number of performed experiments, as this will minimise the financial loss in the event of the product failing (Paul et al., 2010).

The typical approach to characterising chromatography processes while satisfying these demands is to combine design of experiments (DOE) approaches with response surface methodology (RSM) (Kumar et al., 2014; Chhatre et al., 2011; Bhambure and Rathore, 2013). Design of experiments is an approach for designing experimental studies that maximise the information gathered about the impact of the process variables on the responses, while minimising the number of experiments.

After performing the DOE experiments, RSM can be used to produce a model that describes the relationship between the process variables and the responses. This model is produced by fitting a polynomial surface to the experimental data. To prevent overfitting the polynomial is usually limited to the second degree (quadratic polynomial) and it is assumed that this will be a suitable approximation of the experimental space. However, this assumption may not be valid, especially for complex non-linear processes such as chromatography. Furthermore, while this assumption might be valid over short ranges, if the experimental space includes process variables with wide ranges, this assumption is less likely to be valid.

In this chapter the Kriging method (Matheron, 1963) will be explored as an alternative to RSM. Kriging is a technique that was initially developed as a method for predicting

the distribution of mineral deposits over a region of interest from a number of random sampling points (Matheron, 1963). Instead of fitting a parametric model, it produces its predictions from the weighted interpolation of the available data. Therefore it does not assume a form for the experimental space as RSM does. This may also make it better suited to situations where the response is more complex than a single value, such as where the response is a max. purification vs. yield diagram. Kriging also accounts for clustering of the data to prevent this from biasing the prediction. This is potentially useful during early process development where there will be several iterative rounds of experimentation and the experiments may not follow a fixed design. Kriging has been applied to a number of process engineering unit operations including powder feeding (Jia et al., 2009), powder mixing (Boukouvala et al., 2010), and a chemical reaction (Davis and Ierapetritou, 2010) for design space description and optimisation and a similar approach was adopted here.

Cokriging will also be explored as an approach for reducing the experimental burden of characterising a chromatography process. Cokriging also originates from the mining industry and was applied to situations where the primary assay for the mineral of interest was expensive or time consuming. In these situations a large number of samples would be taken across the area that was being investigated for mineral deposits. All of the samples would then be analysed by a cheaper but less accurate assay that was known to be correlated to the mineral of interest. A smaller subset of the samples would also be analysed by the expensive primary assay. The expensive primary assay results would be augmented with the cheap assay results using cokriging to predict the distribution of the mineral in the explored area. This is analogous to chromatography where representive experiments are expensive due to the bed height restriction, but cheaper experiments which are correlated to the final process can be performed using scale down columns with smaller bed heights.

The use of kriging and cokriging was explored using the simple and well understood separation of myoglobin from egg white proteins using cation exchange chromatography (Edwards-Parton et al., 2008). Experiments were performed on columns at three different scales to test whether experiments from a smaller scale could be used to predict the experimental space of larger columns. Maximum purification factor vs. yield

diagrams were calculated for each of the experiments and these diagrams were used to create the input datasets for establishing the kriging and cokriging algorithms.

5.2 Materials and methods

5.2.1 Ion exchange chromatography

A well defined chromatographic separation was employed for these experiments to provide a readily manipulated system. The separation of myoglobin from egg white protein using cation exchange chromatography provides a separation where the elution profiles of the product and the impurities can be determined rapidly (Edwards-Parton et al., 2008). The main components of egg white protein are ovalbumin, ovotransferrin and lysozyme. When a mixture of egg white protein and myoglobin is applied to a strong cation exchange matrix, the ovalbumin will flow through while the remaining proteins bind to the resin. Figure 5.1 is an example chromatogram for this separation. The order of elution for the bound proteins will be ovotransferrin, myoglobin and lysozyme (Edwards-Parton et al., 2008).

In this work the separation was treated as comprising of a product peak of myoglobin within the group of eluting proteins. By designating the myoglobin as the product, this system can be used to mimic a separation where the product has both leading and trailing impurities. Absorbance spectra were used for monitoring the elution. The myoglobin absorbs at 408nm while the impurity proteins absorb at 280nm. As shown by the Beer-Lambert law, the UV absorbance of the eluent is directly proportional to the concentration of the proteins. Therefore, the product and impurity profiles can be rapidly determined by recording the UV absorption of the eluent at these wavelengths.

Chemicals: All chemicals were obtained from Sigma-Aldrich (Gillingham, Dorset, UK). The cation exchange chromatography experiments used S Hypercel resin (Pall Life Sciences, Portsmouth, UK) packed in 1 mL and 5 mL PRC prepacked columns (Pall Life Sciences, Portsmouth, UK) connected to an AKTA Avant 25 (GE Healthcare Life Sciences, Little Chalfont, Bucks, UK).

Feedstock: Egg white protein was obtained by manually separating egg whites from

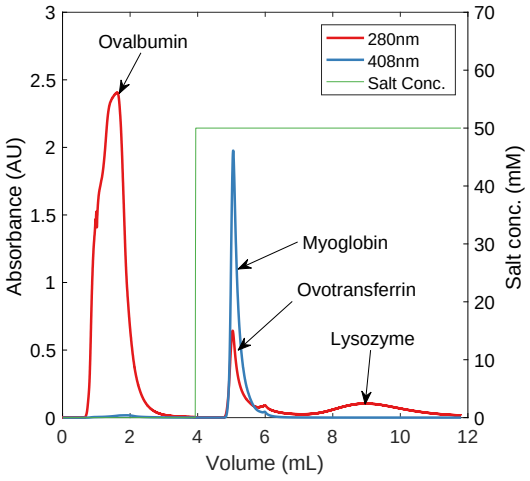

Figure 5.1: Chromatogram for the separation of the egg white proteins from myoglobin using cation exchange chromatography. The elution salt concentration was 0.05 M

egg yolks. To prepare the feedstock, 200 mL of egg whites were mixed with 800 mL of 20 mM sodium phosphate buffer. The mixture was then centrifuged at 10000 rpm for 30 min using a Beckman J2-MI (Beckman Coulter, High Wycombe, UK) to remove any solids. Myoglobin from horse heart was then dissolved in this solution to a final concentration of 0.5 mg/mL. The feedstock was adjusted to pH 5.5. The feedstock was serially vacuum filtered using 1.0m, 0.7m, 0.45m and 0.2m PVDF Durapore membrane filters (Millipore, Billerica, MA, USA) to remove any remaining solids. Before injecting samples of the feedstock into the chromatography column, the samples were filtered using 0.22m cellulose acetate Minisart syringe filters (Sartorius Stedim, Epsom, Surrey, UK) to remove aggregates that may have formed during storage.

Chromatographic separation: The equilibration buffer for these experiments was 20 mM sodium phosphate at pH 5.5. A stock elution buffer of 20 mM sodium phosphate, 2 M NaCl, pH 5.5 was used. The flow rate of the mobile phase was set to maintain a residence time of 2 min in the column. The chromatographic separations were carried out at 3 different scales using a 1 mL, a 5 mL and a 20 mL column. The dimensions of the three columns are detailed in Table 5.1.

Each experiment commenced with the injection of 1 column volume of the feed stock on to the column. After sample application, the column was washed to baseline with 3 column volumes of equilibration buffer. Isocratic elution was carried out with 8 column

volumes of the elution buffer. The salt concentration of the elution buffer was varied by changing the ratio between the equilibration buffer and the stock elution buffer to the column. Finally, the column was regenerated with 8 column volumes of 1 M NaOH and then re-equilibrated with 3 column volumes of the equilibration buffer in preparation for the next run.

At each scale a number of experiments were performed to explore the effect of elution salt concentration on the separation of myoglobin from the egg white proteins. The experimental design for this study is detailed in Table 5.2.

Parameter	Column 1	Column 2	Column 3
Column volume (mL)	0.98	5.03	20.11
Bed height (cm)	5	10	10
Diameter (cm)	0.5	0.8	1.6

Table 5.1: Column parameters for this study.

Elution salt conc. (M)	Column 1	Column 2	Column 3
0.05	X	X	X
0.10	X	X	
0.15	X	X	X
0.20	X	X	
0.25	X	X	X
0.30	X	X	
0.35	X	X	X
0.40	X	X	
0.45	X	X	X
0.50	X	X	
0.55	X	X	X
0.60	X	X	
0.65	X	X	X

Table 5.2: Experimental design for this study. An 'X' indicates an experiment that was performed.

5.2.2 Data processing

A chromatogram was produced from each experiment. As previously shown in Figure 5.1, each chromatogram consisted of the absorbance traces at both 280 nm and 408 nm. The 408 nm and 280 nm traces represented the elution profiles of the product and the impurities respectively.

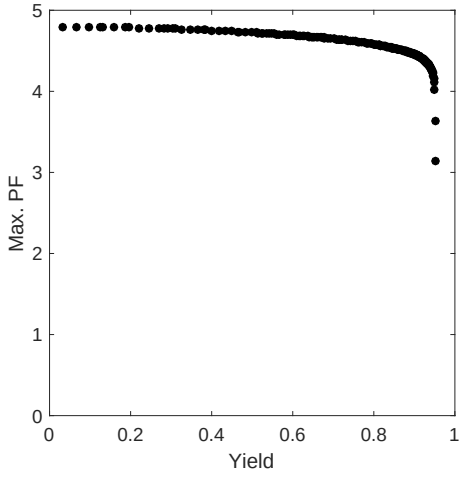

Figure 5.2: Max. purification factor vs. yield diagram for the separation of the egg white proteins from myoglobin using cation exchange chromatography. The elution salt concentration was 0.05 M

Maximum purification factor vs. yield (PFY) diagrams were calculated from the chromatograms to create a simple input dataset expressed in terms of the yield and purity of the separation. The PFY diagrams were calculated using the procedure detailed in Chapter 4. The PFY diagram that corresponds to the chromatogram in Figure 5.1 is shown in Figure 5.2.

After calculating a PFY diagram for each experiment, the dataset consisted of two input variables; the elution salt concentration and the yield, and one response variable; the max purification factor. This is illustrated in Figure 5.3 which shows the dataset for the 1 mL column.

However, to simplify the demonstration of the Kriging and Cokriging algorithms it was necessary to reduce the dataset to a single input variable and a single response variable. This was accomplished by determining the max. PF that corresponded to a yield of 0.9 for each run. The dataset then consisted of one input variable; elution salt concentration, and one response variable; the max. PF. This reduced dataset is shown in Figure 5.4

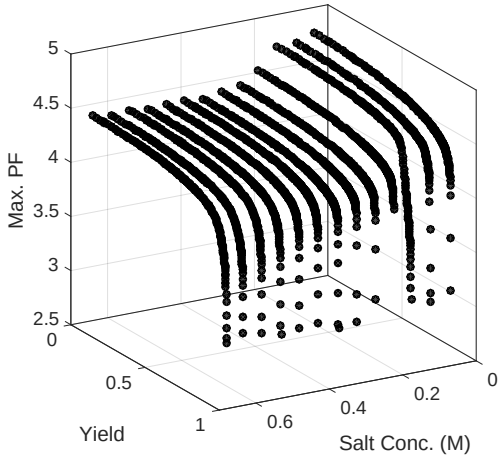

Figure 5.3: Overall input dataset from the experiment performed using the 1 mL column to investigate the effect of elution salt concentration on the separation of myoglobin from egg white proteins.

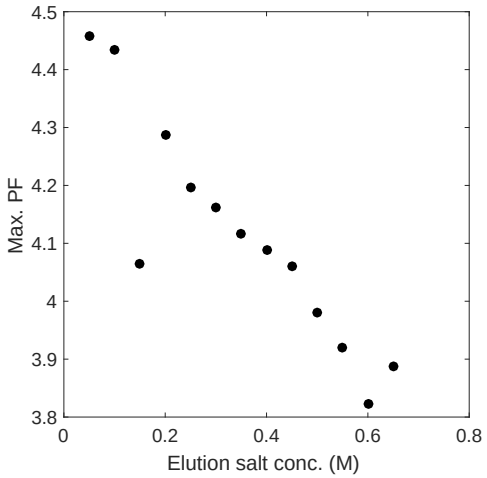

Figure 5.4: Reduced dataset for the 1 mL column consisting of the max. PF at a yield of 0.9 for each experiment.

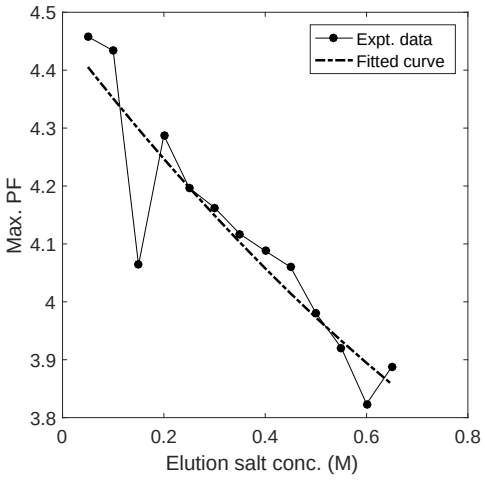

Figure 5.5: Dataset for the 1 mL column with a fitted quadratic polynomial.

5.3 Motivation for exploring alternative process characterisation approaches

Figure 5.5 shows the data from the 1 mL column. It can be seen that at an elution salt conc. of 0.15 M there is a sharp drop in the max. PF that can be achieved. Figure 5.6 shows that as the elution salt concentration increases, the resolution between the myoglobin and lysozyme peaks decreases. At 0.15 M the degree of overlapping between these two peaks means that a high purification factor cannot be achieved. Therefore the drop in max. PF at this elution salt concentation is a real behavior of the process and not an experimental artifact and therefore it is important to include this in any characterisation of the process.

As mentioned previously, a typical approach to characterising processes is to fit polynomial curves or surfaces to experimental data. To prevent overfitting these polynomials are rarely greater than second order. Figure 5.5 shows a quadratic polynomial fitted to the input dataset for the 1 mL column. This figure shows that the polynomial does not accurately model the changes in max. PF that occur at 0.15 M. As Kriging is a non-parametric technique it does not assume a form and maybe more suitable for characterising processes with complex design spaces.

Figure 5.7 shows the datasets that were calculated for each of the columns used in this study. These figures illustrate how the process variable (elution salt conc.) affects the

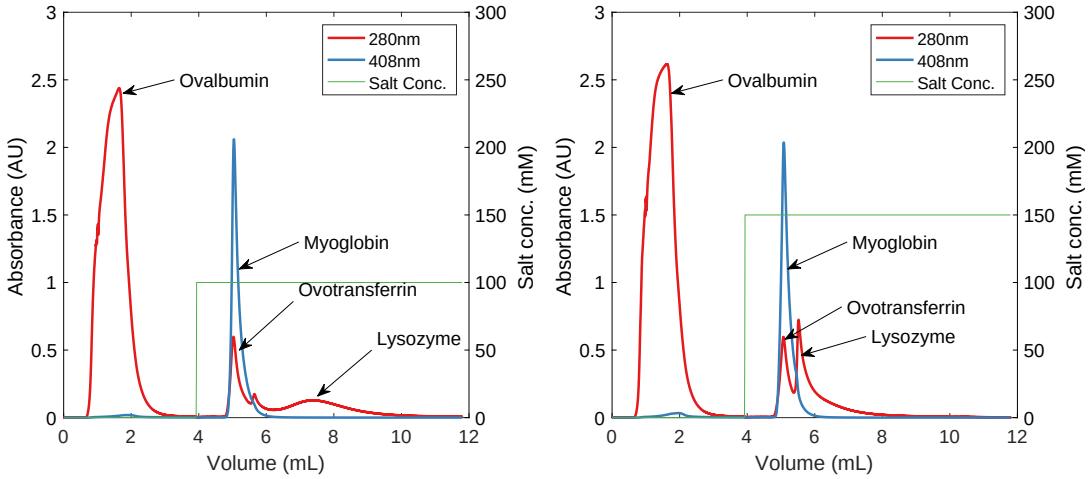

(a) 0.10 M **(b)** 0.15 M

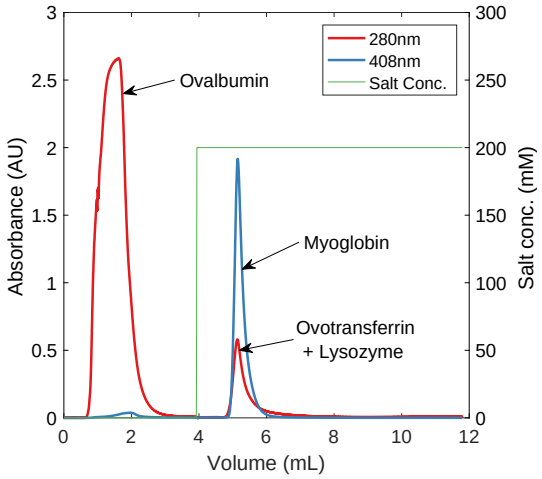

(c) 0.20 M

Figure 5.6: Chromatograms for elution salt concentrations of 0.10, 0.15 and 0.20 M showing the decrease in resolution between the product and impurity peaks.

performance of the column.

These figures show that there are changes in the performance between the differently scaled columns, despite each column having the same residence time and column load. These changes can be attributed to the different dimensions of the columns. The 1 mL column has a bed height of 5 cm while the 5 mL and 20 mL columns have bed heights of 10 cm. Differences between the performance of columns with different bed heights is usually expected. This is because chromatographic separations involve the following 4 modes of mass transfer.

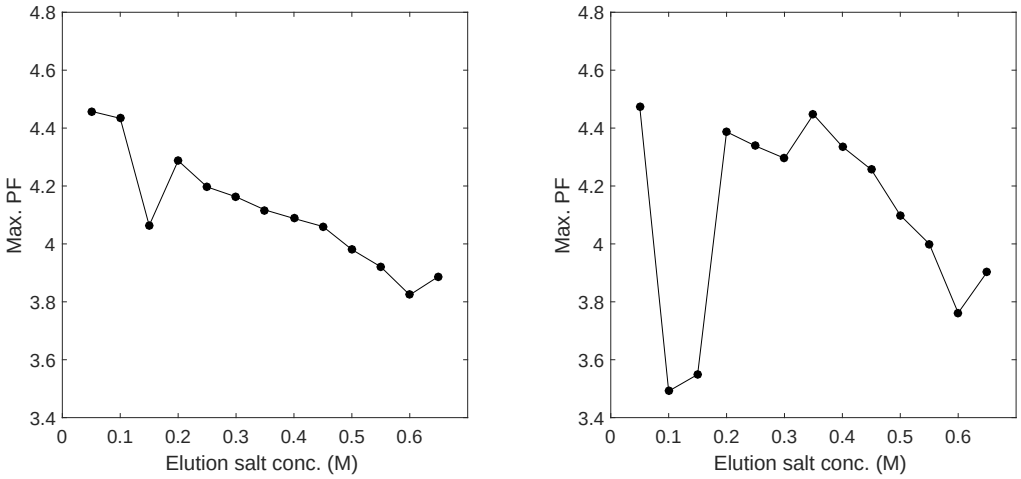

(a) 1 mL (h = 5 cm, d = 0.5 cm)

(b) 5 mL (h = 10 cm, d = 0.8 cm)

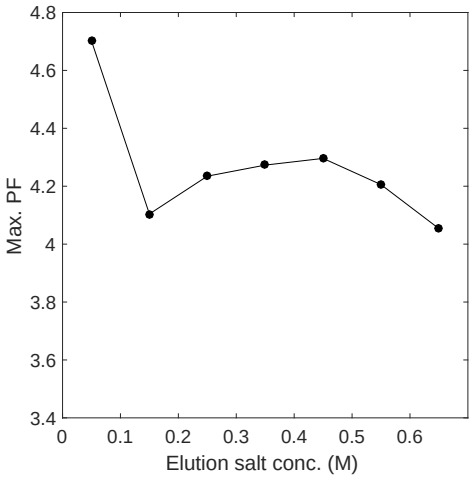

(c) 20 mL (h = 10, d = 1.6 cm)

Figure 5.7: Calculated reduced datasets for each of the columns used in this study.

1. Convection through the bulk phase of the column.

2. The diffusive mass transfer of the solutes in the film surrounding the beads.

3. Diffusion through the pores of the resin.

4. Adsorption/desorption on the surface of the resin.

If the second, third and fourth modes are relatively fast, the rate limiting mode of mass transfer will be the convection through the bulk phase of the column. For these separations, maintaining the residence time should be enough to maintain the performance

between columns of different bed heights. However, for processes such as that used in this study, this is not the case and the differences in the performance were observed.

In theory processes with the same bed height and column load should have the same performance regardless of column diameter. However, due to phenomena such as the wall effect the performance between columns of the same bed height can be different. The wall effect is the interaction between the wall of the column and the resin which helps support the packed bed. As the diameter of the column increases, the wall effect decreases, leading to an increase in the compression of the packed bed (Stickel and Fotopoulos, 2001). The increased compression changes the mass transfer of mobile phase which in turn leads to differences in the performance of the column. Such differences can be seen in Figure 5.7 between the 5 mL column and the 20 mL column that have the same bed height.

The differences seen between the three columns highlight the importance of developing and characterising a process at a representative scale. However, conducting experiments at a representative scale can be expensive due to the large amount of feed material that would be required. Figure 5.7 shows that while there may be differences in the absolute performance of the different columns, the overall trends are similar. Therefore, there is a the potential to reduce the burden of developing and characterising processes by combining expensive larger scale experimental data with cheap small scale experimental data. A technique that has the potential to do this is Cokriging.

5.4 Kriging

Kriging is a non-parametric approach that predicts the value of a response at an unknown point as the weighted sum of the values of the surrounding known points. Kriging assigns weights to the known points based on each point's proximity to the unknown point. Additionally, the weights are reduced for instances where the known points are clustered together, preventing any bias in the predictions. Therefore this approach can be applied to situations where the available data is irregularly distributed. Such a situation may arise during process development as the initial experiments are spread throughout the design space and later experiments focus on the intended oper-

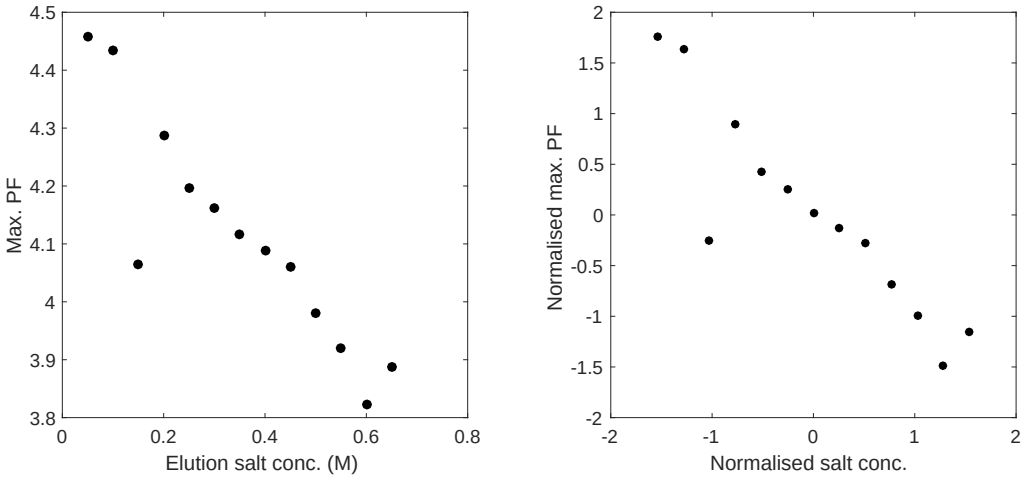

(a) **(b)**

Figure 5.8: Reduced dataset for the 1 mL column consisting of the max. PF at a yield of 0.9 for each experiment. 5.8a shows the original data and 5.8b shows the standardised data.

ating window or process optimum.

The procedure for producing a Kriging prediction involves the following steps (Matheron, 1963).

1. Prepare data for Kriging
2. Calculate the variogram - the variogram describes the variability between points in the input data set.
3. Fit the variogram model
4. Calculate the covariance model
5. Use the covariance model to calculate weights for the available data
6. Use the weights to calculate Kriging prediction

In this section the Kriging algorithm was demonstrated using the reduced dataset that was calculated for the 1 mL column.

5.4.1 Prepare the data

The input data used to demonstrate Kriging is shown in Figure 5.8a. This consists of one input variable (elution salt conc.) and one response variable (max. PF). Kriging assumes that the response variable data is normally distributed with mean zero. To satisfy this assumption the max. PF data was standardised by subtracting the mean and dividing by the standard deviation. Often a process development dataset will consist of more than one input variable and these variables will have different scales, e.g. elution salt concentration and elution pH. As Kriging relies on the distance between data points to predict new data, the input variables are also standardised to prevent any bias towards certain variables. The standardised data is shown in Figure 5.8b.

5.4.2 Calculating the variogram

The first step in the Kriging algorithm is the calculation of the experimental variogram from the input dataset. The variogram describes the spatial correlation between points in the design space. The input dataset consists of $i = 1,2,3,\cdots N$ points where each point is in an n-dimensional space where each dimension is a process variable. The output $f(x)_i$ is the response of the process at that point in the design space. The variogram plots γ against d for each pair of points in the available input dataset. For each pair of points, d is the separation distance as defined in Equation 5.1 and γ is defined in Equation 5.2.

$$h_{i,j} = \sqrt{(x_{i,1} - x_{j,1})^2 + (x_{i,2} - x_{j,2})^2 + \cdots + (x_{i,n} - x_{j,n})^2} \tag{5.1}$$

where $x_{i,n}$ and $x_{j,n}$ are the values of points i and j in the n dimension or process variable.

$$\gamma_{i,j} = \frac{1}{2}\left(f(x_i) - f(x_j)\right)^2 \tag{5.2}$$

where $f(x_i)$ and $f(x_j)$ are the values of the response at points i and j.

As Figure 5.9a shows for the dataset used in this study, raw variogram plots tend to be a rough scatter of points and may not immediately indicate a significant trend. In

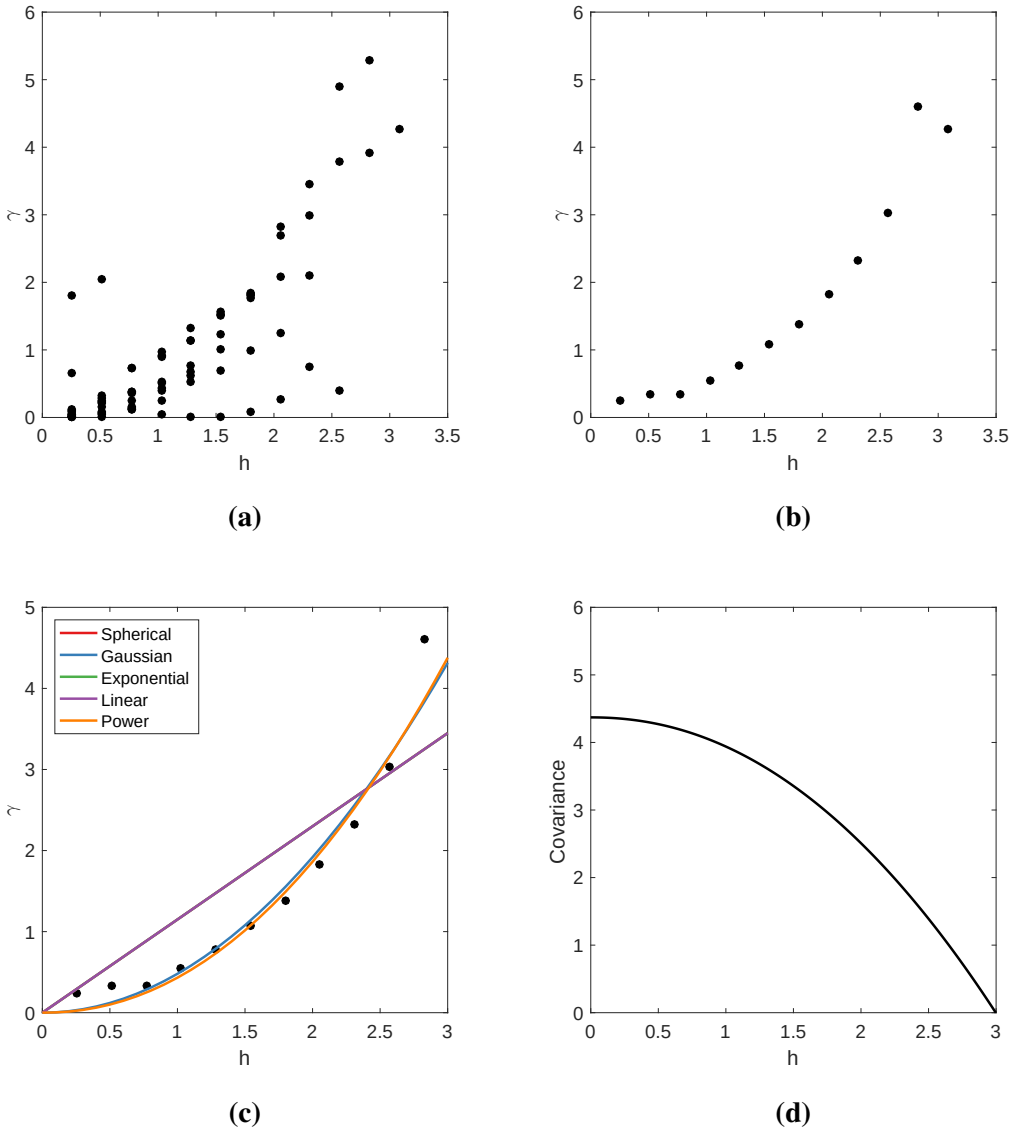

Figure 5.9: The procedure for determining the covariance model used in the Kriging algorithm. 5.9a shows the raw variogram calculated for the dataset shown in Figure 5.4. The raw variogram is then binned by averaging points which have a similar separation distance as shown in 5.9b. As shown in 5.9c a variogram model can then be fitted to the binned variogram data which can be used to predict the variance between points in the design space. In this case the power variogram model provides a good fit. The covariance model shown in 5.9d was calculated from the variogram model which in turn was used to calculate Kriging weights.

order to discern a trend, the variogram points with approximately the same separation distance are averaged to produce a single value as shown in Figure 5.9b. As the data in the input dataset was spaced at regular intervals, the raw variogram was also spaced at regular intervals. Therefore the raw variogram was easily binned into points with the same separation distance. However, for datasets where the data is irregularly spaced, it may be necessary to select an appropriate number of bins through trial and error.

There are a number of variogram models in the form of $\gamma = f(h)$ which can be fitted to the binned variogram data. Some popular variogram models are listed below.

Spherical model

$$\gamma = a\left(1.5\frac{h}{h_{max}} - 0.5\left(\frac{h}{h_{max}}\right)^3\right) \tag{5.3}$$

Gaussian model

$$\gamma = a\left(1 - exp\left(-3\frac{h^2}{h_{max}^2}\right)\right) \tag{5.4}$$

Exponential model

$$\gamma = a\left(1 - exp\left(-3\frac{h}{h_{max}}\right)\right) \tag{5.5}$$

Linear model

$$\gamma = ah \tag{5.6}$$

Power model

$$\gamma = ah^b \tag{5.7}$$

If required an additional term can be added to the variogram model to represent noise or experimental error but this was not applied to this study.

These variogram models can be classified into two types; transition models and non-transition models. As shown in Figure 5.10a, transition models are those where the variogram reaches a plateau. This plateau is also known as the sill and is represented in the variogram models by a. The value of the sill is used as an estimate of the maximum variance between points in the design space. The separation distance at which the sill is reached is represented in the variogram models by h_{max}.

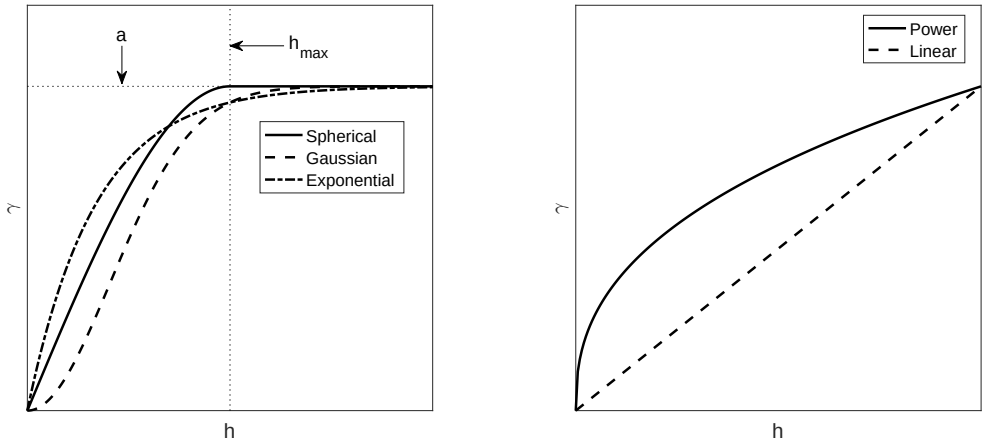

(a) Transition models **(b)** Non-transition models

Figure 5.10: Popular variogram models used for describing the variance between points in a design space. 5.10a shows the spherical, gaussian and exponential transition models and 5.10b shows the linear and power non-transition models.

Figure 5.9c shows these models fitted to the binned variogram calculated in this study. Since the binned variogram does not reach a sill it would be inappropriate to fit a transition model to this data. This is because the fitted model will produce an estimate of the sill which cannot be supported by the available data. The power model had a good fit to the data and was selected as the variogram model. Equation 5.8 is the fitted power variogram model.

$$\gamma = 0.4318h^{2.108} \tag{5.8}$$

5.4.3 Calculating the covariance model

The covariance model for the design space is required to determine the Kriging weights. This is calculated from the variogram model using Equation 5.9.

$$Cov(h) = \sigma^2_{max} - \gamma(h) \tag{5.9}$$

where $Cov(h)$ is the covariance between two points separated by distance h. In this equation $\gamma(h)$ is the previously determined variogram model. σ^2_{max} is the maximum

variance which is estimated from variogram.

As mentioned above in Section 5.4.2, variograms often reach a plateau known as the sill and the value of the sill is the maximum variance in the design space. For variograms that do not have a sill, σ^2_{max} can be estimated as 0.95 times the maximum of the variogram. The variogram calculated for the dataset used in this study did not have a sill and this approach was used to determine the covariance function which is shown in Equation 5.10.

$$Cov(h) = 4.371 - 0.4318h^{2.108} \tag{5.10}$$

5.4.4 Calculating the Kriging prediction

The Kriging prediction of an unknown point is calculated from the weighted sum of the available data. The weights are calculated by solving the relationship in Equation 5.11.

$$Cw = D \tag{5.11}$$

where C is a matrix containing the values of the covariance between each pair of known points in the design space, w is the vector of weights for each of the known points and D is the vector containing the values of the covariance between each known point and the unknown point. Equation 5.11 in its expanded form is shown below in Equation 5.12 where there are N known points and x_k is the unknown point. The previously determined covariance function in Equation 5.10 is used to calculate the required covariance values.

$$\begin{pmatrix} Cov(h_{1,1}) & \cdots & Cov(h_{1,N}) & 1 \\ \vdots & \ddots & \vdots & \vdots \\ Cov(h_{N,1}) & \cdots & Cov(h_{N,N}) & 1 \\ 1 & \cdots & 1 & 0 \end{pmatrix} \times \begin{pmatrix} w_1 \\ \vdots \\ w_N \\ \lambda_k \end{pmatrix} = \begin{pmatrix} Cov(h_{1,k}) \\ \vdots \\ Cov(h_{N,k}) \\ 1 \end{pmatrix} \tag{5.12}$$

where $h_{i,j}$ is the distance between known points x_i and x_j, $h_{i,k}$ is the distance between x_i and unknown point x_k, and w_i is the weight assigned to x_i. λ_k is a parameter used to

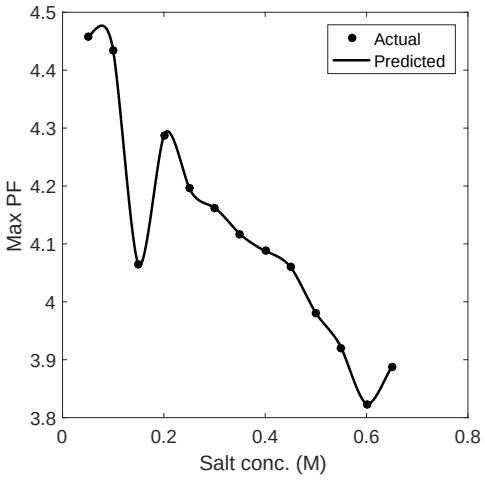

Figure 5.11: Kriging prediction for the 1 mL column

estimate the variance of the Kriging prediction.

Having calculated the weights, the output at the unknown point is calculated as the sum of the weighted known points as shown in the Equation 5.13.

$$\bar{f}(x_k) = \sum_{i=1}^{N} w_i f(x_i) \tag{5.13}$$

Finally, as the predictions were produced from standardised input data, the predicted values are converted back to the original scale.

The Kriging predictions were produced using scripts in MATLAB (The MathWorks Inc., Natick, MA, USA) (see Appendix A).

5.4.5 Kriging results

Figure 5.11 shows the calculated Kriging prediction for the 1 mL column. In contrast to the fitted polynomial shown previously in Figure 5.5, Kriging produces a prediction that accurately describes the effect of the elution salt concentration on the max. PF.

5.5 Cokriging

Cokriging is derived from the Kriging algorithm described above in Section 5.4. Cokriging is also a non-parametric approach that does not require the direct fitting of mod-

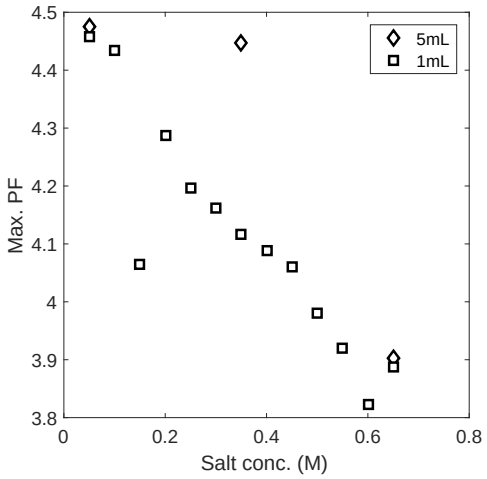

Figure 5.12: Input data for cokriging. The dataset consists of the corner and centre points from the 5 mL column and all the points from the 1 mL column.

els to the input data. However, where Kriging interpolates between values of a single response to predict the value of that response at unknown points, Cokriging is able to use secondary responses that are correlated to the primary response in order to produce predictions of the primary response. This approach is useful in situations where the determination of the primary response is experimentally expensive but determining a secondary response is relatively cheap. In this study the max. PF of the 5 mL column was treated as the primary response while the max. PF of the 1 mL column was treated as the secondary response. As both the bed height and column diameter of the 1 mL column are different those of the 5 mL, it would not normally be possible to use the 1 mL data to characterise the 5 mL column.

The input dataset to demonstrate the Cokriging algorithm consisted of only the two corner data points and the centre data point from the 5 mL column and all data points from the 1 mL column. This mimics the situation where a scale down model of a process is used to characterise a large scale process. The input dataset is illustrated in Figure 5.12.

The Cokriging algorithm follows the same basic procedure as Kriging. However, where Kriging used a single covariance function, Cokriging uses multiple covariance functions. These are used to estimate the covariance between primary data points, secondary data points, and between primary and secondary data points.

5.5.1 Prepare the data

The max. PF response data from each scale was standardised by subtracting the mean and dividing by the standard deviation.

5.5.2 Calculating the primary, secondary and cross variograms

The first step of the Cokriging algorithm was to establish the spatial relationship between the input data. As in the Kriging approach described above in Section 5.4, Equations 5.14 and 5.15 were used to calculate the raw variogram data for the primary response. Additionally Equation 5.16 was used to calculate the raw variogram data for the secondary response. These calculated variograms describe the spatial relationships within each response.

$$h_{i,j} = \sqrt{(x_{i,1} - x_{j,1})^2 + (x_{i,2} - x_{j,2})^2 + \cdots + (x_{i,n} - x_{j,n})^2} \tag{5.14}$$

where $x_{i,n}$ and $x_{j,n}$ are the values of points i and j in the n dimension or process variable.

$$\gamma_{v(i,j)} = \frac{1}{2}\left(v_i - v_j\right)^2 \tag{5.15}$$

where v_i and v_j are the values of the primary response at points i and j.

$$\gamma_{u(i,j)} = \frac{1}{2}\left(u_i - u_j\right)^2 \tag{5.16}$$

where u_i and u_j are the values of the primary response at points i and j.

Equation 5.17 is then used to calculate the cross variogram which describes the relationship between the primary and the secondary responses.

$$\gamma_{uv(i,j)} = \frac{1}{2}\left(v_i - u_j\right)^2 \tag{5.17}$$

As in Kriging, all three variograms were binned and power variogram models were fitted to the binned variograms as shown in Figure 5.13.

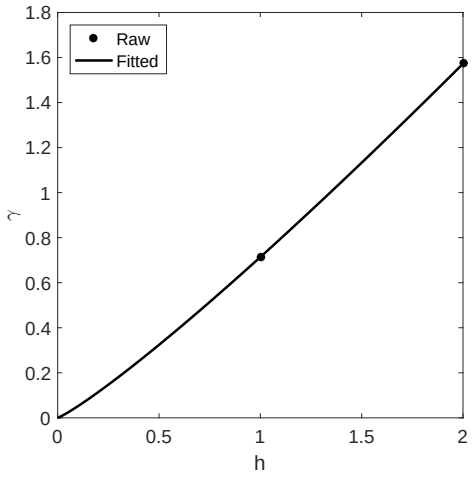

(a) Primary variogram

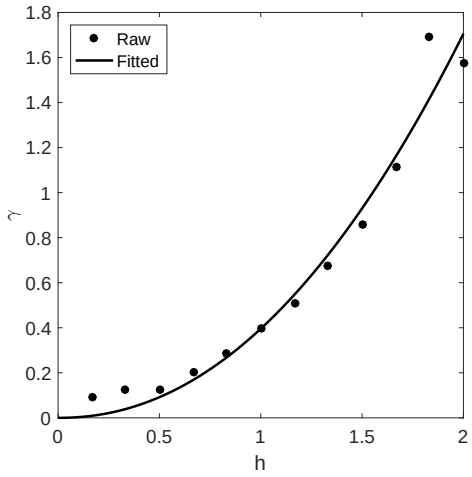

(b) Secondary variogram

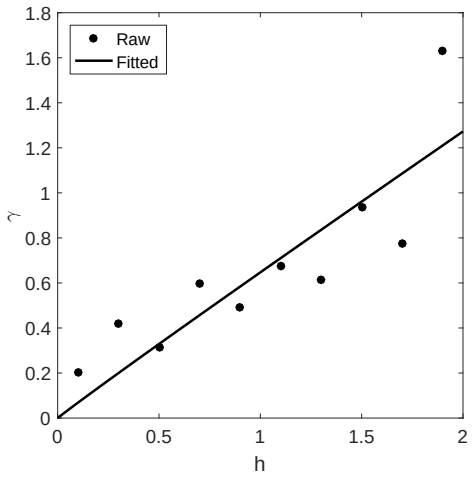

(c) Cross variogram

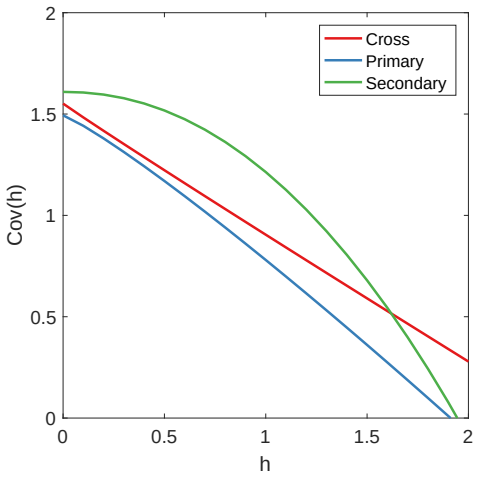

(d) Covariance models

Figure 5.13: Variograms and covariance models for the Cokriging algorithm. 5.13a, 5.13a, and 5.13a show the binned variograms for the Cokriging algorithm and 5.13d shows the covariance models that were calculated from the fitted variogram models.

5.5.3 Calculating the covariance models

The covariance models are required to calculate the weights which in turn are used to calculate the Cokriging predictions. The covariance models are calculated from the variogram models using Equation 5.9 that was used in the Kriging algorithm. The resulting primary, secondary and cross covariance models are shown in Equations 5.18, 5.19 and 5.20 and in Figure 5.13d.

$$Cov_v(h) = 1.494 - 0.7138h^{1.139} \tag{5.18}$$

$$Cov_u(h) = 1.609 - 0.3956h^{2.108} \tag{5.19}$$

$$Cov_{uv}(h) = 1.5516 - 0.6469h^{0.9764} \tag{5.20}$$

5.5.4 Calculating the Cokriging predictions

The covariance function was then used to create the system of equations used to calculate the Cokriging predictions. This system of equations is shown in Equation 5.21.

$$\begin{pmatrix} Cov(v_1,v_1) & \cdots & Cov(v_1,v_m) & Cov(v_1,u_1) & \cdots & Cov(v_1,u_n) & 1 \\ \vdots & \ddots & \vdots & \vdots & \ddots & \vdots & 1 \\ Cov(v_m,v_1) & \cdots & Cov(v_m,v_m) & Cov(v_m,u_1) & \cdots & Cov(v_m,u_n) & 1 \\ Cov(u_1,v_1) & \cdots & Cov(u_1,v_m) & Cov(u_1,u_1) & \cdots & Cov(u_1,u_n) & 1 \\ \vdots & \ddots & \vdots & \vdots & \ddots & \vdots & 1 \\ Cov(u_n,v_1) & \cdots & Cov(u_n,v_m) & Cov(u_n,u_1) & \cdots & Cov(u_n,u_n) & 1 \\ 1 & 1 & 1 & 1 & 1 & 1 & 0 \end{pmatrix} \times \begin{pmatrix} w_{v_1} \\ \vdots \\ w_{v_m} \\ w_{u_1} \\ \vdots \\ w_{u_n} \\ \lambda \end{pmatrix}$$

$$= \begin{pmatrix} Cov(v_1,v_0) \\ \vdots \\ Cov(v_m,v_0) \\ Cov(u_1,v_0) \\ \vdots \\ Cov(u_n,v_0) \\ 1 \end{pmatrix} \tag{5.21}$$

where v_i are the the primary data points, u_j are the secondary data points, and v_0 is the point to be predicted. m is the number of primary data points and n is the number of secondary data points. $Cov(x_1,x_2)$ is the covariance between points x_1 and x_2 and is determined using the covariance models determined from the input data. By solving the system of equations in Equation 5.21 the Cokriging weights w can be determined.

The Cokriging prediction is then produced using the weighted sum of the input data as shown in Equation 5.22.

$$v_0 = \sum_{i=1}^{m} w_i v_i + \sum_{j=1}^{n} w_j u_j \tag{5.22}$$

As the predictions were produced standardised data, the predictions were converted back to the original scale. The Cokriging predictions were produced using scripts in MATLAB (The MathWorks Inc., Natick, MA, USA) (see Appendix A).

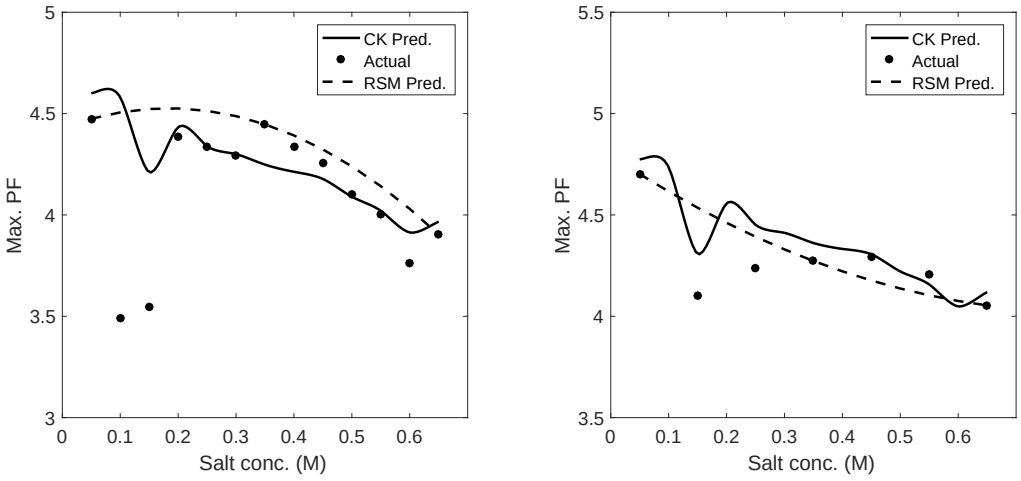

(a) 5 mL **(b)** 10 mL

Figure 5.14: Cokriging predictions for 5.14a the 5 mL column and 5.14a the 10 mL column. Also shown are the quadratic polynomials that were fitted to the 3 available large scale data points.

5.5.5 Cokriging results

Figure 5.14a shows the Cokriging prediction that was calculated for the 5 mL from the previously detailed input data set. A prediction was also calculated for the 10 mL column in a similar manner as shown in Figure 5.14b. These figures also show a quadratic polynomial that was fitted to the large scale data that was made available in this example (2 corners and centre point).

These results show that while the Cokriging predictions are not a perfect fit, when compared to the fitted quadratic polynomial, these better track the actual trend. The Cokriging predictions can then be used to understand the effect of the process variables on the response and guide further experimentation.

5.6 Conclusion

In this chapter Kriging and Cokriging were explored as possible techniques for characterising chromatographic separations. These techniques were tested using simple chromatographic datasets where the process variable had a non-linear relationship with the process response.

It was shown that Kriging could be used as an alternative to response surface method-

ology (RSM) for characterising chromatographic separations, and it better represented the non-linear relationship between the process variable and the response. However, in processes without such non-linear relationships, the use of RSM will provide an accurate model with less modelling effort.

It was also demonstrated that Cokriging could be used to produce characterisations of the experimental space using a limited amount of large scale data augmented with non-representative but cheap scale-down data. While these characterisations were not completely accurate, they provided a better understanding of the effects of the process variable on the response when compared to response surface methodology using large scale data alone. The cokriging predictions could then be used to guide further large scale experimentation in order to characterise any significant non-linear effects.

Chapter 6

A comparison of modelling approaches for producing accurate process models from high throughput experiments which have high variability

6.1 Introduction

In this chapter three modelling approaches were compared for producing process models from the results of high throughput experimentation. High throughput experiments are often subject to relatively high levels of variability which can affect the accuracy of any subsequent modelling attempts. The three modelling approaches were tested to identify which method would be the least affected by such variability.

The exploration and characterisation of the experimental space is a critical part of developing a purification process for a biopharmaceutical product. Through the greater understanding of the experimental space of the process that this delivers, it is possible to design and optimise processes that are robust and less likely to fail. The quality-by-design (QbD) initiative has placed extra emphasis on developing greater process understanding as a route to easing the regulatory approvals process.

In Chapter 3 it was concluded that, despite alternatives such as the use of mechanistic models having certain advantages, the most suitable approach to process development

was to perform physical experiments across the experimental space. The results of these experiments would provide an understanding of how the process parameters affect performance. As these experiments can be expensive and time consuming, scale-down experimental approaches are often used to reduce the burden of this work.

Unfortunately all physical experiments are susceptible to various sources of variability. Due to the very small volumes involved, scale-down methods can be particularly susceptible. As an example, consider a miniature column (such as a Robocolumn) with a column volume of 0.2 mL (bed height = 1 cm, diameter = 0.5 cm) used to develop a cation exchange polishing step. To load the column to a capacity of 40 g/L with post-Protein A material at a concentration of 10 g/L would require an injection volume of 0.785 mL. However, even a deviation as small as 100 µ/L will cause a significant change, in essence equivalent to 5 g/L in the column loading (>10 % difference).

Another source of variability can be the analytical techniques that are used to analyse the samples from the scale down experiments. The use of the scale down methods means that the experiments can be carried out in a high throughput manner which shifts the development bottleneck onto sample analysis. To alleviate this bottleneck it is necessary to use analytical techniques which are fast but may compromise on accuracy and sensitivity (Bensch et al., 2005; Noyes et al., 2014).

While every attempt is made to mitigate the effects of variability during the execution of these experiments, it is important that the techniques used to model the process are capable of reducing the effects of the variability to model accurately the actual underlying process. Response surface methodology (RSM) is the industry-standard regression technique used for producing process models from experimental data. In this study the accuracy of RSM when presented with noisy experimental data was compared with two other modelling techniques, Kriging and partial least squares regression (PLSR). PLSR is similar to principal component analysis and builds models by creating new variables that explain the variance in the response. By careful selection of the new variables or components, a model can be created that does not include the experimental variability. Kriging was selected for this study because it is a non-parametric method and therefore has the potential to better approximate the relationships in the experimental space without relying on fixed models.

These modelling approaches were tested using Monte Carlo simulations. A simulated chromatography process was used in this study as this provided the means to rapidly generate large amounts of data and control the levels of variability in the data. Two types of variability were introduced into the data; experimental error in an assay, and process variability due to deviations from the setpoints of the process parameters. Monte Carlo simulations were carried out using this simulated test bed and the final cumulative results provided a means of comparing the three modelling techniques.

6.2 Materials and methods

6.2.1 Computer simulations

To produce the data for this study it was necessary to perform a large number of experiments with control over the amount of variability in the experimental results. Therefore, it was decided to use a simulated process as this would satisfy both of these requirements. The general rate chromatography model described in Chapter 3 was modified to produce data for this study.

The modelled system consisted of three hypothetical proteins, A, B, and C, which were separated on an ion exchange chromatography column. For the purposes of this study protein B was considered the product while proteins A and C were the leading and trailing impurities respectively. The hypothetical proteins were created to provide a simulated system with certain characteristics that are usually seen in process separations. These characteristics were as follows:

- The product would have trailing and leading impurites, i.e. impurities that eluted before and after the product - Most chromatographic separations involve purifying the product from multiple impurities.
- The peaks of the product and the impurities would not be well-resolved from one another providing a challenge to the purification of the product - In many process separations there is poor resolution between the product and impurity peaks because the major impurities are product-related impurities such as aggregates and fragments/truncates which have similar properties to the product.

Table 6.1: Modulator parameters of the simulated chromatographic system

Component	α	β	γ
A	-3.6	2.6	0.064
B	-2.9	3	0.064
C	-2.6	3.2	0.064

Table 6.2: Parameters for the modelled chromatography column

Bed height (cm)	L	20
Particle diameter (µm)	d_p	50
Resin saturation capacity (g/L)	C^{∞}	10
Bed voidage	ε_b	0.6
Particle voidage	ε_p	0.35

- The peaks would have sharp leading fronts - In preparative chromatography the column will usually be loaded to a high level to maximise the utilisation of the column. This leads to binding in the non-linear region of the adsorption isotherm which in turn can result in peaks with sharp fronts. Additionally, many process separations employ elution steps instead of gradients to improve the robustness of the process. These elution steps can also result in peaks with sharp leading fronts.

Three hypothetical proteins which exhibited these characteristics were created by adjusting the parameter values used in the modulator relationship by trial and error. The modulator parameter values and the parameters for the modelled chromatography column are shown in Table 6.1 and Table 6.2 respectively.

Figure 6.1 shows a chromatogram for the simulated system displaying the required poorly resolved peaks and sharp leading fronts.

Each simulation began with a column that had been equilibrated to the pH and ionic strength of the feedstock. The feedstock was then injected onto the column followed by the elution phase of the process which was a stepped elution. The elution buffer was the equilibration buffer with added salt to displace and elute the bound protein.

The simulations were performed using COMSOL Multiphysics 5.1 (COMSOL Ltd., Cambridge, UK). The finite element method was used to discretise the differential

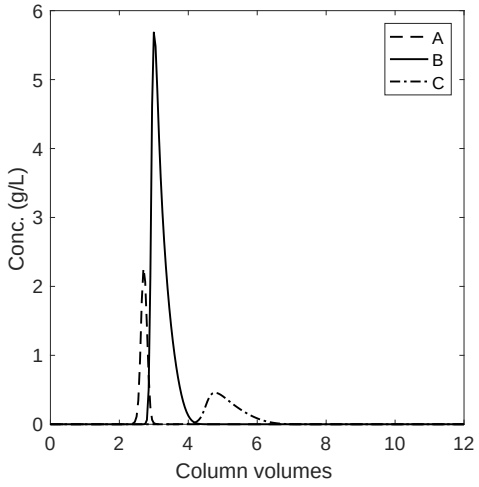

Figure 6.1: Chromatogram for the simulated system at the centre of its experimental space.

equation with 100 axial elements and 5 radial elements being used. The time step used in each simulation was equivalent to the elution of 0.05 column volumes.

6.2.2 Experimental design

Even though a chromatography process can have up to as many as 100 - 200 process variables (Rathore, 2009), process development activities will focus on a few critical variables due to the limitations on the number of experiments that can be performed. A theoretical understanding of the process and prior experience is usually the basis for the selection of the variables. In this study four critical process parameters were identified; the flow rate, the injection volume, the salt concentration of the equilibration buffer, and the salt concentration of the elution buffer. The reasons for their selection are detailed in Table 6.3.

A central circumferential design was used to characterise the effects of these parameters on the performance of the column. This experimental design was chosen as it provides a comprehensive exploration of the design space and allows the fitting of response surfaces up to and including quadratic effects. Figure 6.2 shows an example of such a design for two factors. The central circumferential design consists of a full factorial design with added 'star' points. A full factorial design includes runs at all possible high and low combinations of all the factors. A full factorial design enables the fitting of a response surface consisting of the linear effects and the interactions. By adding

Table 6.3: Process variables that were selected for investigation and the reasons for their selection.

Variable	Reason
Flow rate	The flow rate affects the residence time of the material in column and will therefore affect the binding capacity.
Injection volume	The injection volume dictates the amount of material that is loaded onto the column and if the binding capacity is exceeded the process yield will be less. At a lower loading there will be a greater number of free binding sites and therefore a higher degree of resolution between the product and the impurities can be expected.
Equilibration salt concentration	This is the salt concentration during equilibration and loading of the column. The salt will compete with the product and the impurities for the binding sites on the stationary phase. This salt concentration can be controlled to prevent the leading impurity from binding to the column, improving the purity of the product. However, if the salt concentration is too high it can inhibit or even prevent the product binding leading to a lower binding capacity
Elution salt concentration	This is the salt concentration during the elution of the column. The salt will compete with the product and the impurities for the binding sites on the stationary phase. If the concentration is too low the product will not elute and the yield will be poor. If the concentration is too high the trailing (strongly bound) impurity will elute with the product affecting the purity.

the star points, which are located at the extremes of each factor, it is possible to also fit quadratic effects and model any curvature in the response. Table 6.4 details the central composite circumferential design that was used.

6.2.3 Data processing

The output from each of the simulated experiments was a chromatogram tracing the elution of each protein from the column. As discussed in Chapter 4, the performance of the process cannot be quantified directly from the chromatogram. Therefore a maximum purification factor vs. yield (PFY) diagram was calculated for each experiment. This diagram illustrates the performance of each run in terms of its yield and purity.

The first data processing step was to calculate chromatograms with a realistic level of resolution. As the experiments were simulated, the chromatograms had a high resolution with only 0.05 column volumes (CV) between each pair of datapoints. However, to prevent creating a analytical bottleneck, physical experiments are normally frac-

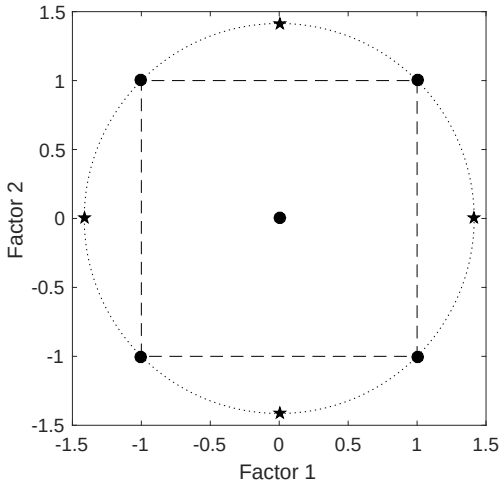

Figure 6.2: Example of a central circumferential experimental design for two factors. The '•' show the experiments that would be included in a full factorial design and the '⋆' show the additional points which enable the fitting of quadratic effects.

tionated into relatively large fractions, e.g. 0.25 - 2 CV. To mimic this approach the chromatograms were 'fractionated' by averaging the concentration of each component in intervals of 0.25 CV as shown in Figure 6.3a.

PFY diagrams were then calculated for each chromatogram using the procedure detailed in Chapter 4 as shown in Figure 6.3. In this study the maximum purification factors were converted into maximum purities by multiplying by the original purity of the feed.

In addition to illustrating the trade off between the purity and the yield, the PFY diagrams can be used to determine the purity for a target yield. A target yield may be set to ensure that the economics of the process are viable. In this study the target yield was set at 0.9 and the maximum purity that could be achieved while satisfying this condition was determined for each experiment. This has the added advantage of reducing each experiment's response from a complex chromatogram to a single value that represents the feasibility of operating the process at that point in the design space. This calculated value served as the primary response of the experiments carried out in this study. The input dataset for this study was made up of the experimental design and the corresponding values of the max. purity.

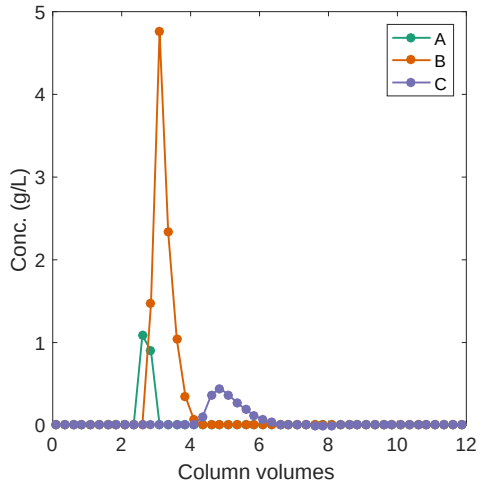

(a) Chromatogram

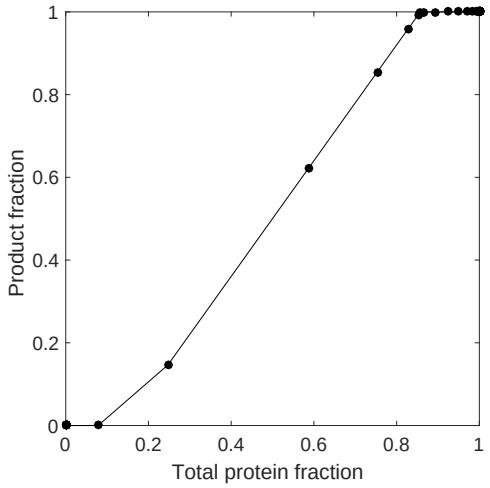

(b) Fractionation diagram

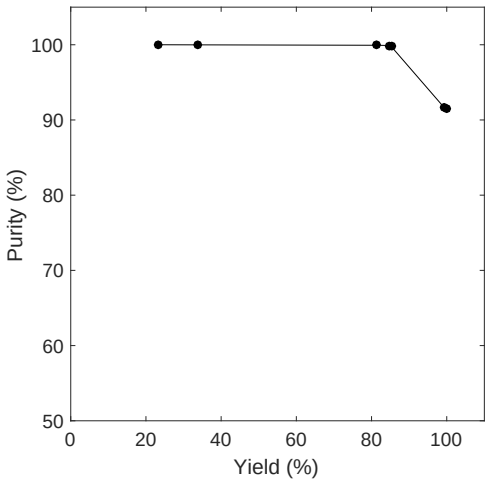

(c) Max. purity vs. yield diagram

Figure 6.3: The fractionated chromatogram and corresponding fractionation diagram and max. purity vs. yield diagram for the centre point of the DOE for the simulated chromatographic process used in this study.

Table 6.4: Experimental design used to characterise the purification process used in this study

Run	Velocity (cm/hr)	Injection volume (CV)	Equilibration salt conc. (mM)	Elution salt conc. (mM)
1	225	0.45	90	190
2	225	0.45	90	210
3	225	0.45	110	190
4	225	0.45	110	210
5	225	0.55	90	190
6	225	0.55	90	210
7	225	0.55	110	190
8	225	0.55	110	210
9	275	0.45	90	190
10	275	0.45	90	210
11	275	0.45	110	190
12	275	0.45	110	210
13	275	0.55	90	190
14	275	0.55	90	210
15	275	0.55	110	190
16	275	0.55	110	210
17	200	0.50	100	200
18	300	0.50	100	200
19	250	0.40	100	200
20	250	0.60	100	200
21	250	0.50	80	200
22	250	0.50	120	200
23	250	0.50	100	180
24	250	0.50	100	220
25	250	0.50	100	200

6.2.4 Model validation dataset

To create a dataset for validating the process models, an additional 100 experiments were simulated at random points throughout the experimental space of the process. The ranges for these experiments are shown in Tabel 6.5 and match the ranges in the experimental design for this study. The chromatograms from each of these runs were also processed in the manner described above to calculate the value of the response for each of these experiments. This dataset was then used to validate the models that were produced during the Monte Carlo simulations.

Table 6.5: Variable ranges that were used to produce the validation dataset

Variable	Range
Velocity (cm/hr)	225 – 275
Injection volume (CV)	0.45 – 0.55
Equilibration salt conc. (mM)	0.09 – 0.11
Elution salt conc. (mM)	0.19 – 0.21

6.2.5 Modelling techniques

In this study three modelling techniques were used to build process models relating the performance of the process (max. purity for a min. yield of 90%) to the 4 process variables. The standard technique used for these applications is response surface methodology and this was compared against Kriging and partial least squares regression.

6.2.5.1 Response surface methodology

Response surface methodology (RSM) involves fitting a response surface function to the data produced from the characterisation experiments. It is widely accepted that for most processes a quadratic function is capable of accounting for the main effects (with curvature) and any interactions between the variables.

The identification of significant effects is an important step in building an accurate response surface model. For a experimental design such as the one used in this study, a full quadratic response surface model can be fitted to the response data. However, the resulting model may be overfitted and produce an unnecessarily complicated model. By identifying the siginificant effects in the dataset a more representative model can be created. The significant effects can be identified manually using tools such as the half normal plot or using automated routines such as stepwise regression. In this study the *stepwiselm* function in MATLAB was used to carry out stepwise regression to identify the best model.

In this study the stepwise regression routine started with a regression model including all 4 linear terms, all 6 interactions terms and all 4 quadratic terms as shown in Equation 6.1.

$$\begin{aligned} y \sim & 1 + x_1 + x_2 + x_3 + x_4 \\ & + x_1x_2 + x_1x_3 + x_1x_4 + x_2x_3 + x_2x_4 + x_3x_4 \\ & + x_1^2 + x_2^2 + x_3^2 + x_4^2 \end{aligned} \tag{6.1}$$

where y was the response (max. purity), x_1 was the flow rate, x_2 was the injection volume, x_3 was the equilibration salt concentration and x_4 was the elution salt concentration.

The *stepwiselm* routine then added and subtracted these terms until a model was found that best explained the input data. The resulting model with only 5 terms is shown in Equation 6.2.

$$y \sim 1 + x_2 \times x_3 + x_2 \times x_4 + x_3 \times x_4 + x_2^2 + x_4^2 \tag{6.2}$$

Figure 6.4 compares the fit of the full quadratic response surface model and the model that was identified by stepwise regression. Each subfigure represents a process variable and shows the effects of that process variable on the response while the other process variables have been held constant. These figures show that the two models have very similar fits despite the stepwise regression model having significantly fewer terms.

6.2.5.2 Kriging

Kriging predicts the value of a response at an unknown point as the weighted sum of the values of the surrounding known points. Kriging assigns weights to the known points based on each point's proximity to the unknown point. Additionally, the weights are reduced for instances where the known points are clustered together, preventing any bias in the predictions. The procedure for producing a Kriging prediction was described in detail in Chapter 5.

The Kriging predictions were produced using scripts in MATLAB (The MathWorks Inc., Natick, MA, USA) (see Appendix A). Figure 6.5 shows the raw variogram, variogram model and covariance model that were produced for the input dataset.

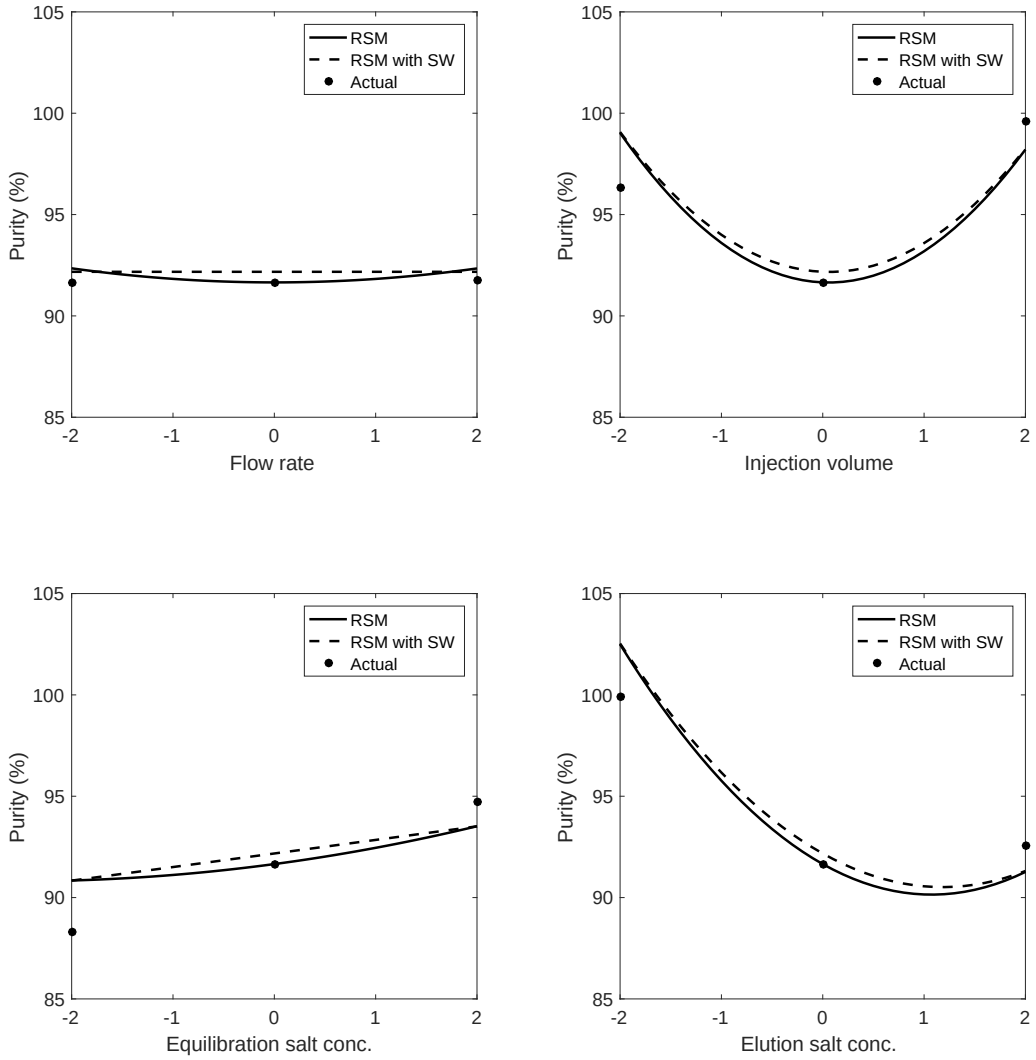

Figure 6.4: Fit comparison of the full quadratic model (RSM) and the model identified by stepwise regression (RSM with SW). These models were fitted to the input dataset that was used in this study. Each figure represents one of the investigated process variables and shows the effects of that process variable on the response while the other process variables had been held constant.

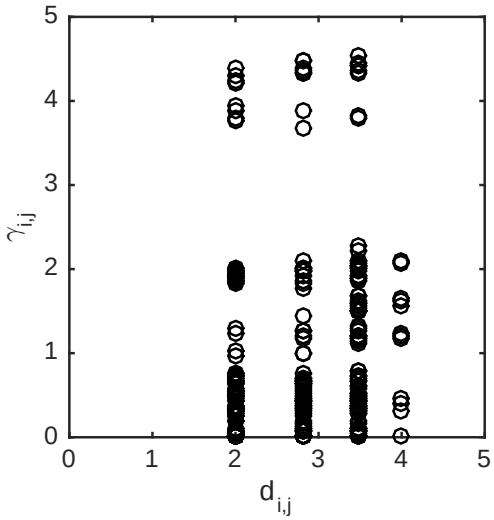

(a) Raw variogram

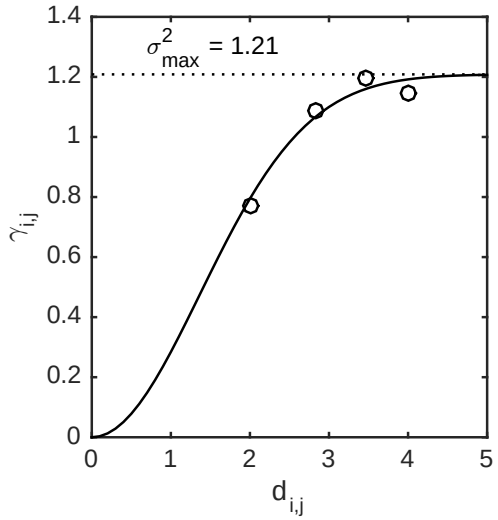

(b) Binned variogram

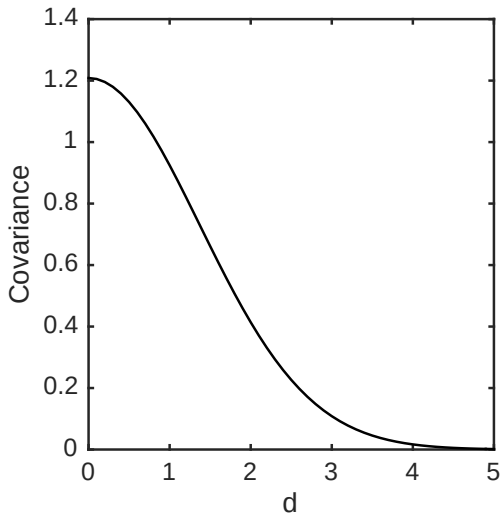

(c) Covariance model

Figure 6.5: Figure illustrating the procedure used to determine the covariance model. 6.5a shows the raw variogram for the input dataset used in this study. This is a plot of $\gamma_{i,j}$ vs. separation distance($d_{i,j}$) for each pair of points in the dataset. In 6.5b the variogram in 6.5a is smoothed by averaging the points in uniform intervals i.e. binning. The variogram model of the form $\gamma = a\left(1 - exp\left(-3\frac{d^2}{b^2}\right)\right)$ was fitted to the binned data. 6.5b shows the covariance model calculated for this dataset by subtracting the variogram model from the maximum variance.

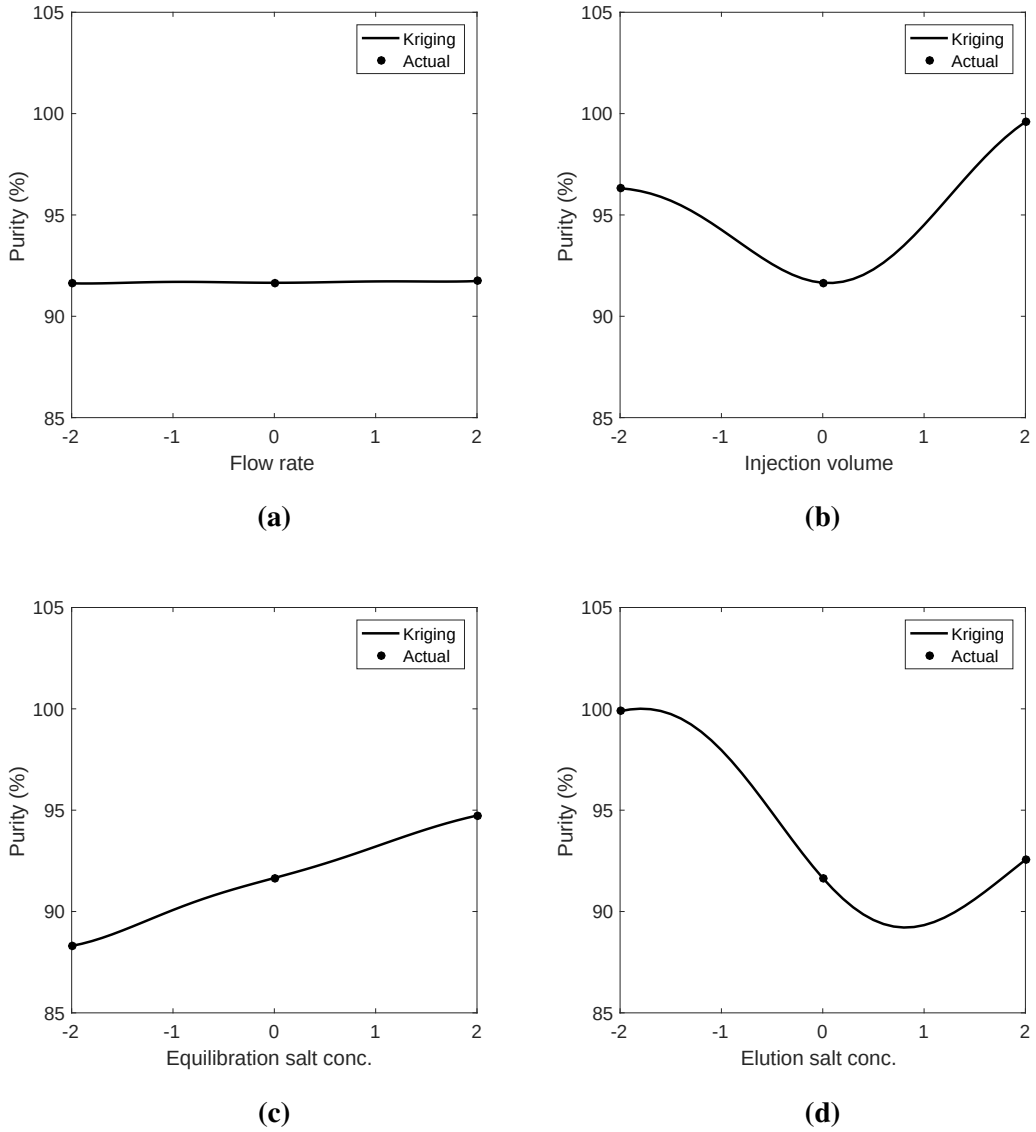

Figure 6.6: Kriging prediction to show the effect of the process variables on the response. Each figure shows the predicted effect of a single process variable while the other process variables are held constant. Also shown are the actual data from the input data set.

The calculated covariance model was then used to produce a Kriging prediction that showed the effect of the process variables on the response. This prediction is shown in Figure 6.6 which compares the prediction to the input dataset.

6.2.5.3 Partial least squares regression

Partial least squares regression seeks to create new variables or components that explain the variance in the response. These components are linear combinations of the original variables and can then be used to construct models that relate the original variables to

the response (Garthwaite, 1994). By identifying an appropriate number of components, it is possible to create models that capture the variance in the response caused by the variables and ignore any noise or error in the input data. The underlying mathematics of this technique are explained in detail by Wold et al. (2001). In this study the the partial least squares regression (PLSR) was performed using the *plsregress* function in MATLAB (The MathWorks Inc., Natick, MA, USA).

Using PLSR, a matrix X of the process variable data and a matrix Y of the response data can be related to each other as follows.

$$Y = XB + F \tag{6.3}$$

where B is a matrix of the PLSR coefficients and F is a matrix of the residuals of the response variables. The objective during the application of PLSR in this study will be to produce a model where XB represents the true effects of the process variables on the response and F represents the experimental error or process variability.

Two PLSR models were created. The first included only the linear effects on the process variables and the second included the linear effects, interactions, and quadratic effects on the process variables. Figure 6.7 shows the capacity of these two models to explain the variance in the response. This figure shows that even with all of the components included, the PLSR model with only linear effects can only explain $\approx$48% of the variance while the PLSR model with quadratic effects was capable of explaining $\approx$90% of the variance. For this study the quadratic PLSR model with 4 components was used. Figure 6.8 shows the results of this model. Each subplot shows the effects of a single process variable on the response while the other variables are held constant. As expected the linear PLSR model has a poor fit to the data while the quadratic PLSR model better approximates the actual trends.

6.2.6 Monte Carlo simulations

Monte Carlo simulations were carried out to investigate the overall effects of variability when deriving process models from experimental data. At the start of each Monte Carlo simulation the source of variability was defined as a distribution. During each cycle

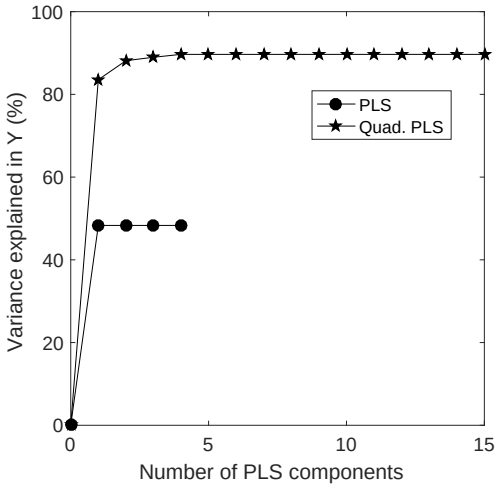

Figure 6.7: Comparison of PLSR and quadratic PLSR showing the relationship between the number of components and amount of variance explained in the response.

of the simulation, variability was applied to the input data by randomly sampling the distribution. The overall effects of the variability could be observed by repeating this procedure for a large number of cycles and analysing the cumulative results. MATLAB scripts were written to carry out the Monte Carlo simulation (see Appendix A).

The effects of two sources of variability that are commonly associated with high throughput process development were investigated in this study. These were:

1. The error introduced by the assay used to analyse the samples.

2. Variability in the process parameters from their setpoints.

6.2.6.1 Monte Carlo simulation of the error introduced by the assay

This Monte Carlo simulation was carried out to examine how experimental errors in a high throughput assay might affect the resulting process model. Figure 6.9 shows how this Monte Carlo simulation was carried out. The general rate model described above was used to produce the 25 chromatograms that made up the experimental design. Each chromatogram was fractionated into 0.25 column volume (CV) fractions and the concentration of A, B, and C was determined in each fraction. Random error was then applied to the concentrations of A, B, and C in each fraction to simulate the introduction of error via a high throughput assay. For each of these chromatograms a

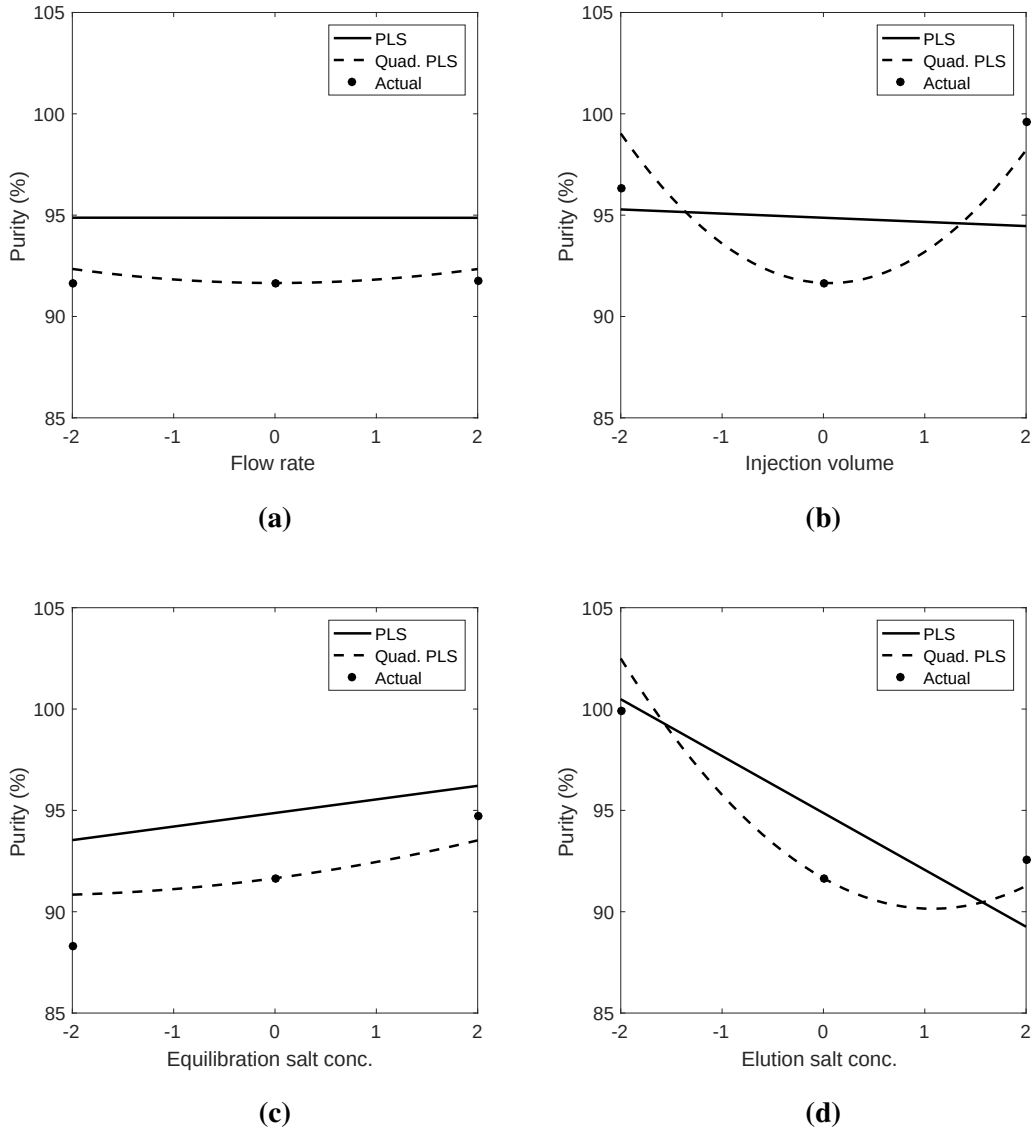

Figure 6.8: Fit comparison of PLSR and quadratic PLSR. Each figure represents one of the investigated process variables and shows the effects of that process variable on the response while the other process variables had been held constant.

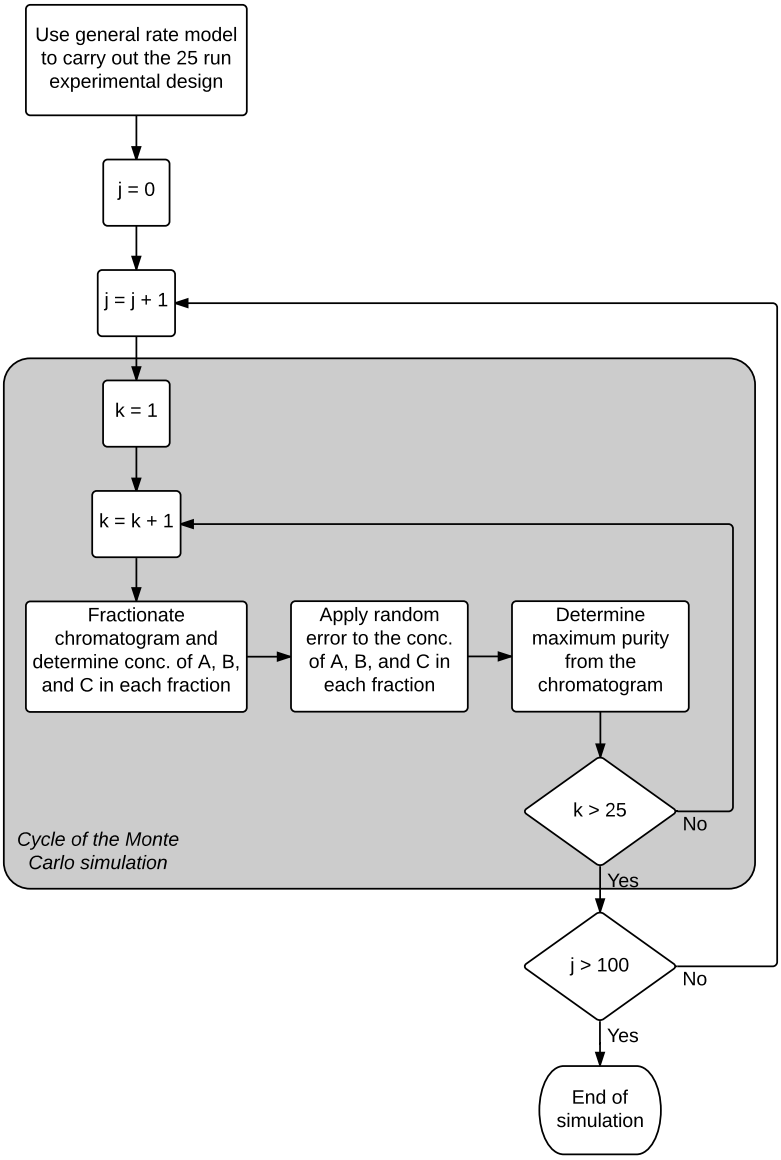

Figure 6.9: Flow chart showing the procedure for the Monte Carlo simulation examining the effect of experimental error introduced by a high throughput assay. In this flow chart j is the number of cycles of the Monte Carlo simulation and k is the number of chromatograms.

max. PF vs. yield diagram was produced and used to determine the maximum purity for a minimum yield of 90%. These purity values were used to produce the process models. This procedure was repeated for 100 cycles.

For this study it was assumed that the error introduced by the assay was normally distributed. A normal distribution was established for the concentration of each protein in each fraction. The mean of this distribution was the original error free concentration and the standard deviation of this distribution was defined in terms of the relative standard deviation as defined in Equation 6.4. The value of the relative standard deviation was defined at the start of the Monte Carlo simulation. The random error was applied in the Monte Carlo simulation by using a random number generator to randomly sample this distribution.

$$RSD = \frac{s}{\overline{x}} \times 100\% \tag{6.4}$$

where RSD is the relative standard deviation, s is the standard deviation, and $\overline{x}$ is the mean.

6.2.6.2 Monte Carlo simulation of process variability

In this Monte Carlo simulation the effects of process variability were examined. Process variability stems from small deviations away from the set-point of the process parameters that occur during the execution of the process. Figure 6.10 shows how this Monte Carlo simulation was carried out. In each cycle of the Monte Carlo simulation the general rate mode was used to produce the 25 chromatograms that made up the central circumferential experimental design. Random error was applied to the process parameters to simulate the effects of process variability. The chromatograms were then produced at the new values of the process parameters. The chromatograms were then fractionated and the concentration of each component in the fraction calculated. These values were used to construct maximum purity vs. yield diagrams which were used to determine the maximum purity for a minimum yield of 90%. Process models were then constructed using these maximum purity values as the response. This procedure was repeated for 100 cycles to investigate how the variability affected the results of the

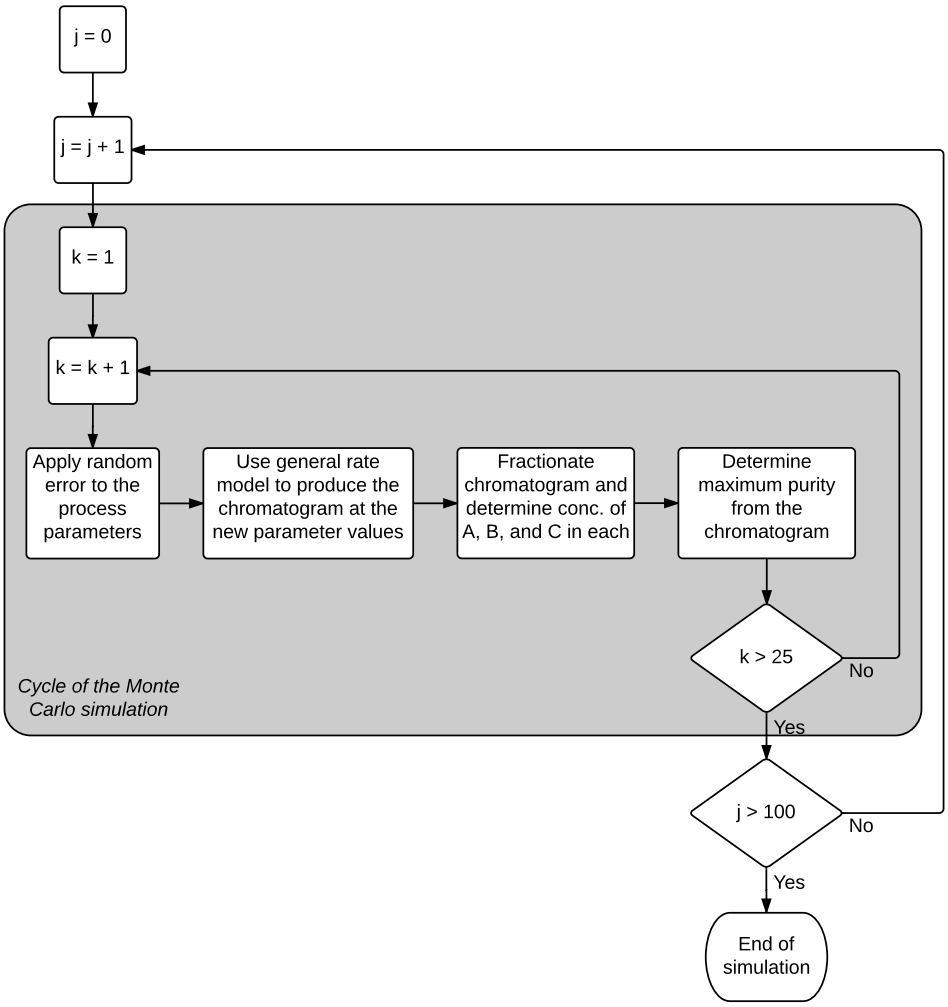

Figure 6.10: Flow chart showing the procedure for the Monte Carlo simulation examining the effect of process variability. In this flow chart j is the number of cycles of the Monte Carlo simulation and k is the number of chromatograms.

Table 6.6: Standard deviations of the process variability for each of the process parameters

Parameter	Standard deviation
Velocity (cm/hr)	1
Injection volume (CV)	0.01
Equilibration salt conc. (mM)	5
Elution salt conc. (mM)	5

experiments.

In this study it was assumed that deviations from the process parameters were normally distributed around the actual set point. The error distribution for each process parameter was defined in terms of its mean and standard deviation. The mean of the distribution was the set-point of the process parameter and the standard deviation was as detailed in Table 6.6. For normally distributed variability, 99.99% of the deviations from the set-point will be in the range of ± 3 standard deviations. These ranges were selected as they were similar to the level of control that would be expected during a chromatography run. In Monte Carlo simulation the random error was applied by sampling the error distribution for each of the parameters.

6.2.6.3 Model validation

During each cycle of the Monte Carlo simulations, the accuracy of the models was assessed by predicting the value of the response at each point in the validation dataset and calculating the percentage error. The percentage error was calculated using Equation 6.5.

$$\text{Relative error} = \frac{\sqrt{(y' - y)^2}}{y} \times 100\% \tag{6.5}$$

where y' is the predicted value and y is the actual value.

6.3 Results and discussion

6.3.1 Performance of the modelling techniques in the absence of variability

As an initial test the three modelling approaches described above (RSM, PLSR and Kriging) were fitted to the original input dataset. Since the experiments were simulated and a source of variability had not been applied to the results, this created a deterministic input dataset. Fitting the models to this error free dataset provided a baseline indication of how well the models described the trends in the experimental space. The models were fitted to the input dataset and the fitted models were used to predict the results of the experiments in the validation dataset. The relative error was calculated for each of the predictions and the distributions for each model are shown in Figure 6.11.

Figure 6.11a shows a boxplot comparing the three distributions. The box represents the range between the first and third quartiles and also shows the the median of the distribution while the whiskers show the maximum and minimum of each distribution. This box plot shows that the median and overall ranges for all three methods are similar. However, this also shows that the interquartile range (range between the third and first quartile) was smaller for Kriging compared to RSM and PLSR. This implies that the errors are tightly distributed around the median and thst more points will have a smaller error.

The histograms in Figures 6.11b, 6.11c and 6.11d also highlight this behavior. It can be seen that there are fewer points in the tail of the Kriging distribution. Furthermore, the RSM and PLS distributions show an additional peak around a relative error of 4%.

This behaviour was further analysed by plotting the relative error vs. the actual max. purity for each of the model as shown in Figure 6.12. To improve the clarity of the plot, the points were averaged into intervals of 1%. This figure shows that the relative error increases at extreme values of the response (max. purity) and the worst performers are the RSM and PLSR models. This behaviour is to be expected as RSM and PLSR are regression based methods which are fitted to the available data using least squares

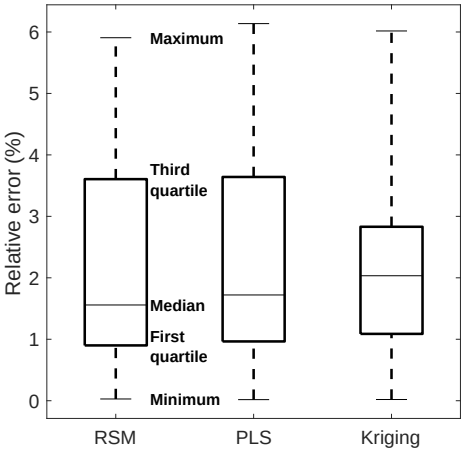

(a)

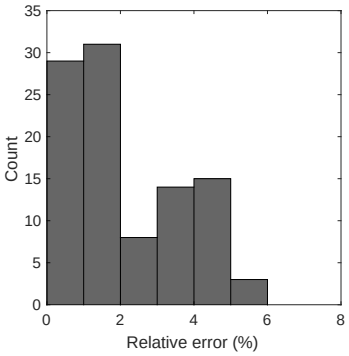

(b) RSM

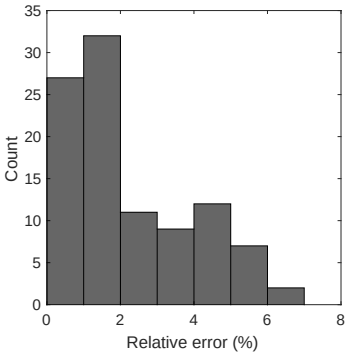

(c) PLSR

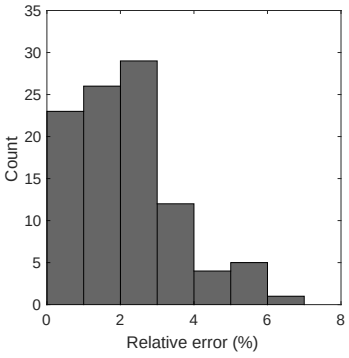

(d) Kriging

Figure 6.11: Results of the models fitted to the error free input dataset. 6.11a shows a boxplot comparing the relative error distributions of the three models. The box represents the range between the first and third quartiles while the whiskers represent the maximum and minimum of the distribution. 6.11b, 6.11c and 6.11d show the histograms for each model's error distribution

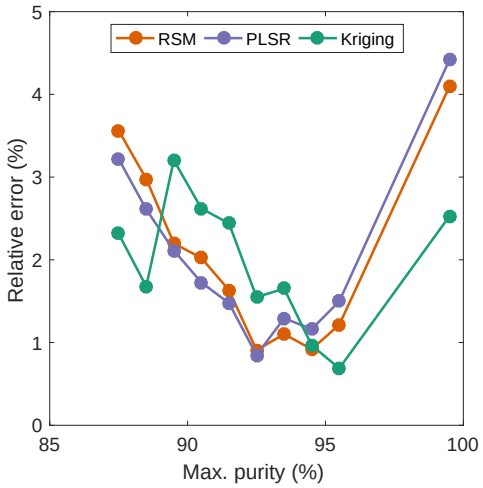

Figure 6.12: Graph of error vs. max. purity for the RSM, Kriging, and PLS models trained using the error free input dataset.

techniques and therefore the model is unlikely to pass through the input data points. While this has the advantage of eliminating some of the effects of variability, it also has the effect of smoothing out the extremes of the response range. On the other hand, Kriging uses weighted interpolations to produce models and therefore the predictions are more likely to reflect the full range of the response.

6.3.2 Propagation of variability in the experiments through to the response results

In the Monte Carlo simulations that were performed in this study, the sources of variability were simulated by applying error to the experimental parameters or to the chromatogram data. However, there were data processing steps between the application of the error and the final calculation of the response. The propagation of the error through the data processing workflow was examined using the Monte Carlo simulation that mimicked the effect of assay variability on the chromatogram data.

In this Monte Carlo simulation, the effects of assay variability were simulated by applying random error to the concentration of each component in each fraction of the 25 input chromatograms. The max. purity was calculated for each of these chromatograms, and the error was calculated between that value and the max. purity from the corresponding chromatogram with no applied error.

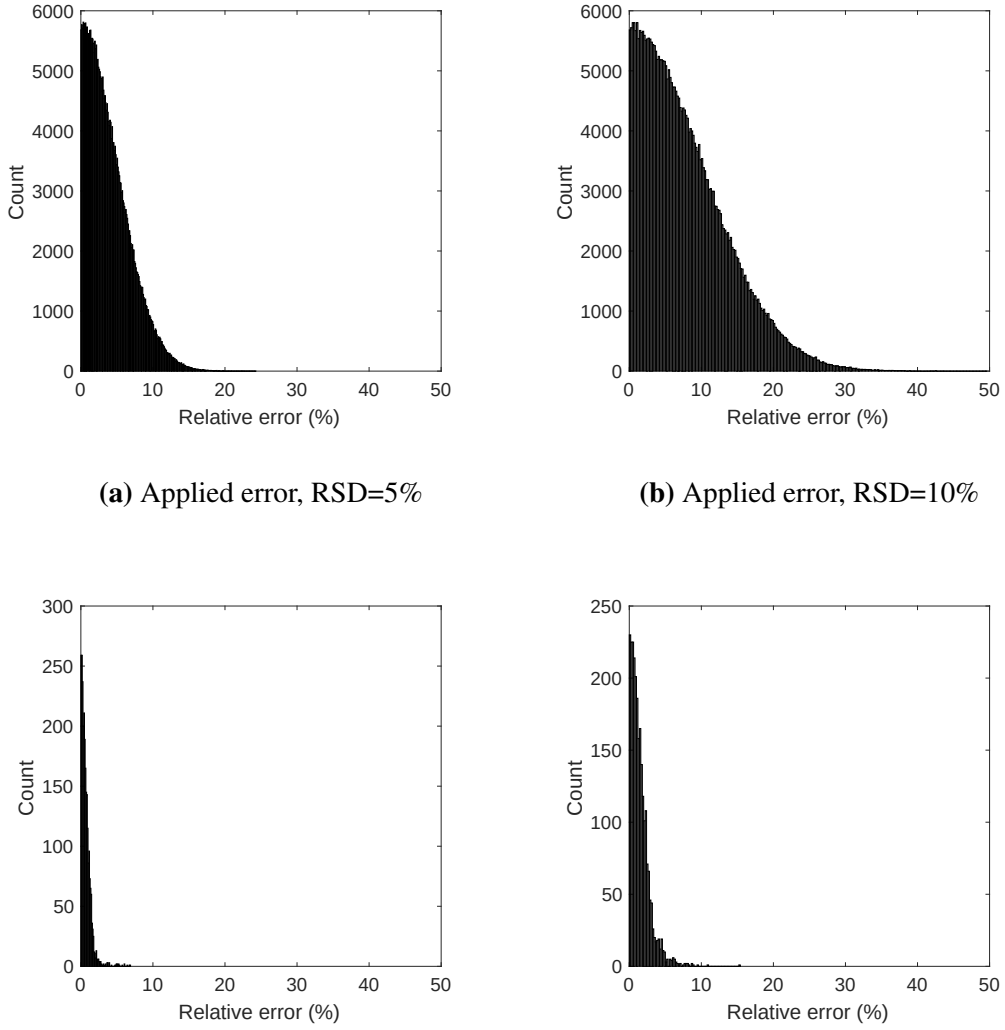

(a) Applied error, RSD=5%

(b) Applied error, RSD=10%

(c) Propagated error, RSD=10%

(d) Propagated error, RSD=10%

Figure 6.13: Histograms showing the propagation of error through the processed experimental data. 6.13a and 6.13b show the distributions of error that were applied to chromatograms. The relative standard devaiations of the applied error was 5% and 10% respectively. 6.13c and 6.13d show the distribution of the error that was present in the response (max. purity) which had been calculated from the chromatogram data to which the error had been applied.

This Monte Carlo simulation was performed twice; first applying error with a relative standard deviation (RSD) of 5% and then applying error with an RSD of 10%. These simulations were performed for 100 cycles. During each cycle the randomly applied error and the calculated relative error on the response were recorded and their distributions are shown in Figure 6.13.

This figure shows that the error is significantly reduced through the processing of the

Table 6.7: Standard deviations of half-normal distributions fitted to the error distributions

	RSD = 5%	RSD = 10%
Applied error	5.0039	10.003
Propagated error	1.04688	1.95483

chromatogram data to calculate the max. purity. Half normal distributions were fitted to the distributions and the standard deviations of the fitted distributions are shown in Table 6.7. This table highlights the substantial reduction in error that occurs through the data processing. This reduction is due to the method of calculating the max. purification factor vs. yield (PFY) diagrams. These diagrams are produced by calculating the yield and purification factor across multiple fractions which has the effect of cancelling out the errors. This can be considered another benefit of using the PFY diagrams.

6.3.3 A comparison of regression methods for reducing the effects of variability in the input data

6.3.3.1 Experimental error

The first source of variability that was investigated was that of experimental error. High throughput analytical techniques are often employed during process development to avoid the formation of an analytical bottleneck. However, the high throughput nature of these methods may lead to greater levels of experimental error compared to that of standard methods.

The effects of experimental error were simulated by applying random error to the concentration of each component in each fraction of the chromatograms that made up the initial input dataset. These chromatograms were then processed to calculate the value of the max. purity for each of the experiments. The max. purity values were then used as the response in the final input dataset that was used to create process models using RSM, PLSR and Kriging. This procedure was repeated for 100 cycles and during each cycle the produced process models were used to predict the values of the validation dataset. The relative errors were calculated for each of these predictions which provided an indication of the accuracy of the corresponding modelling technique.

The relative standard deviation of the introduced error was varied to investigate how the level of variability affected the accuracy of the produced models. The first Monte Carlo simulation was carried out using a error distribution with a relative standard deviation of 5%. For the second Monte Carlo simulation the relative standard deviation was increased to 10%. Figure 6.13 above shows the levels of variability that were present in the input data that was used to produce the models. The distribution of prediction errors for each model are shown in Figures 6.14 and 6.15. These figures represent the results from the Monte Carlo simulations which had an applied error RSD of 5% and 10% respectively. In these plots a distribution of prediction errors with a low median and small distribution would be considered beneficial as this would imply that the majority of predictions had a low relative error.

As expected, increasing the input error from 5% to 10% resulted in a increase in the prediction error for all three methods. For the Monte Carlo simulation with an applied error of 5%, the box-whisker plots show that the median and distribution for all three methods is comparable. However, examination of the histograms show additional peaks for RSM and PLSR around a relative error of 4%. A similar behaviour was seen above in section 6.3.1 and was attributed to difficulties that these techniques had in predicting extreme values of the response.

Similar behaviours can be seen in the results for the Monte Carlo simulation with an applied error of 10% as shown in Figure 6.15. Again the distribution and median of the errors are similar for all three modelling approaches. However, in these results, the additional peak is less pronounced for PLSR.

6.3.3.2 Process variability

The second Monte Carlo simulation investigated variability that was introduced by deviations in the process parameters. This was implemented during the simulation of the experiments that made up the input dataset. Randomly sampled error was introduced into the set points of the process variables during each simulation. The resulting chromatograms were then processed to create the input dataset from which the process models were created. The process models were used to predict the response of the validation dataset and the results were evaluated by calculating the relative error. This was

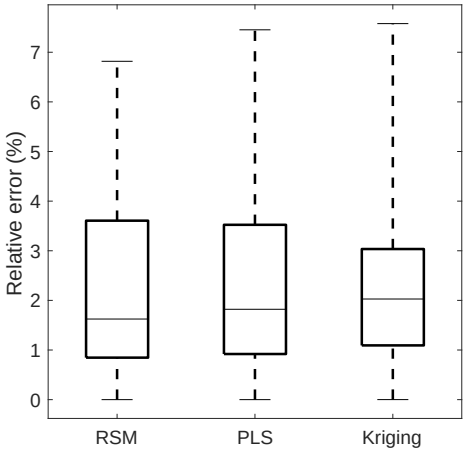

(a)

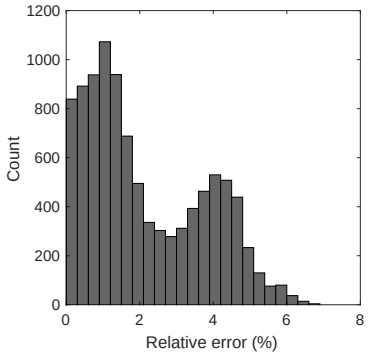

(b) RSM - RSD=5%

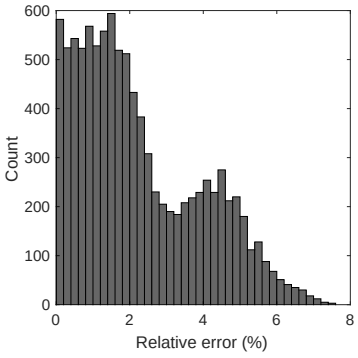

(c) PLSR - RSD=5%

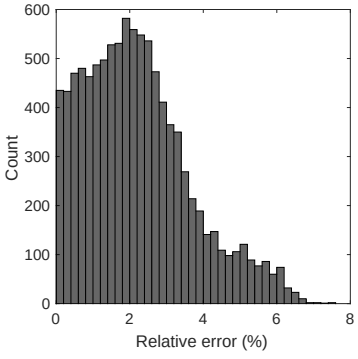

(d) Kriging - RSD=5%

Figure 6.14: Distributions of prediction errors for each of the regression methods investigated using Monte Carlo simulations which introduced experimental error into the input data. The distribution of the applied error for this Monte Carlo simulation was 5%. The box represents the range between the first and third quartiles while the whiskers represent the maximum and minimum of the distribution.

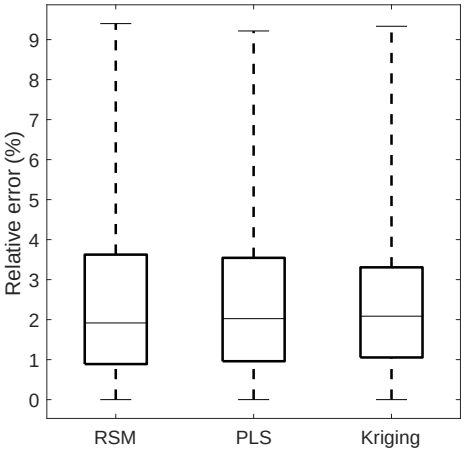

(a)

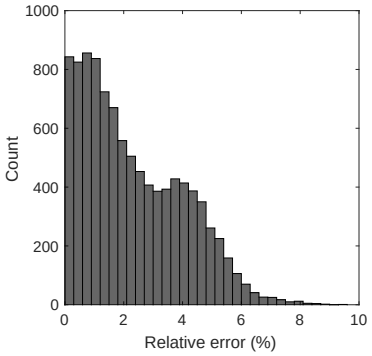

(b) RSM - RSD=10%

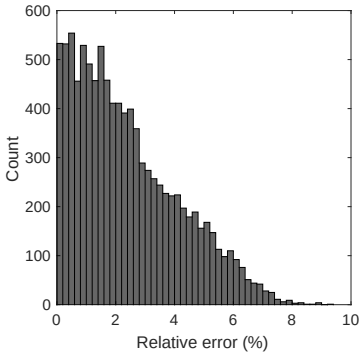

(c) PLSR - RSD=10%

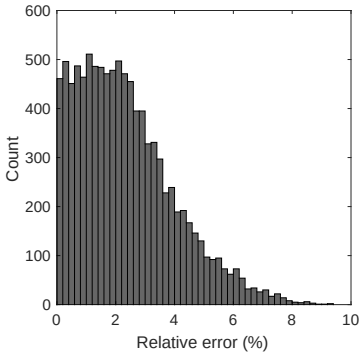

(d) Kriging - RSD=10%

Figure 6.15: Distributions of prediction errors for each of the regression methods investigated using Monte Carlo simulations which introduced experimental error into the input data. The distribution of the applied error for this Monte Carlo simulation was 10%. In 6.15a box represents the range between the first and third quartiles while the whiskers represent the maximum and minimum of the distribution.

performed for 100 cycles and the aggregated results are shown in Figure 6.16.

The boxplot in Figure 6.16a shows that the errors for all three methods have similar medians and distributions. However, in a similar manner to the previous Monte Carlo simulations, the RSM and PLSR distributions have an additional peak which indicated a poor fit to points with extreme response values.

6.4 Conclusion

The objective of this study was to compare the use of three modelling approaches (RSM, PLSR, and Kriging) for producing process models from high throughput process development data which tends to include error introduced by various sources of variability.

In this study it was shown that using max. purity vs. yield diagrams to reduce complex chromatogram data had the added benefit of reducing the propagation of error from the experimental data through to the process models.

As an initial test, the three chosen modelling techniques, RSM, PLSR, and Kriging were applied to an error free input dataset. The overall results showed that all three techniques produced models with similar levels of accuracy. However, detailed analysis showed that RSM and PLSR struggled to predict points at the extremes of the response's range. This indicated that Kriging was better overall at approximating the trend of the response than the other methods.

The Monte Carlo simulations were then performed to test the modelling techniques in the presence of different sources and magnitudes of variability. The results of these simulations showed that all three modelling techniques were susceptible to the error at similar levels. However, the results again indicated that Kriging could approximate the entire trend better than the other two methods. This, combined wth the benefit of not having to perform manual model selection/fitting, indicates that Kriging is a viable technique for producing process models from high throughput experimentation.

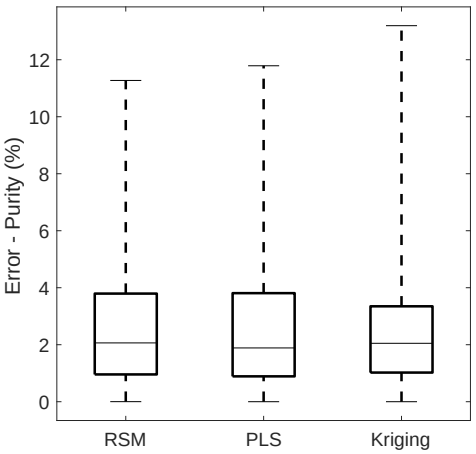

(a)

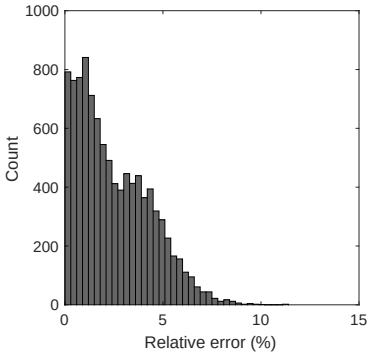

(b) RSM

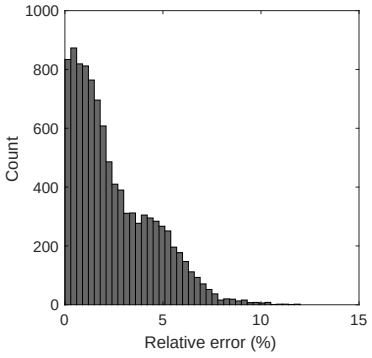

(c) PLSR

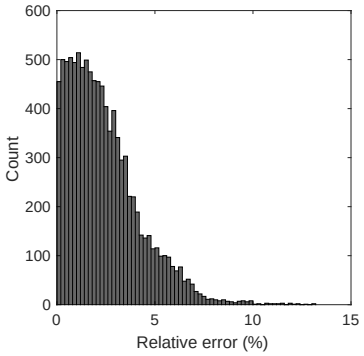

(d) Kriging

Figure 6.16: Distributions of prediction errors for each of the regression methods investigated using the Monte Carlo simulation which introduced process variability into the input data. In 6.16a the box represents the range between the first and third quartiles while the whiskers represent the maximum and minimum of the distribution.

Chapter 7

A comparison of approaches for using scale down experimentation to develop chromatographic separations

7.1 Introduction

In this chapter alternative approaches for developing chromatographic separations from scale down experiments were developed and tested.

Previously, in Chapter 5, the benefits of using scale down experiments during the development of chromatographic separations was discussed. The benefits included the ability to perform a greater number of experiments due to the lower cost and higher throughput of these experiments. The results of these experiments can provide a better understanding of the process which in turn can be used to optimise the process and ensure that the developed process produces a product with a consistent quality.

The usual approach to scaling a chromatographic process is to maintain the column height, the load per unit volume of sorbent and the residence time while changing the diameter of the column as required. This ensures that the dynamics within the column are constant across the different scales. However, scale down devices have significantly smaller bed heights in order to minimise the amount of material required for each experiment. Equivalence with large scale columns can be achieved by maintaining the same residence time, but differences between the performance of the large scale column and

the scale down device are often seen. The factors that contribute to these differences include relatively large extra-column volumes and low flow rates in the column that cause significant levels of dispersion and differing wall effects due to the comparatively narrow diameters of scale down devices (Sofer and Hagel, 1997). The effects of various scaling factors mean that scale down experiments are not always directly representative of the final process, and this can limit the usefulness of these experiments.

The aim of this study was to develop an approach that would circumvent the various scaling effects associated with the use of scale-down methods. This would enable the use of the data from these methods for the characterisation of the large scale process. The approach taken in this study was to carry out a comprehensive characterisation of the process using a small scale column which had a low material requirement. The data from the scale down method was then augmented with a few selected large scale runs in order to produce a comprehensive characterisation of the experimental space of the large scale process.

One approach used regression techniques to create mathematical relationships between the small scale and large scale experimental spaces. This enabled the transformation of the small scale data into the large scale experimental space. Response surface methods were then used to fit models to the transformed data to characterise the large scale experimental space. The other approach used the cokriging method that was introduced in Chapter 5

All of these methods were tested using the cation exchange separation of the myoglobin from egg white proteins as a platform separation. This study used a single small scale column with a 1 mL column volume and two different larger scale columns with 20 mL and 30 mL column volumes respectively. Additionally the results of these methods were compared against a more traditional approach that involved performing design of experiments studies at both small and large scale.

7.2 Materials and methods

The separation of myoglobin from egg white protein using cation exchange chromatography was discussed in Chapter 5. This separation provided two key benefits; a readily

manipulated system and the ability to determine rapidly the concentration profiles of the product and the impurities directly from the UV chromatograms. Due to these benefits this separation was adopted for use in this study.

7.2.1 Materials

7.2.1.1 Chemicals

All chemicals were obtained from Sigma-Aldrich (Gillingham, Dorset, UK). The cation exchange chromatography experiments were carried out using S HyperCel™ sorbent (Pall Life Sciences, Portsmouth, UK) packed in prepacked PRC columns (Pall Life Sciences, Portsmouth, UK) and XK16 columns (GE Healthcare Life Sciences, Little Chalfont, Bucks, UK) connected to an AKTA™ Avant 25 (GE Healthcare Life Sciences, Little Chalfont, Bucks, UK).

7.2.1.2 Feedstock

The feedstock was created by dissolving egg white powder and horse heart myoglobin in 30 mM sodium citrate at pH 5 at concentrations of 1 g/L and 5 g/L respectively. These concentrations were chosen to mimic a typical capture chromatography step where the concentration of the product is significantly larger than the concentration of the impurities that bind to the column. The mixture was then centrifuged at 10000 rpm for 30 min using a Beckman J2-MI (Beckman Coulter, High Wycombe, UK) to remove any undissolved solids.

7.2.2 Cation exchange chromatography

The base experiment was carried out as follows:

1. **Equillibration** - The column was equilibrated with 5 column volumes (CV) of 30 mM sodium citrate at pH 5.
2. **Load** - The egg white/myoglobin feed was injected onto the column.
3. **Wash** - The column was washed with 10 CV of 30 mM sodium citrate at pH 5 to clear any unbound proteins.

Table 7.1: Characteristics of the columns used in this study

Parameter	Column 1	Column 2	Column 3
Height (cm)	5	10	15
Diameter (cm)	0.5	1.6	1.6
Column volume (mL)	0.982	20.1	30.2

4. **Elution** - An elution gradient of 30 mM sodium citrate, at pH 5 with NaCl was used to elute the bound proteins (the NaCl conc. at the end of the gradient was a variable in these experiments).

5. **Strip** - The column was stripped with 5 CV of 1 M NaOH to remove any remaining bound proteins.

The chromatography experiments were carried out on three columns with three different column volumes; 1 mL, 20 mL and 30 mL. During this study the the 1 mL column was designated as the small scale column while the 20 mL and 30 mL columns were designated as the large scale columns. Table 7.1 details the dimensions of these columns and shows that the small scale column and the large scale columns were not geometrically related.

7.2.3 Experimental design

Experiments were performed on all three columns described above. To maintain equivalence between the three columns, the experimental space was defined in terms of scale independent variables, e.g. column load per unit volume of resin and residence time. The extents of the experimental space that was explored in this study are detailed in Table 7.2. The extents are shown in terms of the codings that were used to normalise the process parameters.

A central composite circumscribed experimental design with 7 centre points was used to characterise the experimental space of the separation at the 1 mL scale. This experimental design is detailed in Table 7.3.

Table 7.4 and Table 7.5 show the experimental designs carried out at the 20 mL and 30 mL scale. The experimental designs were fractional factorial with 8 runs and 3

Table 7.2: Extents of the explored experimental space and their corresponding codings that were used to normalise the process parameters.

Parameter	**0**	**± 1**	**± 2**
Column load (g/L)	6	± 1.5	± 3
Residence time (min)	3	± 0.15	± 0.3
Gradient target (mM)	200	± 20	± 40
pH	5	± 0.1	± 0.2

Table 7.3: Experimental design for the 1 mL column. Also shown is the productivity that was determined for each experiment.

Run	**Velocity**	**Sample size**	**Gradient target**	**Elution pH**	**Productivity**
1	0	0	0	0	0.274
2	0	-2	0	0	0.129
3	0	2	0	0	0.469
4	0	0	0	0	0.348
5	-2	0	0	0	0.281
6	2	0	0	0	0.362
7	0	0	0	0	0.306
8	0	0	-2	0	0.320
9	0	0	2	0	0.321
10	0	0	0	0	0.312
11	0	0	0	0	0.267
12	0	0	0	0	0.297
13	0	0	0	0	0.305
14	1	1	-1	-1	0.432
15	1	1	1	-1	0.364
16	1	-1	-1	-1	0.473
17	-1	1	1	-1	0.343
18	-1	1	-1	-1	0.359
19	-1	-1	1	-1	0.213
20	-1	-1	-1	-1	0.213
21	1	-1	1	-1	0.234
22	1	-1	1	1	0.487
23	-1	1	1	1	0.372
24	-1	-1	1	1	0.224
25	-1	-1	-1	1	0.235
26	-1	1	-1	1	0.400
27	1	1	-1	1	0.425
28	1	1	1	1	0.430
29	1	-1	-1	1	0.285
30	0	0	0	2	0.592
31	0	0	0	-2	0.345

Table 7.4: Experimental design for the 20 mL column and the productivity calculated for each run. Runs 12, 13 and 14 are the runs used to validate models produced for the process at this scale.

Run	Velocity	Sample size	Gradient target	Elution pH	Productivity
1	-2	-2	2	2	0.290
2	-2	2	-2	2	0.812
3	2	-2	-2	2	0.395
4	2	2	2	2	0.912
5	-2	-2	-2	-2	0.309
6	-2	2	2	-2	0.689
7	2	-2	2	-2	0.367
8	2	2	-2	-2	1.021
9	0	0	0	0	0.651
10	0	0	0	0	0.660
11	0	0	0	0	0.667
12	1.301	1.173	1.591	1.834	0.876
13	-1.637	0.727	-0.366	-0.793	0.693
14	-1.174	-0.120	0.634	0.899	0.608

centre point runs. However, as shown in the experimental design, the explored range was greater for the 20 mL column. This was done to examine what effect the explored range had on the accuracy of the produced models. An additional 3 runs were carried out at random points in the experimental space at each of these scales. These additional runs were for model validation purposes.

7.2.4 Data processing

In this study a data processing approach was used that allowed for the rapid determination of the response, the productivity, from the chromatogram of the experiment without any further sample analysis. This approach involved the following steps.

1. Deconvolute the chromatogram to produce concentration profiles for the product and the impurities.
2. Calculate the maximum purification factor vs. yield diagram and determine the yield that can be achieved for a purity of 99%.
3. Calculate the productivity of the process.

This data processing approach is detailed in further detail below.

Table 7.5: Experimental design for the 30 mL column and the productivity calculated for each run. Runs 12, 13 and 14 are the runs used to validate the models produced for the process at this scale.

Run	Velocity	Sample size	Gradient target	Elution pH	Productivity
1	0	0	0	0	0.608
2	-1	-1	1	1	0.486
3	1	-1	1	-1	0.529
4	-1	1	1	-1	0.650
5	1	1	1	1	0.850
6	0	0	0	0	0.672
7	-1	1	-1	1	0.748
8	-1	-1	-1	-1	0.470
9	1	-1	-1	1	0.546
10	1	1	-1	-1	0.770
11	0	0	0	0	0.648
12	-0.649	-0.649	-1.033	0.301	0.543
13	1.600	1.600	-0.384	-1.761	0.850
14	-0.523	-0.523	-1.614	-1.061	0.572

7.2.4.1 Calculating the concentration profiles from the chromatogram

During these experiments the 280nm and 408nm chromatograms were recorded. The Beer-Lambert law relates UV absorbance to concentration as shown in Equation 7.1.

$$A = \varepsilon CL \tag{7.1}$$

where A is the absorbance, ε is the extinction coefficient, C is the concentration and L is the path length.

While all the proteins in the feedstock absorb UV at 280 nm, only myoglobin absorbs at 408 nm due to the presence of heme groups in its structure. Equations 7.2 and 7.3 show how this behaviour can be represented using the Beer-Lambert law.

$$A_{408} = \varepsilon_{M,408} C_M L \tag{7.2}$$

$$A_{208} = \varepsilon_{E,280} C_E L + \varepsilon_{M,280} C_M L \tag{7.3}$$

where A_{408} is the absorbance at 408 nm, A_{208} is the absorbance at 280nm, $\varepsilon_{M,408}$ is the

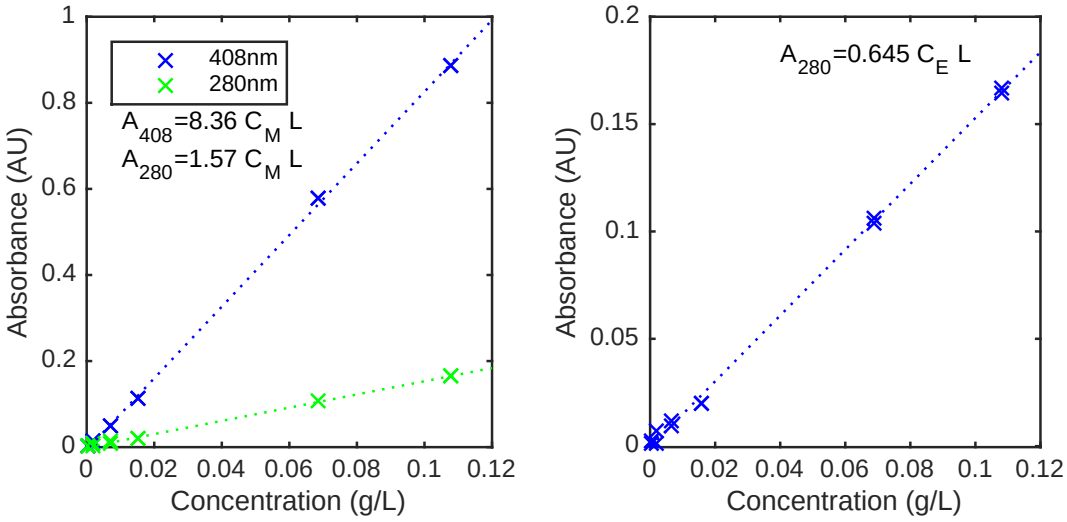

(a) Myoglobin **(b)** Egg white protein

Figure 7.1: Standard curves used to determine the extinction coefficient of myoglobin at 280nm and 408nm and the egg white protein at 280nm.

extinction coefficient for the myoglobin at 408nm, $\varepsilon_{E,280}$ and $\varepsilon_{M,280}$ are the extinction coefficients of the egg white proteins and the myoglobin at 280nm, and C_M and C_E are the concentrations of the myoglobin and the egg white proteins.

By solving Equations 7.2 and 7.3, the concentration profiles for myoglobin and the egg white proteins in the eluate can be determined directly from the chromatograms.

Solving these equations required the extinction coefficients which were determined experimentally using the standard curves shown in Figure 7.1. The extinction coefficients of myoglobin at 280nm and 408nm are 1.57 g^{-1}Lcm and 8.36 g^{-1}Lcm respectively. The extinction coefficient of egg white protein at 280nm was 0.645 g^{-1}Lcm.

7.2.4.2 Baseline correction of the impurity traces

The calculated egg white protein traces were found to have a drift in the baseline as Figure 7.2a shows. As this drift would impact the calculation of the PFY diagrams, it was corrected by calculating a new baseline using the second derivative method detailed by Dietrich et al. (1991). In this approach the second derivative of the trace was calculated and was used to identify the locations of the peaks. As shown in Figure 7.2b the second derivative reaches a maximum at the start and end of each peak. A piecewise cubic Hermite interpolating polynomial was fitted to the remaining portions of the

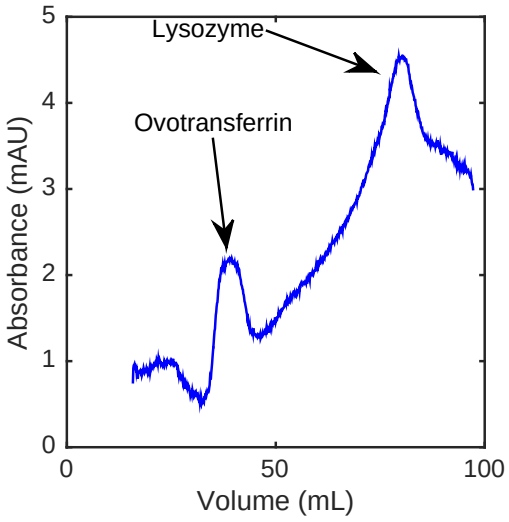

(a) Impurity trace with baseline drift

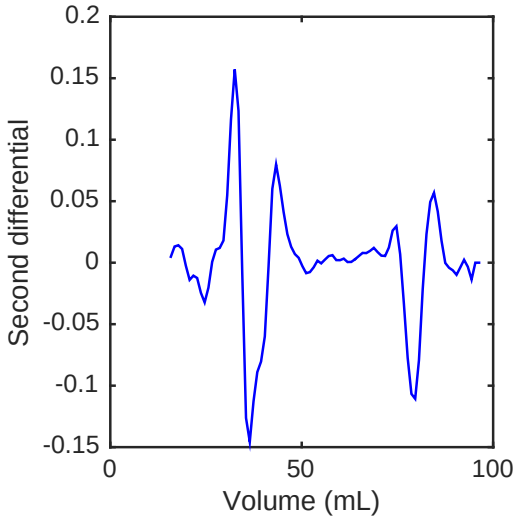

(b) Second differential of the impurity trace to identify the start and end of each peak

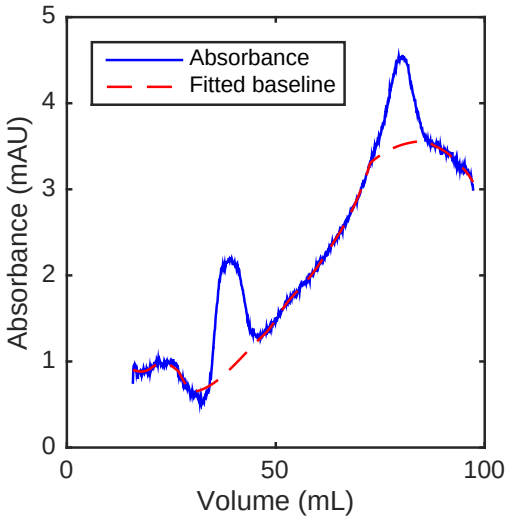

(c) New baseline calculated from the second differential

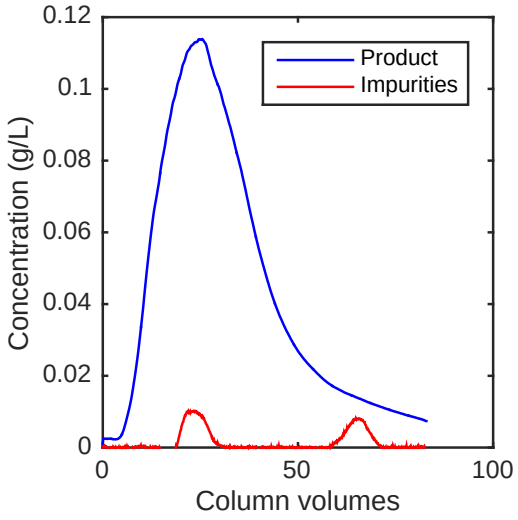

(d) Corrected impurity trace and the product trace

Figure 7.2: Figures showing the stages of the procedure used to correct the baseline of the chromatograms.

trace (Figure 7.2c) using the *fit* function in MATLAB and this was subtracted from the trace to correct the baseline (Figure 7.2d).

7.2.4.3 Max. purity vs. yield diagrams

For each chromatogram a max. purification factor vs. yield (PFY) diagram was calculated using the procedure detailed in Chapter 4. This diagram was converted to a max. purity vs. yield diagram by multiplying the max. purification factor by the purity of

the feed. The max. purity vs. yield diagram was then used to calculate the yield that corresponded to a product purity of 99%.

7.2.4.4 Productivity

As described above, the yield that corresponded to a product purity of 99% was determined for each experiment. This yield was in turn used to calculate the productivity of the process. The productivity was calculated using Equation 7.4. This value was used as the response for characterising the process.

$$\text{Productivity} = \frac{C_L V_L Y}{t_{cyc} V_{Col}} \tag{7.4}$$

where C_L is the concentration of the load, V_L is the volume of the load, Y is the yield, t_{cyc} is the cycle time and V_{Col} is the column volume.

7.2.5 Model validation

The process models produced in this study were validated by predicting the value of the productivity response for the 3 validation runs that were carried out on the 20 mL and 30 mL columns. These points were selected at random from within the range coded [-2,-2,-2,-2] to [2,2,2,2]

During model validation a plot of the predicted value vs. the actual value was used to provide a visual indication of the prediction accuracy. The error of the prediction was quantified by calculating the root mean squared error of prediction (RMSEP) using Equation 7.5.

$$RMSEP = \frac{1}{n}\sum_{i=1}^{n}\left(Y_i - Y_{i,pred}\right)^2 \tag{7.5}$$

where there are $i = 1,2,3\cdots n$ points to be predicted, Y_i was the actual value of point i and $Y_{i,pred}$ was predicted value.

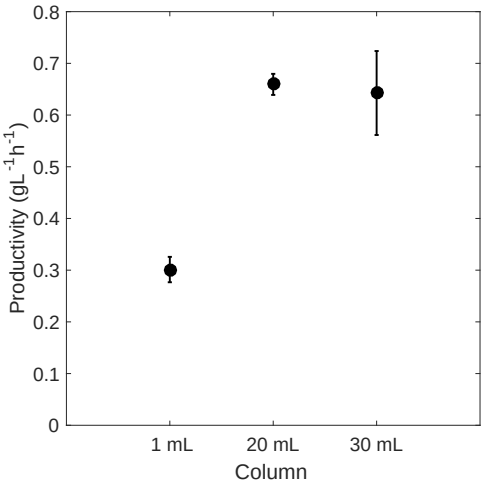

Figure 7.3: Average productivity at the centrepoint of the experimental space for each of the columns used in this study. The error bars indicate the 95 % confidence intervals.

7.3 Results and discussion

7.3.1 Influence of scale up factors on the performance of the process

The main objective of this study was to test approaches for using scale down experimentation to reduce the burden of developing chromatographic separations. The experiments were performed using 3 columns with different dimensions and column volumes to produce data for testing these approaches. In this study the small scale column had a volume of 1 mL while the large scale columns had volumes of 20 mL and 30 mL.

The experimental designs for each column included multiple centre points, which allowed the calculation of the average productivity at the centre of the experimental space and its corresponding 95% confidence interval. The average productivity and the 95% confidence interval for each column is shown in Figure 7.3. This figure shows that while the performance of the 20 mL and 30 mL columns were comparable to each other, their performance was significantly different to that of the 1 mL column. This confirms that it would not be possible to develop a process for the larger scale columns using experimental data from the 1 mL column alone.

7.3.2 A typical approach to process characterisation

A single uniform approach to developing chromatography processes does not exist and different individuals and organisations will base their approach on the tools that are available to them and their experience. The use of scale down experimentation during process development has become more commonplace due to the various advantages that come with it. However, as highlighted in the previous section, the results of scale down experiments cannot be used to describe the final process. Therefore multiple stages of experimentation will be required, but attempts are made to perform as many experiments as possible at the smaller scale. An example of such a process development work flow is described below.

1. Explore the experimental space of the process using scale down experimentation. As these experiments are high throughput and cheap, a detailed experimental design can be performed.
2. Use the resulting data to identify a suitable process model.
3. Perform an appropriate experimental design at large scale to produce data for fitting the process model that was identified at small scale.
4. Fit the previously identified process model to the large scale data to characterise the process.

In this study alternative approaches for using small scale chromatography experiments to develop chromatography processes were explored and the procedure described above was used as the basis for comparison.

A central composite circumferential experimental design consisting of 31 runs was performed at small scale (detailed in Table 7.3). This design was used as it can be used to identify any significant main effects, second degree interaction effects or quadratic effects. The experimental data was then processed to calculate the productivity for each experiment. A suitable process model was identified from the resulting dataset using stepwise regression. Stepwise regression was performed using the *stepwiselm* function in MATLAB. The routine began with all main effects, second degree interaction effects and quadratic effects included as shown in Equation 7.6.

$$\begin{aligned} y \sim & 1 + x_1 + x_2 + x_3 + x_4 \\ & + x_1x_2 + x_1x_3 + x_1x_4 + x_2x_3 + x_2x_4 + x_3x_4 \\ & + x_1^2 + x_2^2 + x_3^2 + x_4^2 \end{aligned} \tag{7.6}$$

where y is the productivity, x_1 is the velocity, x_2 is the sample size, x_3 is the gradient target, and x_4 is the elution pH.

The stepwise regression routine then subtracted and added these terms in a stepwise manner until the model that best explained the response was identified. This model is shown in Equation 7.7.

$$y \sim 1 + x_1 + x_2 + x_3 + x_4 + x_1x_2 + x_3x_4 + x_4^2 \tag{7.7}$$

After identifying a model that was capable of describing the process, an appropriate experimental design was selected for characterising the process at large scale. The experimental designs in Table 7.4 and Table 7.5 were performed on the 20 mL and 30 mL columns respectively and the identified model in Equation 7.7 was fitted to the results. The models were validated by predicting the productivity of the validation runs and comparing the predictions to the actual results.

Figure 7.4 shows the results of the model validation for the models fitted to the 20 mL and 30 mL data. The dotted line is the parity line. The distance between the predictions and the parity line is the error and therefore indicates the accuracy of the fitted models. This figure shows that these models are accurate. However, fitting this model required 11 experimental runs (8 corners + 3 centre points) and since the objective of this study was to minimise the number of large scale runs, the experimental burden was considered excessive.

The RMSEP value for 20 mL column is greater than that for the 30 mL column. The experimental space for the 20 mL column was twice as large as the 30 mL column and it is likely that this has resulted in a less precise model.

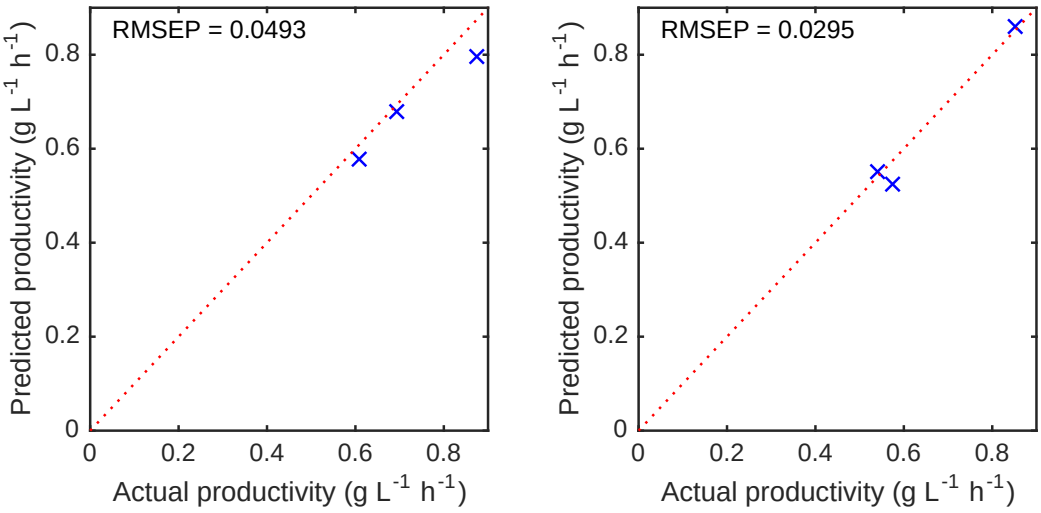

(a) 20 mL column **(b)** 30 mL column

Figure 7.4: Validation results for the fitting of the regression model identified at small scale to the available 20 mL and 30 mL column data.

7.3.3 Using an offset calculated from the centre points of the data

The first alternative approach that was tested in this study involved using a fixed constant to transform the small scale data into the large scale experimental space. Figure 7.3 above highlights the changes in performance that occured during scale up and the information in this figure was exploited to calculate an offset between the scales. The procedure for this approach was as follows:

1. Perform a detailed exploration of the process at small scale including experiments at the centre points of experimental space.
2. Perform large scale experiments at the centrepoint of the experimental space.
3. Calculate the offset between small and large scale centre point experiments.
4. Transform the small scale experimental results into the large scale experimental space by adding the offset to each data point.
5. Fit model to transformed data to produce characterisation of the large scale process.

This approach only requires an evaluation of the centre point of the large scale experimental space and would be an inexpensive way of transforming the small scale data.

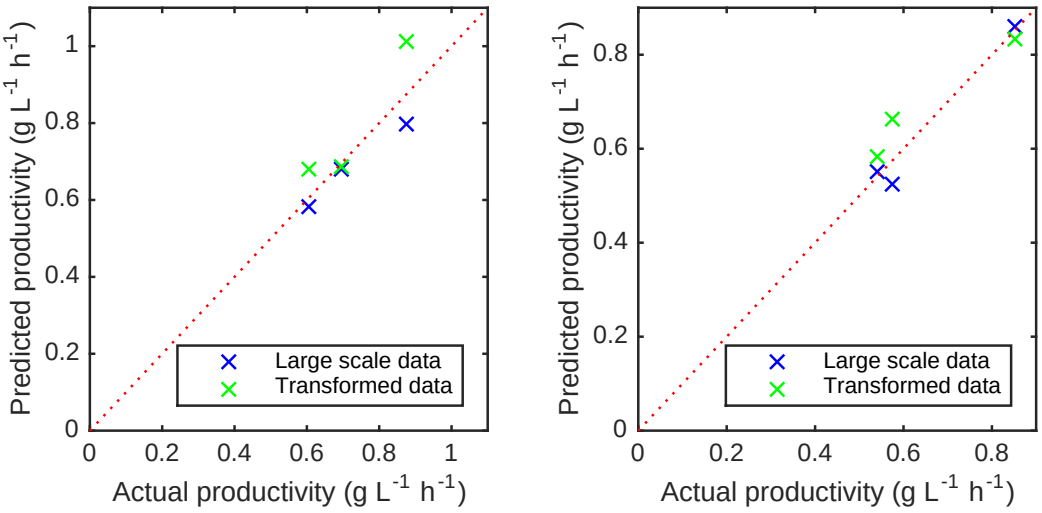

(a) 20 mL column **(b)** 30 mL column

Figure 7.5: Validation of the models fitted to the transformed small scale data. The data was transformed by adding the difference between the centre points to the small scale data. These predictions of these models are compared to the predictions of the models that were fitted to the actual large scale data

This could be done with a single large scale run at the centre point. However, repeats of the centre point run were used to minimise the effects of experimental error. In this study, 3 centre point repeats were carried out on the large scale columns (20 mL and 30 mL) and 7 centre point repeats were carried out for the small scale column (1 mL column). The averaged values of these centre point runs were used to calculate the offsets. The offsets between the 1 mL column and the 20 mL and 30 mL columns were 0.36 $gL^{-1}h^{-1}$ and 0.34 $gL^{-1}h^{-1}$ respectively.

The calculated offset was added to each of the small scale data points to transform that data into the large scale experimental space. The previously identified model (Equation 7.7) was then fitted to the transformed data to produce a process model detailing the large scale experimental space.

The resulting models were validated by predicting the values of the validation runs. The results of the model validation are shown in Figure 7.5.

Figure 7.5 shows the model validation results. This figure and the RMSEP values shown in Table 7.6 show that the use of the transformed data resulted in a reduction in the accuracy of the prediction. However, this could be considered acceptable as the required number of large scale runs was reduced from 11 to 3.

Table 7.6: The calculated root mean squared error of prediction for the validation of the fitted models.

Scale	*Large scale data*	*Transformed data*
20 mL	0.0493	0.0895
30 mL	0.0295	0.0583

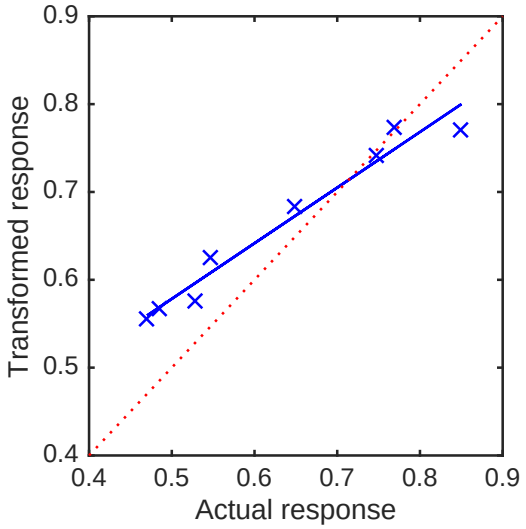

Figure 7.6: Results of transforming the small scale data into the experimental space of the 30 mL column using a constant offset. The constant offset was calculated from the difference between responses at the centre points of the large scale and small scale experimental spaces. The transformed small scale data is plotted against the actual large scale data.

7.3.4 Using a transformation function calculated using additional large scale points

The approach described in the Section 7.3.3 used a constant offset to transform the small scale data and produced a model with a good level of accuracy. But detailed analysis of the transformed data showed that this approach had the potential to produce unsatisfactory results in processes where the changes in the performance are not uniform across the entire experimental space. This is illustrated in Figure 7.6 which shows the transformed data plotted against the actual values for the 30 mL column dataset. In this figure the plotted data points deviate away from the parity line, indicating that the relationship between the small scale response and the large scale response is not constant. At the extremes this variation is approximately 0.1 $gL^{-1}h^{-1}$ which is a significant error as the overall range in response values is only ~ 0.45 — 0.85 $gL^{-1}h^{-1}$.

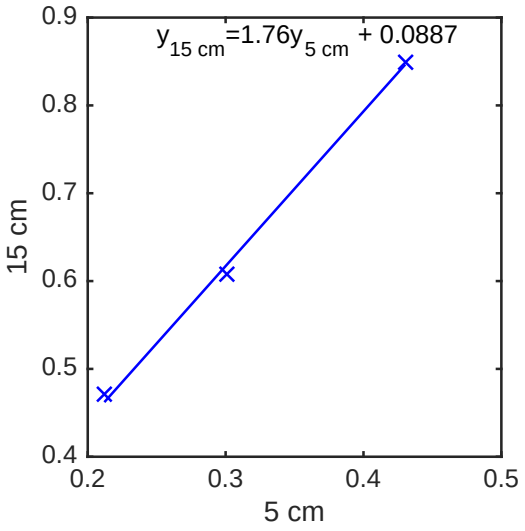

Figure 7.7: Regression between the selected large scale and small scale points to derive a function for transforming small scale data into the large scale experimental space (30 mL column)

This deviation is because the response undergoes greater changes across the experimental space at large scale compared to the small scale. Therefore, a constant offset cannot account for this kind of difference. An alternative approach that would mitigate this effect would be the use of a transformation function that reflected the range of the response in the large scale experimental space.

A simple transformation function can be derived by regressing a small number of large scale data points onto their corresponding small scale data points. In this study, the centre point and the two points located at the extremes of the experimental space (points coded -1,-1,-1,-1 and 1,1,1,1) were used to derive this function as illustrated in Figure 7.7. These points were selected by examining the small scale data and identifying the points which had the highest and lowest response values, and were common to both the small and large scale experimental designs.

The function fitted in Figure 7.7 was used to transform the small scale data into the large scale experimental space. The transformed data was plotted against the actual values in Figure 7.8. There is a good agreement between the actual data and the transformed data, and the deviation seen with the constant offset approach in Figure 7.6 is not seen.

The model previously identified at small scale (Equation 7.7) was fitted to the transformed data to produce a model describing the experimental space of the 30 mL col-

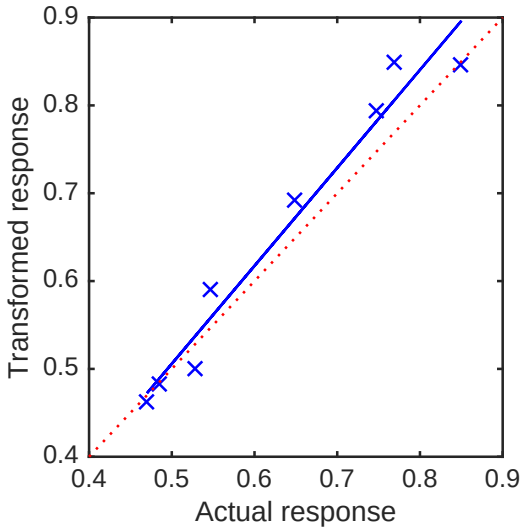

Figure 7.8: Values of the transformed small scale data plotted against the actual data from the experiments carried out on the 15cm column. The transformation was carried out using a function derived from the regression of 3 large scale data points onto the small scale data.

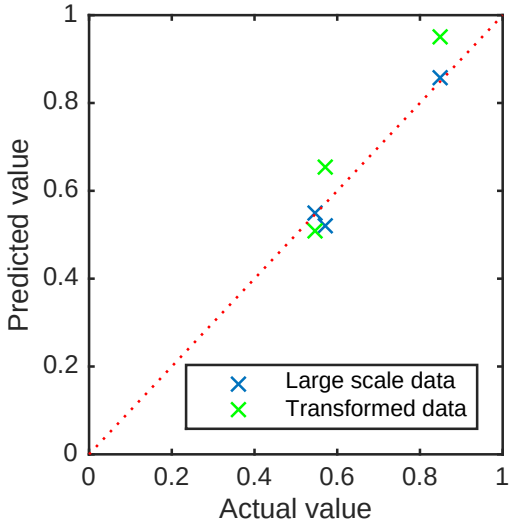

Figure 7.9: Validation of the process model for the 30 mL column produced using small scale data transformed into the large scale experimental space. The data was transformed using a function calculated from the regression of 3 large scale data points onto 3 small scale data points. The predictions are compared to the predictions produced using a model fitted to all available large scale data points.

umn. This model was validated by predicting the values of the validation runs and the results are shown in Figure 7.9. The RMSEP for the model produced from the transformed data is 0.0793. This is unexpectedly greater than the RMSEP for the model produced from the offset data which was 0.0583 but might be considered sufficiently comparable for scale up studies.

7.3.5 Cokriging

In the above sections, two regression methodologies for modelling the experimental space of a purification using transformed small scale data were established. This approach produced accurate predictions but required two modelling steps; the fitting of the transformation functions and the fitting of an appropriate process model to the transformed data. Another approach that has a similar potential to reduce the required amount of large scale experimentation is cokriging. The procedure for producing a cokriging prediction was described in detail in Chapter 5. The cokriging predictions were produced using scripts in MATLAB (The MathWorks Inc., Natick, MA, USA) (see Appendix A).

For this study, all the available data from the 1 mL column and 3 data points from the large scale columns were used. For the 20 mL column, the large scale data points were the points coded as [-2,-2,-2,-2], [0,0,0,0], and [2,2,2,2] in the experimental design. For the 30 mL column, the large scale data points were the points coded as [-1,-1,-1,-1], [0,0,0,0], and [1,1,1,1] in the experimental design. The response data from each scale was standardised by subtracting the mean and dividing by the standard deviation. The spatial relationships between the standardised input datasets were determined by fitting variogram models as shown in Figure 7.10.

In this study the Gaussian variogram model that was used in Chapter 6 was fitted to the raw variogram data to produce variogram models. However, since the input datasets for this study included multiple centre points it was possible to estimate the effect of the experimental error by adding another parameter, c, into the variogram model as shown in Equation 7.8.

$$\gamma = a(1 - exp(-3\frac{h^2}{b^2})) + c \tag{7.8}$$

This parameter represents the intersect and the addition of this parameter helps to prevent the overfitting of the cokriging model. Figure 7.10 shows the variogram models that were fitted to the raw variogram data for the 30 mL column. The covariance functions were then calculated from each of the variograms and used to produce the

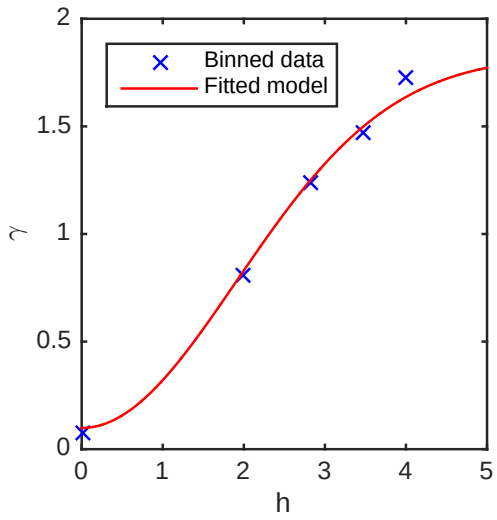

(a) Secondary variogram

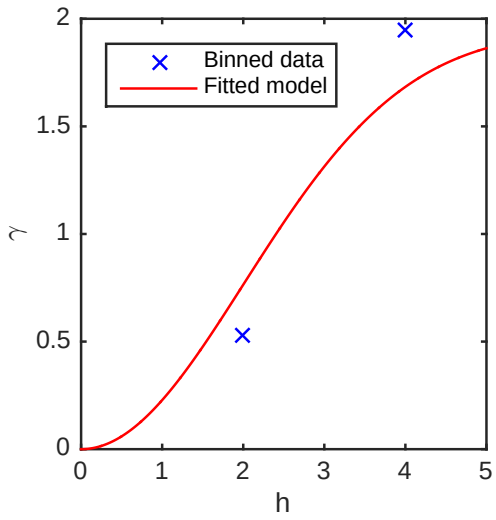

(b) Primary variogram

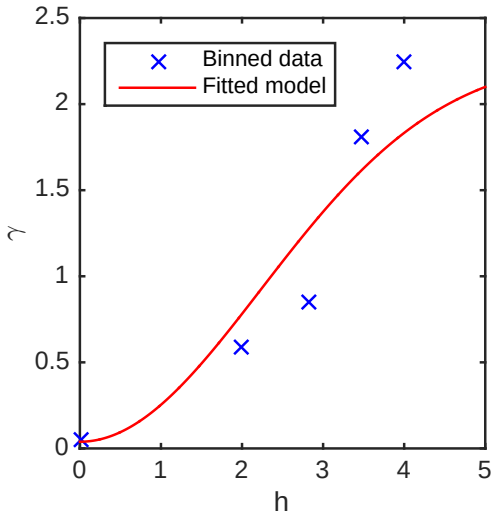

(c) Cross variogram

Figure 7.10: Calculated raw variograms for the secondary response (1 mL) and primary response (30 mL), and the cross variogram between the two responses. Also shown are the fitted Gaussian variogram models. The fitted variogram models were used to calculate the weights for Cokriging prediction of the 30 mL column experimental space.

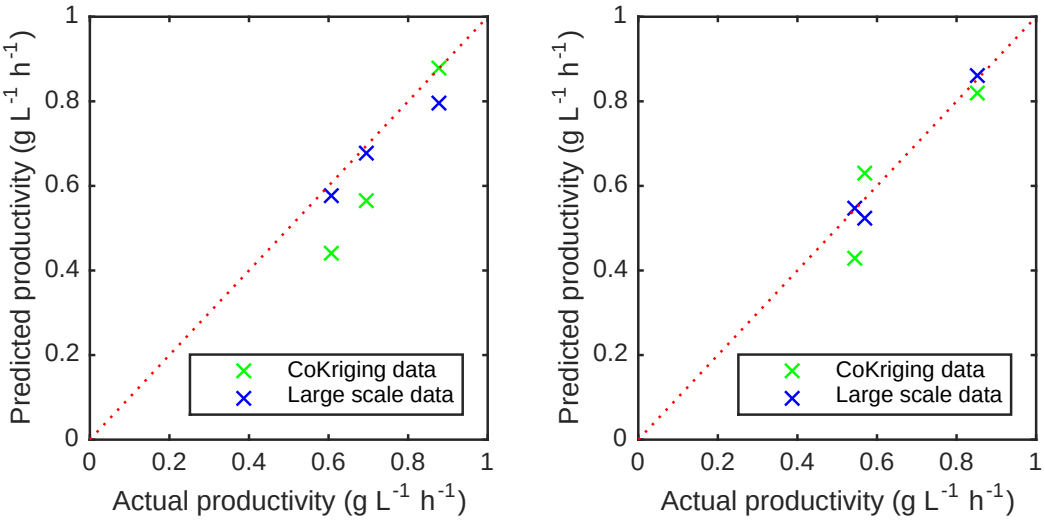

(a) 20 mL **(b)** 30 mL

Figure 7.11: Validation of the Cokriging models produced using 3 large scale data points and the entire small scale data set.

cokriging predictions as previously described in Chapter 5.

Cokriging was used to predict the values of the validation data points for the 20 mL column and the 30 mL column. The results are shown in Figure 7.11. The RMSEP values for the 20 mL column and 30 mL column predictions were 0.1232 and 0.0752 respectively. The input data for the 20 mL column was gathered from a larger range than the 30 mL column, which is the probable cause of the poorer prediction accuracy.

7.4 Conclusion

It was demonstrated that there was a substantial difference between the performance of the small scale scale and large scale columns which prevents the direct use of scale down experiments to describe the large scale experimental space. In this study three approaches were tested for exploiting the small scale data to describe the large scale design space. These approaches were compared to a baseline approach which involved fitting a process model directly to large scale data.

Figure 7.12 summarises the results of this study. As expected the typical approach of fitting a suitable model to large scale data yielded the best results in terms of accuracy. The suitable model was identified at small scale which helped to minimise the number of experiments that were required at large scale. However, this approach still required

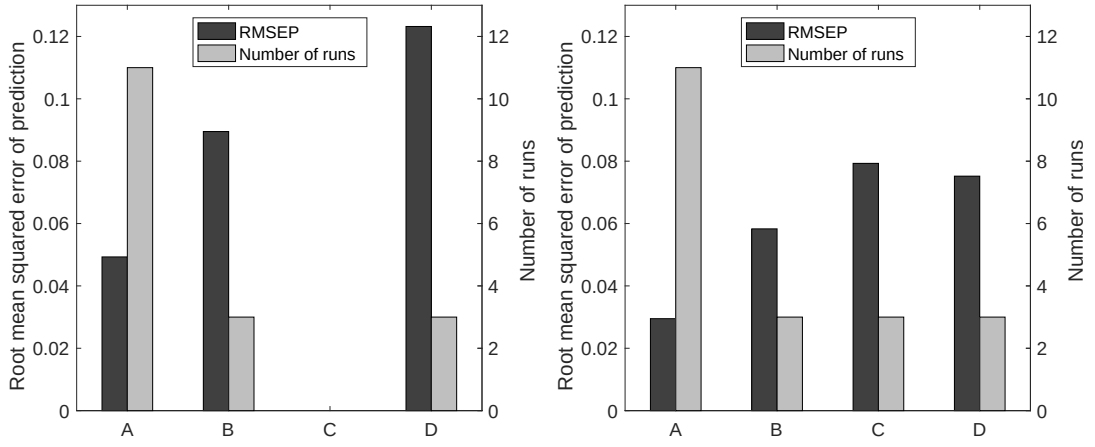

(a) 20 mL **(b)** 30 mL

Figure 7.12: Comparison of the methods used to characterise the large scale chromatographic separation at the 20 and 30 mL column scale. *A* is the use of a model fitted to all the available large scale data. *B* is the use a constant offset to transform the small scale data into the large scale experimental space. The model was then fitted to transformed data. *C* is the same as B but with a transformation function used to transform the data into the large scale. *D* is the use of a cokriging algorithm to produce predictions of the large scale experimental space.

11 runs to be performed at large scale.

The method using a constant offset to transform the small scale data into the large scale space produced good predictions of the large scale experimental space. In this study 3 repeats of the centre point were carried out at large scale but data from a single experiment could be used. However, it was established that this method can lead to transformed data that deviates from the results of the actual large scale experimental space.

These deviations were eliminated through the use of a transformation function created by regressing a few large scale data points onto their equivalent small scale data points. However, unexpectedly this produced a model with a slightly higher RMSEP.

Cokriging was explored as an alternative to using response surface based methods and was also found to have a similar level accuracy to the regression based alternatives.

Figure 7.12 also shows that the predictions for the 20 mL column were consistently worse than the 30 mL column. This can be attributed to the fact that the large scale

input data for this column came from a larger experimental space. This behaviour can be expected for response surface based methods as the examined experimental space widens. As the experimental space widens, the assumption that a response surface can accurately approximate the process can begin to fail. Therefore there was the potential that the non-parametric cokriging approach would perform better under these conditions but this was also found to produce worse predictions.

However, the observed drop in accuracy may be considered acceptable due to the clear savings that were made. For the 30 mL column, the baseline approach required 361 mL of feed material compared to the alternatives which only required 121 mL. Ultimately the choice of method will depend upon speed, material inventory and cost, time, etc. but this work has demonstrated that judicious se of models and DOE can help to expedite scale up.

Chapter 8

Extending the scale-down characterisation methodology to enable the optimisation of a two step purification process with multiple responses

8.1 Introduction

Previously in Chapter 7 two approaches were established for characterising large scale chromatographic purifications. These methods used comprehensive small scale experimentation augmented with a small number of selected large scale experiments. The study detailed in this chapter aims to extend and further test these approaches.

In order to reach the required levels of purity, a typical purification process for a biopharmaceutical product will consist of multiple chromatography or equivalent steps. Other unit operations such as filtration, centrifugation, and precipitation may also be employed to clear impurities. The action of each unit operation will affect the performance of those further downstream, e.g. by changing the impurity burden. Therefore modelling the whole process sequence is important for the definition of robust operating windows. Furthermore, as each unit operation will have different impurity clearance

capabilities, modelling the whole process sequence together will aid the identification of the optimum process conditions. However, it may not be feasible to carry out the amount of experimentation required to produce a detailed characterisation of the whole purification process sequence at a representative scale. A scale down experimental approach coupled with the modelling approaches developed in Chapter 7 has the potential to circumvent this problem.

In Chapter 7 two approaches were established for characterising the experimental space of a process. One approach involved transforming small scale experimental data into the large scale design space, while the other involved using cokriging to combine small scale and large scale data into a single process model. In this study these two approaches were applied to the purification of an antibody fragment (Fab) from *E. coli* lysate. The purification process for the Fab consists of two steps. In the first step the *E. coli* lysate was subjected to a heat treatment which promoted the aggregation of impurities. The supernatent from the heat treatment step was then further purified using a cation exchange chromatography step. The aim of the purification process was to reduce the impurities to an acceptable level while minimising the loss of the product.

In addition to meeting an overall purity specification, many biopharmaceutical products will have minimum specifications set on certain individual impurities. For the Fab purified in this study it was deemed necessary to clear the *E.coli* DNA and host cell proteins down to an acceptable level. The ability to predict the elution profiles of the product and the various impurities at a given set of process conditions can serve as a useful tool for the identification of windows of operation that will satisfy all of the purification criteria. Fractionation diagrams were adapted in this study to enable the modelling of these elution profiles.

8.2 Materials and methods

8.2.1 Materials

All chemicals were obtained from Sigma-Aldrich (Gillingham, Dorset, UK). The cation exchange chromatography experiments were carried out using S HyperCel™ sorbent packed in 1 mL (5 cm bed height and 0.5 cm diameter) and 5 mL (10 cm bed height and

0.8 cm diameter) pre-packed PRC columns (Pall Life Sciences, Portsmouth, UK) connected to an AKTA Avant™ 25 (GE Healthcare Life Sciences, Little Chalfont, Bucks, UK).

8.2.2 Feedstock

An *E. coli* w3110 strain (ATCC 27325) containing the plasmid pTTOD A33 IGS2 coding for a 46 kDa antibody fragment (Fab) utilising a tac promoter was kindly donated by UCB Pharma Ltd. (Slough, UK). High cell density fed-batch fermentations were performed in a 7L Applikon vessel (Applikon Biotechnology B.V., Schiedam, Holland), with a 5 L working volume.

The Fab was expressed in the periplasmic space of the *E. coli* cell. In this study the fermenter was harvested approximately 80 hours after inducing the expression of the Fab. At the point of harvesting the majority of the cells had lysed, releasing the product into the fermentation broth. The harvested fermentation broth was centrifuged at 10000 rpm in JA-10 rotor in a Beckman Coulter J2 for 30 minutes to remove the *E. coli* cell debris.

8.2.3 Heat treatment

The expressed Fab is stable at 60 °C. Incubating the fermentation broth at this temperature causes some of the impurities to aggregate while leaving the product in solution. The harvested fermentation broth was placed in shake flasks and incubated at 60 °C while shaking at 400 rpm. The length of the incubation was varied according to the experimental design detailed in Section 8.2.5. After the heat treatment the aggregated impurities were removed by centrifuging the suspension at 10000 rpm in a JA-10 rotor in a Beckman Coulter J2 for 30 minutes.

At this point the supernatent retained most of the components of the fermentation media. Therefore the supernatent had a high conductivity which would hinder the binding of the Fab to the cation exchange chromatography resin. Therefore the Fab was buffer exchanged into 100 mM tris at pH 7.4 using Slide-A-Lyzer dialysis flasks (Life Technologies, Paisley, UK) with a 10 kDa molecular weight cut-off. The feed stock was then adjusted to pH 4.5 with 1 M acetic acid to promote the binding of the Fab to

the chromatography resin. Finally the pH adjusted solution was filtered using 0.2 μm PVDF filters to remove any aggregates.

8.2.4 Cation exchange chromatography

Cation exchange chromatography was used to separate the Fab from the remaining impurities present in the feedstock. This purification was performed using the following procedure:

1. **Equillibration** - The column was equilibrated with 5 column volumes (CV) of 20 mM sodium acetate, pH 4.5.

2. **Load** - The heat treated Fab feedstock was injected onto the column (the injection volumn was a variable in these experiments).

3. **Wash** - The column was washed with 5 CV of 20 mM sodium acetate, pH 4.5 to clear any unbound proteins.

4. **Elution** - An elution gradient from 20 mM sodium acetate, pH 4.5 to 20 mM sodium acetate, 400 mM NaCl, pH 4.5 was used to elute the bound proteins (the length of the gradient was a variable in these experiments). 1 CV fractions were collected during the elution phase.

5. **Regeneration** - The column was stripped with 3 CV of 6 M guanidine-HCl to remove any remaining bound proteins. This harsh regeneration solution was used because less aggressive solutions such as 1 M NaOH did not demonstrate complete regeneration of the column, which affected the binding capacity of subsequent runs.

A residence time of 4 minutes was maintained for all experiments. The injection volume and the gradient length for each experiment were as defined in the experimental design in Section 8.2.5. The dimensions of the small and large scale columns that were used in this study are detailed in Table 8.1. An example chromatogram for this separation is shown in Figure 8.1.

Table 8.1: Characteristics of the columns used in this study

Parameter	Small scale column	Large scale column
Height (cm)	5	10
Diameter (cm)	0.5	0.8
Column volume (mL)	0.982	5.03

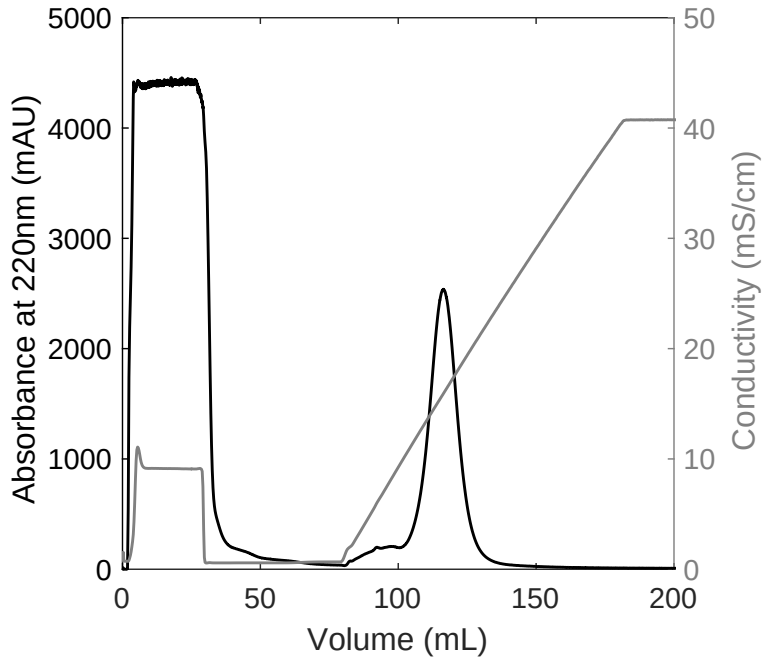

Figure 8.1: Chromatogram for experiment carried out at the centre point of the large scale design space. For this experiment the injection volume was 25 mL, the gradient length was 20 CV and the feed material had been heat treated for 10 h.

8.2.5 Experimental design

The factors which had the most impact on the process were identified as the length of the heat treatment, the injection volume and the length of the elution gradient of the cation exchange step. The length of the heat treatment step has a direct impact on the impurity profile of the feed to the chromatography experiments. The injection volume can affect the recovery of the product and the clearance of the impurities. If the injection volume is too large the binding capacity of the column may be exceeded. However, a large injection volume can be beneficial as the product may displace impurities with a

Table 8.2: Central composite circumferential experimental design carried out on the small scale column column with a 1 mL column volume. Runs 9, 10 and 11 are centre points while Runs 12 — 17 are located at the extremes of each of the process variables.

Run	Injection volume (mL)	Gradient length (CV)	Heat treatment (h)
1	4	16	4
2	4	16	16
3	4	24	4
4	4	24	16
5	6	16	4
6	6	16	16
7	6	24	4
8	6	24	16
9	5	20	10
10	5	20	10
11	5	20	10
12	3.32	20	10
13	6.68	20	10
14	5	13.27	10
15	5	26.73	10
16	5	20	0
17	5	20	20

lower affinity to the resin which improves the purity of the bound product. The length of the elution gradient affects the resolution between the product and the impurities.

For this study the small scale column had a 1 mL column volume and the large scale column had a 5 mL column volume. At the small scale a central composite circumferential design consisting of 14 runs and 3 centre point runs was performed to produce a thorough characterisation of the purification process. At the large scale a fractional factorial experimental design with 4 runs and 3 centre point runs was performed. Two additional runs were also performed at large scale for model validation purposes. The experimental designs are detailed in Tables 8.2 and 8.3.

8.2.6 Assays

The Fab concentrations in each of the eluate fractions were determined by Protein G chromatography. The Protein G method was carried out using a HiTrap™ Protein G HP column (GE Healthcare Life Sciences, Little Chalfont, Bucks, UK) connected to a Agilent 1200 HPLC system (Agilent Technologies, Santa Clara, CA, USA).

Table 8.3: Experimental design for the large scale column with a 5 mL column volume. Runs 1 — 7 are a fractional factorial design with 3 centre points. Runs 8 and 9 were used for model validation.

Run	Injection volume (mL)	Gradient length (CV)	Heat treatment (h)
1	20	16	16
2	20	24	4
3	30	16	4
4	30	24	16
5	25	20	10
6	25	20	10
7	25	20	10
8	22.5	18	5
9	17.5	14	3

The total protein concentration in the eluate fractions was determined in order to quantify the overall impurity levels. The purity of the eluate fractions was determined by dividing the Fab concentration by the total protein concentration. The concentrations of two specific residual impurities, *E. coli* DNA and host cell proteins were also determined. To improve the analytical throughput, these assays were only carried out on eluate fractions with a Fab concentration greater than 0.075 g/L.

The total protein concentration was determined using the Pierce™ BCA protein assay kit (Life Technologies, Paisley, UK). The DNA concentration was determined using the Quant-iT™ PicoGreen® dsDNA assay kit (Life Technologies, Paisley, UK). The *E. coli* host cell protein concentration was determined using the *E. coli* HCP ELISA kit (Cygnus Technologies, Southport, NC, USA). The assays were carried out according to the manufacturer's instructions.

8.3 Results and discussion

8.3.1 Clearance of impurities across the heat treatment and chromatography unit processes

Figure 8.2 shows how the duration of the 60 °C heat treatment affected the composition of the lysate. Figures 8.2a and 8.2b show that the concentration of the heat stable Fab remained constant while there was a reduction in the total protein concentration over

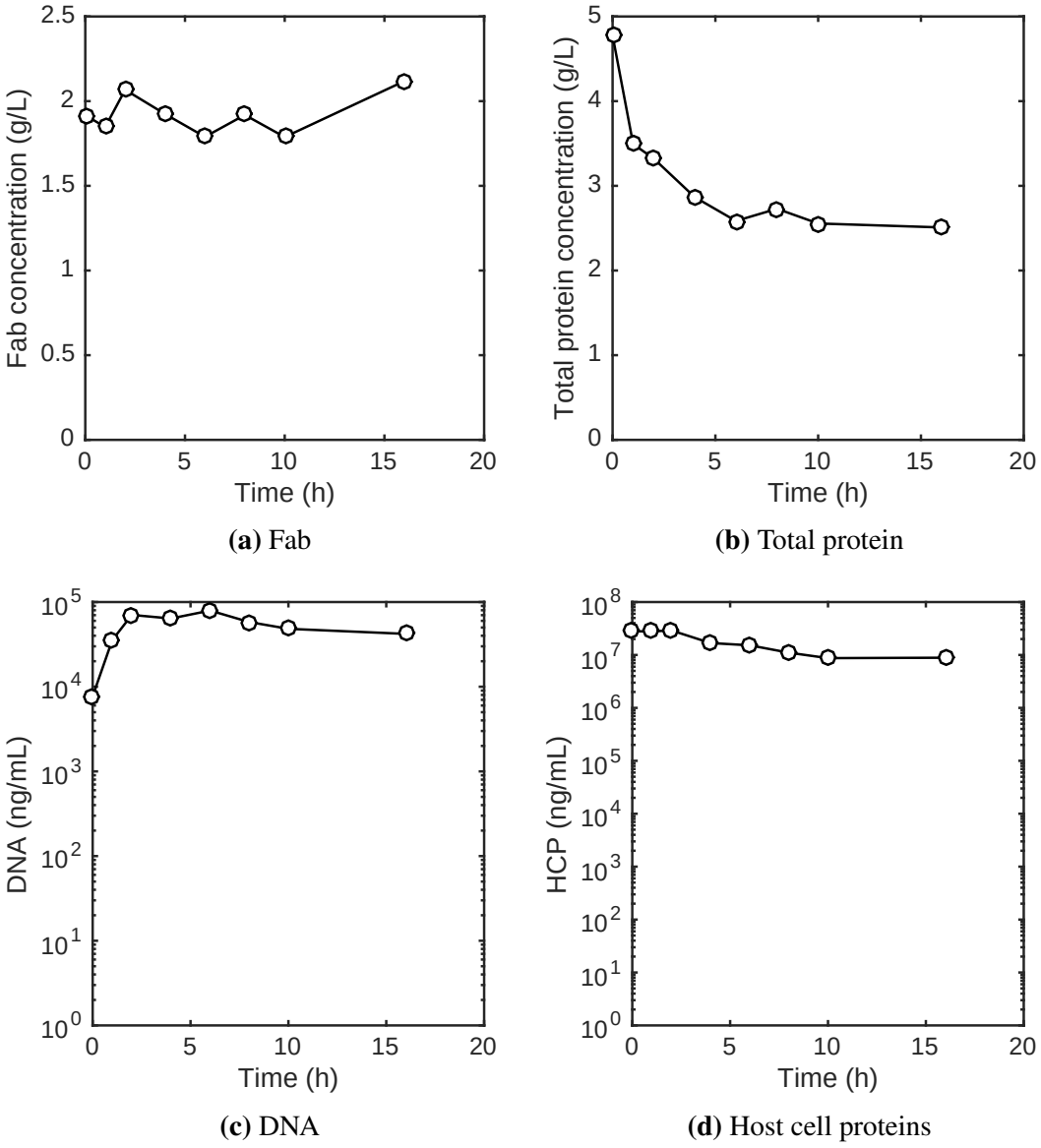

(a) Fab **(b)** Total protein

(c) DNA **(d)** Host cell proteins

Figure 8.2: Effect of the heat treatment duration on the concentration of Fab, total protein, DNA, and host cell proteins in the clarified *E. coli* lysate.

the course of the heat treatment. Over the first 6 hours of the heat treatment step there is an approximately 46% reduction in total protein concentration from 4.78 g/L to 2.59 g/L. This reduction in total protein concentration corresponds to an increase in purity from 40.1% to 69.2%. However, after the initial 6 hours, a further reduction in the total protein concentration is not observed over the next 10 hours of the heat treatment step.

Figures 8.2c and 8.2d show the effect of the heat treatment step on the host cell DNA and host cell protein (HCP) levels. As these contaminants are potentially immunogenic or may trigger other harmful side effects it is important to reduce their levels to very low

or undetectable levels. The acceptable levels of these contaminants are established for each product but as a general guideline less than 100 pg of DNA per therapeutic dose (Wolter and Richter, 2005) and a HCP concentration of less than 100 ng/mg (Wang and Richardson, 2015) is considered acceptable. The initial DNA and HCP concentrations in the lysate were 7730 ng/mL and 2.8×10^7 ng/mL which are substantially higher than the guideline acceptable levels.

Figure 8.2c shows that a substantial reduction in DNA levels was not observed throughout the duration of the heat treatment step which was expected as DNA is stable at 60 °C (Bartlett and Stirling, 2003). However, an initial increase from 7730 ng/mL to 70400 ng/mL was measured during the first two hours of the heat treatment. This may be due other proteins in the lysate causing interference with the PicoGreen DNA assay. Such interferences can be caused by host cell proteins in the lysate that bind to DNA which in turn prevents the binding of PicoGreen. As the heat treatment proceeds the interfering proteins are cleared from the lysate which results in an increase in the measured DNA concentration.

Figure 8.2d shows that the HCP concentration reduces by an order of magnitude from 2.80×10^7 ng/mL to 8.87×10^6 ng/mL over the course of the 16 h heat treatment. However, further purification is required to reduce the HCP concentration to an acceptable level.

Figure 8.3 shows the changes in the composition of the product over the purification sequence for the experiment carried out at the centre of the design space (Run 6). For this experiment the clarified lysate was heat treated for 10 h and the injection volume of the cation exchange chromatography column was 25 mL. The bars in this figure show the impurity levels in the clarified lysate before the purification sequence, in the lysate after 10 h of heat treatment, and in the cation exchange chromatography column eluate. This figure highlights that while the heat treatment step was the most effective at increasing the overall purity of the product, the CEX step had a greater capability to reduce the DNA and HCP levels which are reduced by several orders of magnitude.

Figure 8.4 shows the chromatograms for the experiment carried out at the centre of the large scale design space (Run 6). In this experiment the injection volume was 20

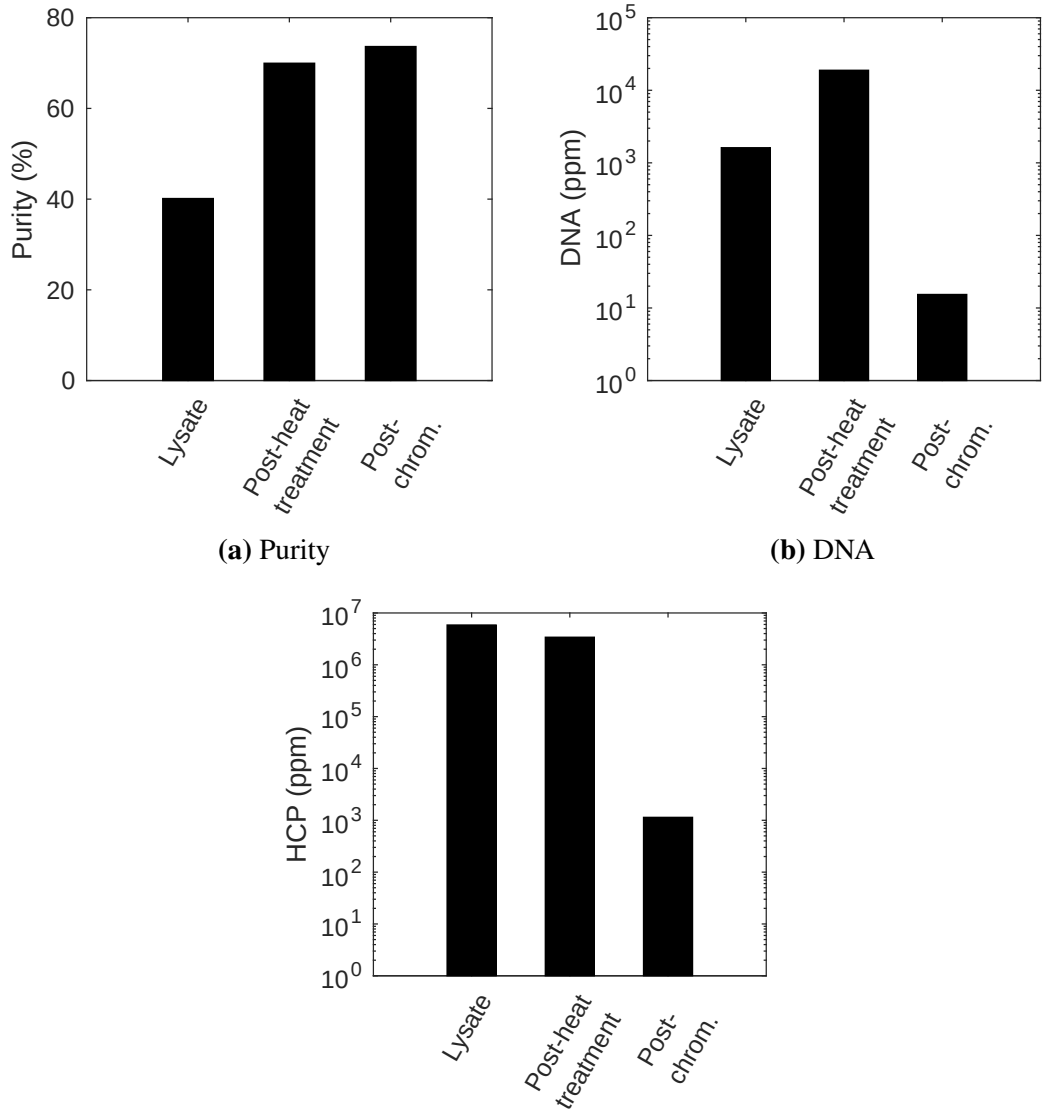

(a) Purity

(b) DNA

(c) Host cell proteins

Figure 8.3: Bar graphs showing the changes in the impurity profile across the two-step purification process at the centre of the large scale design space (Run 6). In this experiment the duration of the heat treatment was 10 h. The cation exchange chromatography column was then loaded with 25 mL of the lysate. Figure 8.3a shows the changes to the purity of the product while Figures 8.3b and 8.3c show the changes to the DNA and host cell protein levels.

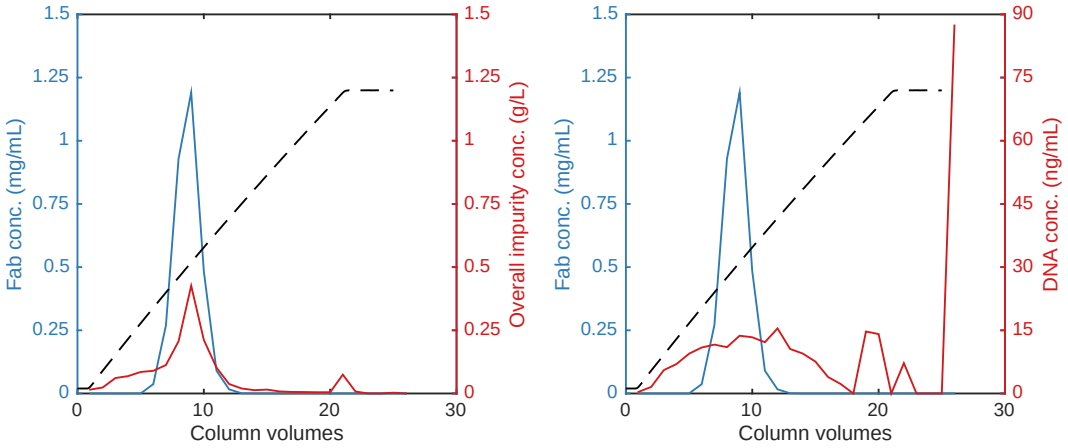

(a) Overall impurities **(b)** DNA

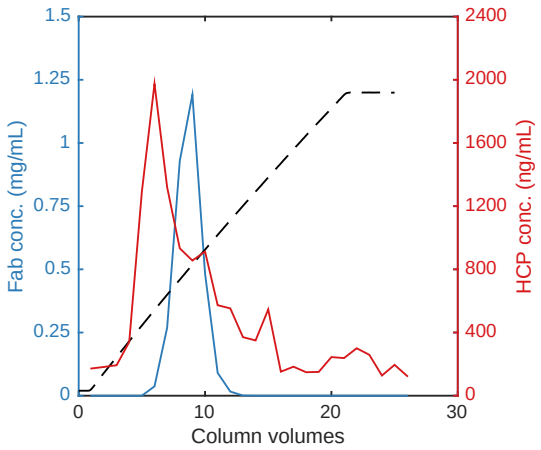

(c) Host cell proteins

Figure 8.4: Elution profiles from the cation exchange column for the product and impurities in this study. These profiles are for the experiment carried out at the centre point of the large scale design space (Run 6). The dashed line shows the change in the conductivity caused by the elution gradient. In Figure 8.4a the overall impurity concentration was determined by subtracting the Fab concentration from the total protein concentration.

mL while the gradient length was 20 column volumes. A large proportion of the HCP and DNA clearance stems from these impurities not binding to the column during the load phase. Figure 8.4 shows that there are varying levels of resolution between the product and the different impurities. Therefore, in order to optimise the cuts used to collect the product during the elution phase, it was necessary to model each individual impurity. As the resolution of these impurities from the product will also be influenced by the injection volume and the gradient length, as well as the composition of the feed to the column, it was important to include these factors in any process model used for optimisation.

As Figure 8.3 showed, the heat treatment step and the CEX step have different impurity clearance capabilities. To ensure that both the final purity specification of the product was met and the best utilisation of each process step was made, it was necessary to optimise the entire process sequence together. This required process models of the entire sequence. In this study consisting of two process steps, the design space for the process sequence was reduced to three critical process parameters. However, in other process sequences many more process parameters may need to be included in the design space. Furthermore, a typical downstream process will consist of around three chromatography steps and 2 - 3 clarification and filtration steps. This can lead to a very large design space with interactions between the parameters spanning the various process steps. Fitting adequate models to such a design space will require a large amount of experimentation which highlights the benefit of using a scale down approach.

8.3.2 Simplification of the chromatograms to cumulative elution profiles

The importance of reducing specific impurities to acceptable levels was highlighted above in Section 8.3.1. In these situations being able to predict the elution profile of each impurity will allow the determination of the optimum elution pools that satisfy all the impurity clearance criteria set on the process. The chromatogram is the usual form of presenting the elution profile. However, these include multiple peaks of different shapes and sizes and due to this complexity they cannot be easily used as the basis for

building process models.

Salisbury et al. (2006) described an approach for calculating a fractionation diagram from a chromatogram. The typical fractionation diagram plots the fraction of product in the eluate vs. the fraction of total protein in the eluate. The calculation of these diagrams was discussed in greater detail in Section 6.2.3. In this study this approach was adapted to plot the cumulative elution profile (CEP) of each species in the eluate (Fab, total protein, DNA, and HCP) against the fraction of Fab product. The fraction of Fab was calculated using Equation 8.1 and the cumulative masses of the Fab, total protein, DNA, and HCP were calculated using Equations 8.2, 8.3, 8.4 and 8.5.

$$x = \frac{\sum_{i=0}^{i} M_{Fab,i}}{\sum_{i=0}^{N} M_{Fab,i}} \tag{8.1}$$

where the eluate is divided into $i = 1,2,3\cdots N$ fractions and $M_{Fab,i}$ is the mass of Fab in fraction i.

$$y_{Fab} = \sum_{i=0}^{i} M_{Fab,i} \tag{8.2}$$

$$y_{T} = \sum_{i=0}^{i} M_{T,i} \tag{8.3}$$

$$y_{DNA} = \sum_{i=0}^{i} M_{DNA,i} \tag{8.4}$$

$$y_{HCP} = \sum_{i=0}^{i} M_{HCP,i} \tag{8.5}$$

where $M_{Fab,i}$, $M_{T,i}$, $M_{DNA,i}$ and $M_{HCP,i}$ are the respective masses of Fab, total protein, DNA and HCP in fraction i.

The cumulative elution profiles (CEPs) are then plots of y vs. x for each of the species as shown in Figure 8.5. These CEPs correspond to the chromatograms in Figure 8.4. These plots have a common x axis and the content of the eluate pool collected between two points on this can be calculated from the difference between the corresponding y

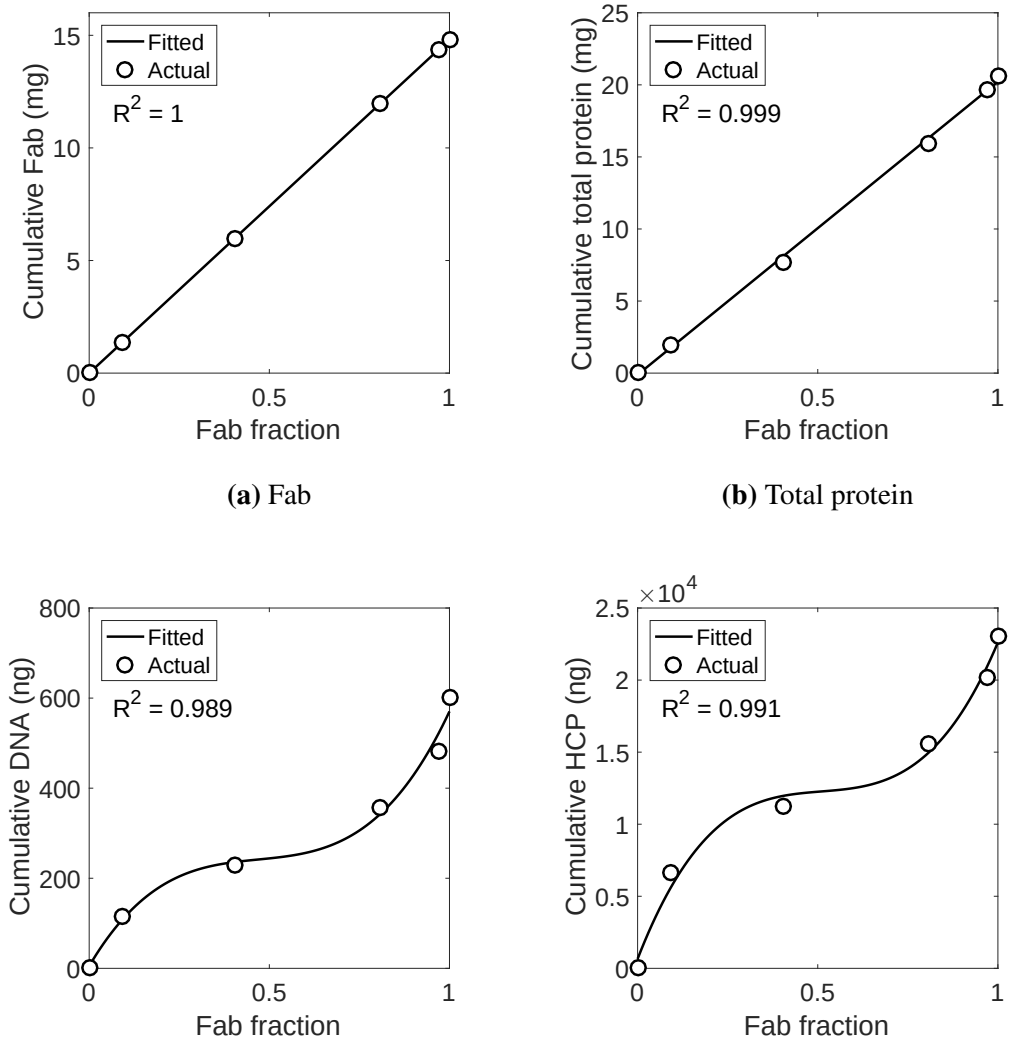

(a) Fab **(b)** Total protein

(c) DNA **(d)** Host cell proteins

Figure 8.5: Cumulative elution profiles (CEPs) calculated for the chromatograms from the centre point of the large scale design space (Run 6). Also shown are curves fitted to the CEP data and their corresponding R^2 values. First degree polynomials were fitted to the Fab and total protein CEPs while third degree polynomials were fitted to the DNA and HCP CEPs.

values of these curves.

In this study CEPs were calculated from the chromatograms for each experiment. The data from the CEPs can then be used to create the datasets for building the process models. This is achieved by adding the Fab fraction as a variable in addition to the process variables. The responses are then the cumulative masses of Fab, total protein, DNA and HCP.

Table 8.4: Format of the data after the processing of the chromatograms to produce cumulative elution profiles. x_{inj}, x_{grad}, x_{heat}, and x_{frac} are the injection volume (mL), gradient length (CV), heat treatment duration (h) and product fraction respectively. y_{Fab}, y_{total}, y_{DNA}, and y_{HCP} are the cumulative mass of Fab (mg), cumulative mass of total protein (mg), cumulative mass of DNA (ng) and cumulative mass of HCP (ng) respectively.

Run	x_{inj}	x_{grad}	x_{heat}	x_{frac}	y_{Fab}	y_{total}	y_{DNA}	y_{HCP}
1	20	16	16	0	0	0	0	0
1	20	16	16	⋮	⋮	⋮	⋮	⋮
1	20	16	16	1	2.99	3.34	50.0	3300
2	20	24	4	0	0	0	0	0
2	20	24	4	⋮	⋮	⋮	⋮	⋮
2	20	24	4	1	3.69	3.71	140	3810
⋮	⋮	⋮	⋮	⋮	⋮	⋮	⋮	⋮

Table 8.4 shows the format of the experimental data after it was processed to produce the corresponding CEPs. By fitting a model to this data, the cumulative mass of Fab, total protein, DNA and HCP in the eluate can be predicted at any point in the design space of the process. The yield, overall purity, DNA content and HCP content for any eluate pool can then be easily calculated.

8.3.3 Model fitted to the available large scale data

The fractional factorial experimental design detailed in Table 8.3 was carried out on the large scale column. For the three process parameters included in this study this experimental design consisted of 4 runs. This experimental design allowed for the estimation of the main effects. This would result in a model of the form shown in Equation 8.6. Centre points may be added to test for curvature in the response but will not enable the estimation of interactions or quadratic effects.

$$y \sim x_{inj} + x_{grad} + x_{heat} + 1 \tag{8.6}$$

where y was a given response and x_{inj}, x_{grad}, and x_{heat} were the process variables (injection volume, gradient length, heat treatment duration).

The use of the cumulative elution profile (CEPs) approach detailed in the previous sec-

tion creates an additional variable x_{frac} which was included in the model. Polynomials were fitted to the CEPs to determine the suitable approach for including the Fab fraction in the process model. The lowest order polynomials that provided $R^2 \approx 1$ were first order for the Fab and total protein and third order for the DNA and HCP cumulative elution profiles as shown in Figure 8.5. The generic model in Equation 8.6 was then updated to reflect this additional variable as shown in Equations 8.7, 8.8, 8.9, and 8.10.

$$y_{Fab} \sim x_{inj} + x_{grad} + x_{heat} + x_{frac} + 1 \tag{8.7}$$

$$y_{total} \sim x_{inj} + x_{grad} + x_{heat} + x_{frac} + 1 \tag{8.8}$$

$$y_{DNA} \sim x_{inj} + x_{grad} + x_{heat} + x_{frac}^3 + x_{frac}^2 + x_{frac} + 1 \tag{8.9}$$

$$y_{HCP} \sim x_{inj} + x_{grad} + x_{heat} + x_{frac}^3 + x_{frac}^2 + x_{frac} + 1 \tag{8.10}$$

where y_{Fab} was the cumulative mass of Fab, y_{total} was the cumulative mass of total protein, y_{DNA} was the cumulative mass of DNA, y_{HCP} was the cumulative mass of HCP and x_{frac} was the fraction of product in the eluate. These models were then fitted to the available data.

8.3.4 Using splines to align the small and large scale data

Sections 8.3.5 and 8.3.6 below will show that the data tranformation and cokriging approaches used in this study required that the small scale and large scale data be aligned to each other. However, using the cumulative elution profile approach produced data where the product fraction values varied from run to run. Therefore, sets of points that were at identical locations in both the large and small scales were created by interpolation using piecewise cubic Hermite interpolating polynomials as shown in Figure 8.6. The interpolation was perfomed using the *pchip* function in MATLAB.

8.3.5 Model fitted to the transformed small scale data

The small scale data transformation approach established in Section 7.3.4 was used in this study to produce a process model using the minimum amount of large scale data. At the small scale a central composite circumferential experimental design was performed

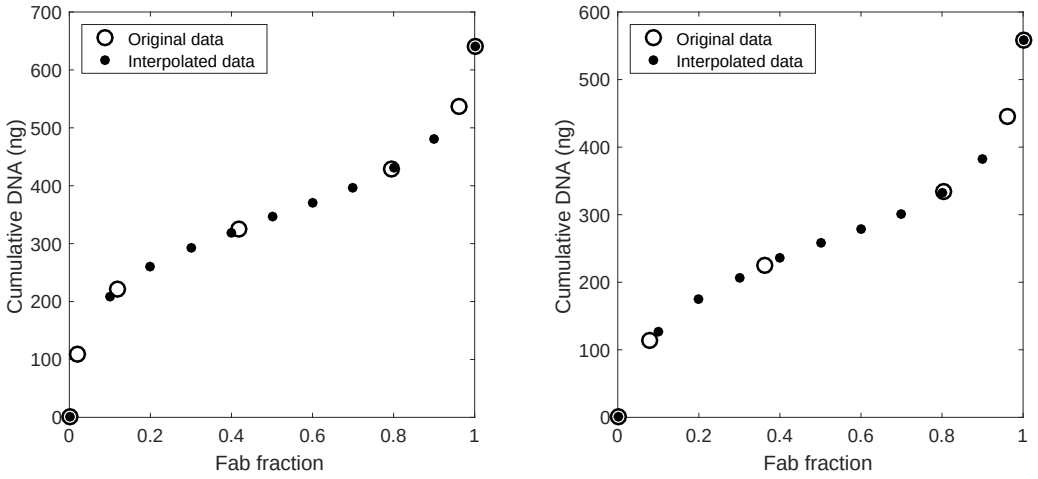

(a) Small scale **(b)** Large scale

Figure 8.6: Figure illustrating the interpolation of new points from the original data to enable the calculation of tranformation functions. The new points were interpolated using piecewise cubic Hermite interpolating polynomial splines.

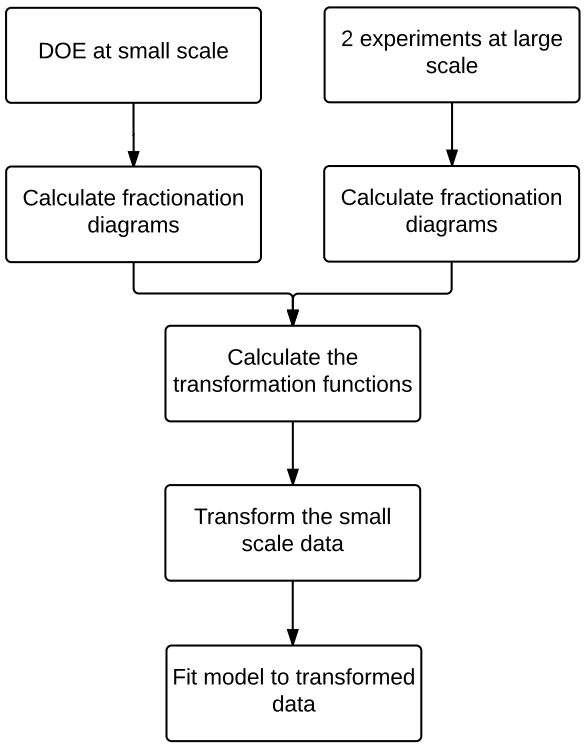

Figure 8.7: Flow chart showing the procedure for using transformed small scale data to characterise the large scale process

consisting of 14 runs and 3 centre point runs as detailed in Table 8.2. Two large scale runs, at [0, 0, 0] and [1, -1, -1], were used to derive the transformation functions. These runs were selected as they represented the highest and lowest values of the responses.

As described in Section 7.3.4 the derivation of the transformation function required regressing the large scale data against the small scale data located at the same points in the design space. To enable this regression the small and large scale datasets were aligned by interpolating new data points at regular intervals using the approach described above in Section 8.3.4.

The interpolated large scale and small scale data were then plotted against each other as shown in Figure 8.8. First order polynomials were found to be sufficient to model the transformation of the Fab, total protein and DNA concentrations while a second order polynomial was required to model the transformation of the HCP data. The cause of the second order relationship is potentially due to increased resolution that occurs between the product and HCP peaks at large scale. At large scale the velocity of the mobile phase is higher which reduces the diffusive effects and in turn may improve the resolution of the peaks.

The transformation functions then take the forms shown in Equations 8.11 to 8.14.

$$y_{Fab,LS} \sim y_{Fab,SS} \tag{8.11}$$

$$y_{total,LS} \sim y_{total,SS} \tag{8.12}$$

$$y_{DNA,LS} \sim y_{DNA,SS} \tag{8.13}$$

$$y_{HCP,LS} \sim y^2_{HCP,SS} \tag{8.14}$$

where $y_{Fab,LS}$, $y_{total,LS}$, $y_{DNA,LS}$, and $y_{HCP,LS}$ were the cumulative masses of Fab, total protein, DNA and HCP at large scale and $y_{Fab,SS}$, $y_{total,SS}$, $y_{DNA,SS}$, and $y_{HCP,SS}$ were the cumulative masses of Fab, total protein, DNA and HCP at small scale.

As the transformed dataset consists of a more comprehensive central composite circumferential experimental design, a more robust model can be fitted. The generic model consisted of all quadratic terms, second order interactions, main effects as shown in

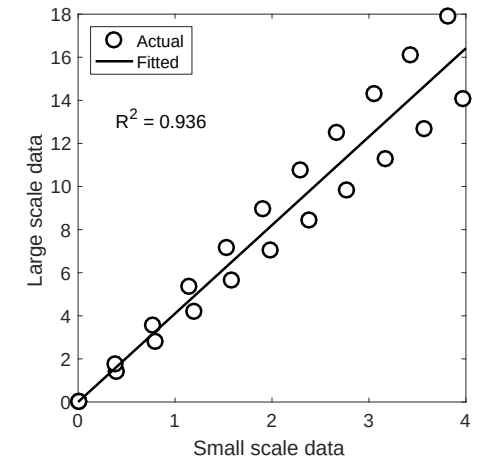

(a) Fab (mg)

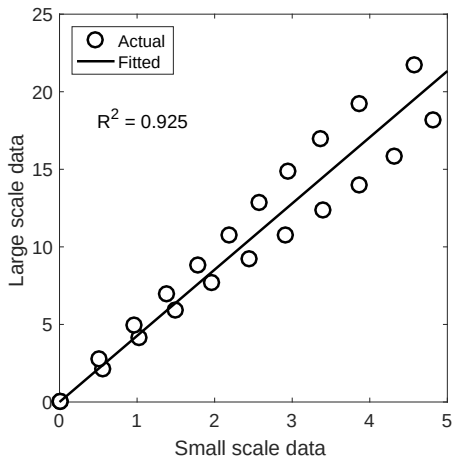

(b) Total protein (mg)

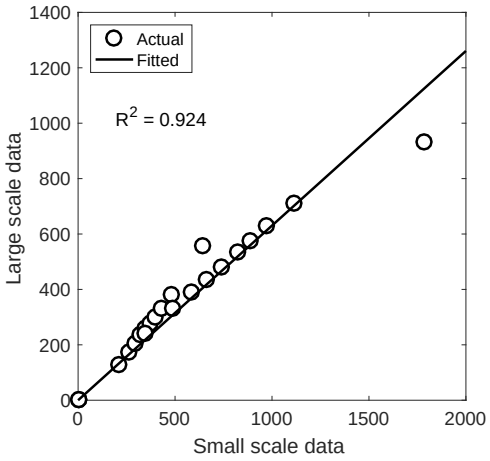

(c) DNA (ng)

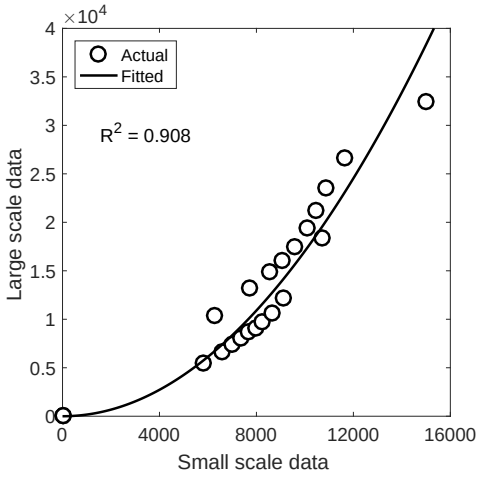

(d) Host cell proteins (ng)

Figure 8.8: Derivation of the functions used to transform the small scale data into the large scale design space. The functions were derived by plotting corresponding large and small scale data against each other. The R^2 values for the fitted transformation functions are also shown.

Equation 8.15.

$$y \sim x_{inj}^2 + x_{grad}^2 + x_{heat}^2 + x_{inj}x_{grad} + x_{inj}x_{heat} + x_{grad}x_{heat} + x_{inj} + x_{grad} + x_{heat} + 1 \quad (8.15)$$

Further terms were added to this model to incorporate the product fraction using the same approach as in Section 8.3.3 above resulting in the models shown in Equations 8.16, 8.17, 8.18, and 8.19.

$$y_{Fab} \sim x_{inj}^2 + x_{grad}^2 + x_{heat}^2 + x_{inj}x_{grad} + x_{inj}x_{heat} + x_{grad}x_{heat} + x_{inj} + x_{grad} + x_{heat} + x_{frac} + 1 \quad (8.16)$$

$$y_{total} \sim x_{inj}^2 + x_{grad}^2 + x_{heat}^2 + x_{inj}x_{grad} + x_{inj}x_{heat} + x_{grad}x_{heat} + x_{inj} + x_{grad} + x_{heat} + x_{frac} + 1 \quad (8.17)$$

$$y_{DNA} \sim x_{inj}^2 + x_{grad}^2 + x_{heat}^2 + x_{inj}x_{grad} + x_{inj}x_{heat} + x_{grad}x_{heat} + x_{inj} + x_{grad} + x_{heat} + x_{frac}^3 + x_{frac}^2 + x_{frac} + 1 \quad (8.18)$$

$$y_{HCP} \sim x_{inj}^2 + x_{grad}^2 + x_{heat}^2 + x_{inj}x_{grad} + x_{inj}x_{heat} + x_{grad}x_{heat} + x_{inj} + x_{grad} + x_{heat} + x_{frac}^3 + x_{frac}^2 + x_{frac} + 1 \quad (8.19)$$

8.3.6 Using cokriging to produce predictions of the large scale design space

In this study the cokriging approach described in Section 7.3.5 was used to produce predictions of the design space of the large scale process. The data from all 17 small scale runs and the 5 large scale runs that made up a fractional factorial design with 1 centre point were used to create the secondary and primary input datasets for the cokriging algorithm.

These initial datasets took the form shown in Table 8.4 where the product fraction was treated as an additional input variable. However, using this dataset to produce cokriging

predictions resulted in predictions that had very large errors. Analysis showed that this stemmed from the cokriging algorithm calculating very large weights for some data points and very small weights for others. As described in Chapter 7, cokriging predictions are calculated as a weighted sum of the known points in the experimental space. The cokriging approach used in this study was formulated to produce weights that sum to a total of one. For a well formulated cokriging prediction each weight should be between 0 and 1. However, in this case it was found that some of the weights were greater than 1 while others were less than 0. These extreme weights were then contributing to the cokriging predictions which had a large error.

These negative weights arise when data points close to the point being predicted screen outlying data points (Deutsch, 1996). The initial dataset described above included the product fraction as a variable. Therefore each run was represented as a clustered subset of datapoints within the overall dataset. The runs closest to the point to be predicted would then screen the outlying runs which resulted in the extreme weights that were calculated. This is illustrated in Figure 8.9. In this example x_2 is similar to the product fraction variable which is clustered into the values of x_1 which is similar to the process variables in this study.

To avoid this issue new large scale and small scale input datasets were created from the initial datasets where each run was represented by a single data point. The first step was to identify product fraction value for the point to be predicted. The interpolation technique described above in Section 8.3.4 was then used to calculate the response value at this product fraction value for each run. A new dataset was then constructed from the calculated response values which was specific to this product fraction value and therefore did not include the product fraction as a variable.

To reduce further the screening effect a neighbourhood approach was used for the calculation of the cokriging prediction. In this approach, the input dataset was reduced to a neighbourhood around the prediction points. The neighbourhood for each prediction point was defined as being the nearest 3 large scale datapoints and 5 small scale data points.

After creating the input datasets for each prediction the raw primary, secondary and

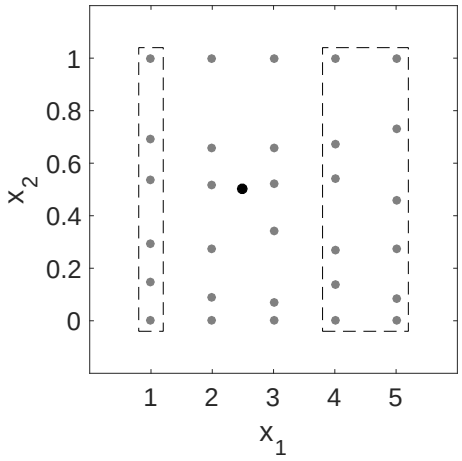

Figure 8.9: Figure illustrating the screening effect that causes the calculation of extreme cokriging weights. In this example x_1 and x_2 are the input variables, the grey dots represent known data points and the black dot represents the point to predicted. The rectangles highlight the outlying data points that are screened by the data points that lie closer to the point to be predicted. This screening effect leads to extremely high weights for the points that form the screen and extremely low weights for the points that are screened.

cross variograms were calculated and variogram models were fitted to the raw variograms. For this study a linear variogram model with a constant was fitted. The form of this variogram model is shown in Equation 8.20. The fitted variogram models were then used to perform the calculations required to produce the cokriging prediction as described in Chapter 7.

$$\gamma = ah + c \tag{8.20}$$

8.3.7 Comparison of the predictions produced using the models fitted to the large scale data and the transformed data, and using cokriging

In this study runs 8 and 9 in the large scale experimental design were performed to produce a validation dataset. These experiments were performed at points away from the original large scale data points and therefore the accuracy of different prediction approaches could be investigated by predicting the data of these two runs. The predictions of the three prediction methods that were used in this study are plotted in Figure 8.10

along with the actual data. This figure can be used to make a qualitative comparison between the prediction quality of the models. However, it can be seen that there was no consistently better performing prediction method and that accuracy of each prediction method changed from response to response.

The accuracy of each prediction method was quantified by calculating the average percentage error for the prediction of the validation dataset as shown in Figure 8.11. This figure shows that apart from the prediction of the HCP response, the transformed data approach and cokriging approach outperformed the use of the model fitted directly to the large scale data. Furthermore, for three of the four responses the accuracy of cokriging was better than that of the model fitted to the transformed data.

The accuracy of the three approaches were further explored by using leave-one-out cross-validation. Cross-validation uses all available data to assess the predictive capability of models. In the cross-validation approach used in this study, the large scale dataset was separated into subsets where each subset contained the data from one run. The data from a single subset was used to create the validation dataset and the remaining subsets were used to create the input dataset that was used to train the model. The resulting model was then used to predict the data in the validation dataset. This procedure was repeated until the entire dataset had been predicted. The errors were calculated for each subset and the averaged errors are presented in Figure 8.12. This figure shows that cokriging produces the most accurate predictions for three of the four responses.

In this study the column volume of the scale down column was 20% of the large scale column meaning that around 5 scale down runs could be performed using the amount of material used for a single large scale run. As shown in Table 8.5, 17 small scale runs and 2 large scale runs were required for the transformed data approach. This represents a 35% increase in material required for characterising the process. However, as shown in the results above, using the transformed data approach yielded a more accurate and comprehensive model than fitting a simple main effects model to 5 large scale runs would yield. The cokriging approach was shown to produce even more accurate predictions but required more large scale runs which resulted in a 110% increase in the material requirement. However, this can be contrasted with fitting a response surface

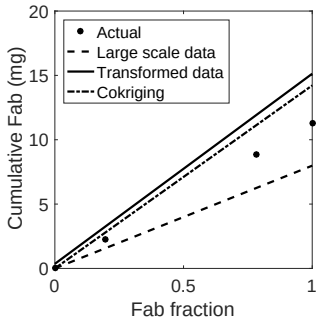

(a) Run 8 - Fab

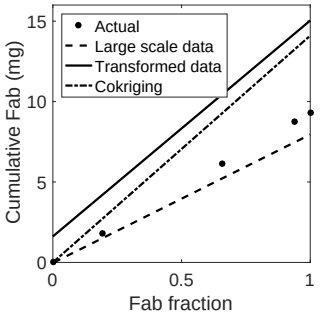

(b) Run 9 - Fab

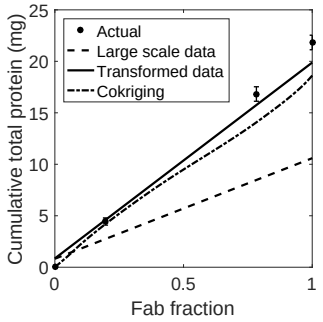

(c) Run 8 - Total protein

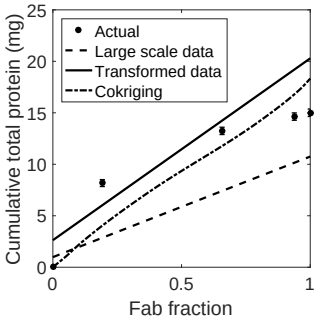

(d) Run 9 - Total protein

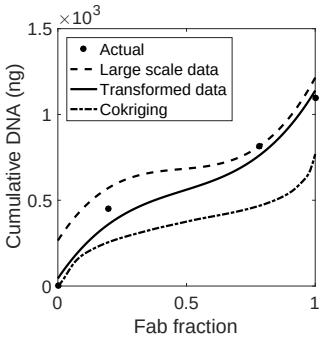

(e) Run 8 - DNA

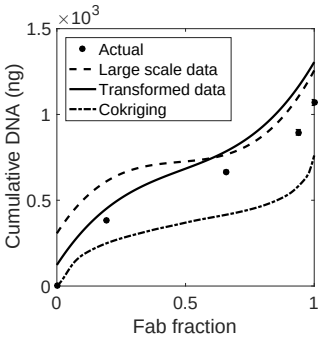

(f) Run 9 - DNA

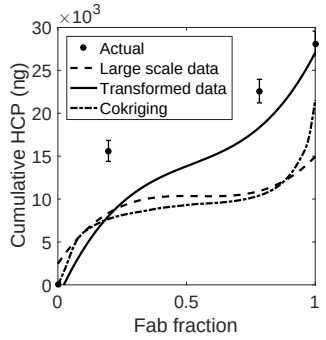

(g) Run 8 - HCP

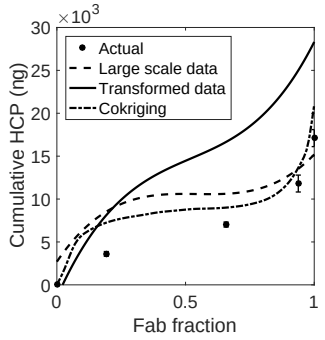

(h) Run 9 - HCP

Figure 8.10: Predictions of the validation runs (Run 8 and Run 9) produced using the model fitted to the large scale data, the model fitted to the transformed data and cokriging. Also shown are error bars showing 3 standard deviations around the mean for the actual data which shows indicates the magnitude of the error in the assay methods.

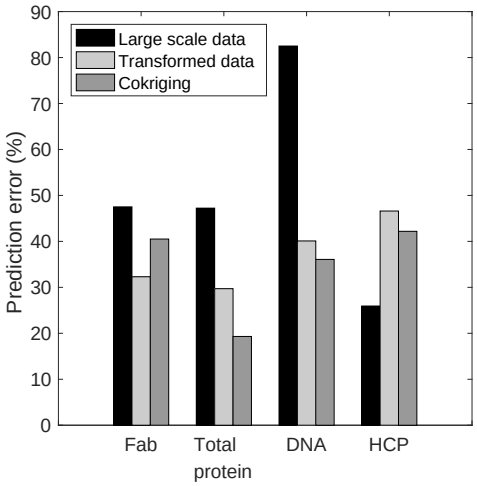

Figure 8.11: Average prediction error (%) for the prediction of the validation dataset. The predictions were made by using models fitted to the large scale data, models fitted to the small scale data transformed into the large scale design space and cokriging.

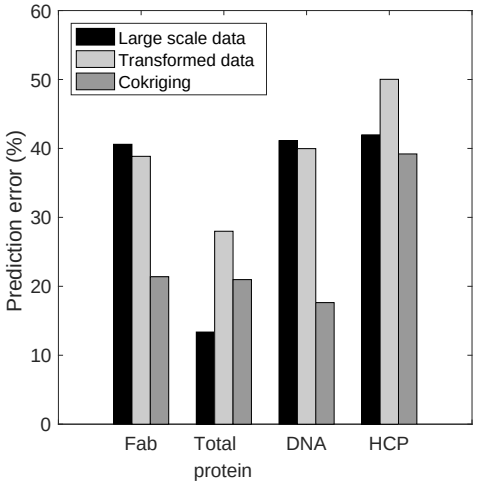

Figure 8.12: The average prediction error (%) for each of the prediction methods evaluated by cross-validation.

Table 8.5: Number of small scale and large scale runs required for each characterisation approach used in this study. Also shown is the change in material requirement from the first method involving a model fitted to a fractional factorial design performed at large scale. The compared methods are a model that is fitted to tranformed small scale data, a cokriging model using small scale data and a model fitted to a central composite design perfomed at large scale.

Method	Number of small scale	Number of large scale	Change in material needs (%)
Model fitted to large scale fractional factorial design data	0	4	-
Model fitted to transformed data	17	2	+35
Cokriging	17	5	+110
Model fitted to large scale central composite design data	0	17	+325

directly to large scale data which would require 17 large scale runs which would result in a 325% increase in feed material.

A benefit of the transformation approach is that, even for a complex experimental space consisting of a large number of process variables, the number of required large scale runs will not increase significantly. The number of small scale experiments will increase in order to characterise the process. However, the number of large scale runs required to derive the transformation function need not necessarily increase beyond 2-3 runs. Therefore, the relative experimental saving will increase with increasing process complexity.

8.4 Conclusion

In this study the previously established modelling approaches were applied to a multi-unit operation process which required multi-response optimisation to ensure that all of the specific impurities were cleared to a satisfactory level. The fractionation diagrams were adapted to simplify the chromatograms to an output that could be modelled with

relative ease. By using this output, the cumulative elution profiles, as the basis of the process models it was possible to create process models that were capable of predicting the elution profile of the product and each impurity at a given set of process conditions. This enables the multi-response optimisation of the purification process.

The data transformation and cokriging methods established in Chapter 7 were used to produce predictions of the large scale design space. Using the data transformation approach, process models were then built using data from a comprehensive small scale experimental design augmented with 2 large scale runs. The cokriging method was modified to handle the more complex input dataset found in this study. The cokriging method required the entire small scale dataset and the data from five large scale runs. The predictions of these two approaches were compared to the predictions of a model fitted directly to a fractional factorial study carried out at large scale.

The three approaches were compared by predicting the results of a validation dataset and by cross-validation. It was found that in most cases the data tranformation approach and the cokriging approach produced more accurate predictions. These improvements in prediction accuracy were achieved despite relatively small increases in the required feed material demand.

This study suggests that a generic approach to large scale process characterisation could begin by performing a comprehensive experimental study at small scale and a few large scale runs. The tranformation function approach can then be used to create a model describing the experimental space of the large scale process as this approach requires a mimimum of two large scale experiments. If the resulting model is found to be insufficiently inaccurate (e.g. by cross-validation), further large scale experiments can be performed and the entire dataset can be used to train a cokriging model which can better utilise the additional data.

Chapter 9

Conclusions

Alternative approaches for characterising the experimental spaces of chromatographic separations from scale down experiments were investigated in this thesis. Typical approaches to characterising chromatographic separations require a large number of expensive and time consuming experiments. Scale down experimentation can be used to reduce this experimental burden. However, issues such as being susceptible to variability and not being representative of the large scale process can limit their usefulness. Therefore alternative modelling approaches which can reduce the impact of these issues would be beneficial and were explored in this thesis.

The use of mechanistic models as an alternative approach to characterise and predict the performance of chromatographic processes was examined in **Chapter 3**. The benefit of using mechanistic models is that they can be used to rapidly and cheaply simulate a large number of experiments. While these models can be used to provide a very detailed understanding of the process, a significant amount of experimentation and modelling effort would be required to establish them. This would prevent the use of these models during the early stages of process development where the objective is to rapidly develop the process. The required level of detail in the process characterisation is relatively low during the early stages of process development and the higher levels of detail provided by mechanistic models are typically only required during the later stages of process development when the process for commercial manufacture is being defined. Therefore it was concluded that a more suitable approach to early process characterisation would be the use of small scale high throughput experimentation combined with empirical

modelling to populate the process space.

The typical output from a chromatographic experiment is a chromatogram which traces the time dependent changes in parameters such as the UV absorbance, conductivity, pH, concentration of individual components, etc. in the eluate. Due to the quantity of data generated, the chromatograms can become complex and furthermore they often do not directly indicate the performance of the process. In **Chapter 4** it was shown that maximum purification factor vs. yield diagrams could be calculated from chromatograms to show the trade off between the purity and yield for a given chromatographic experiments. Therefore these diagrams could be used to highlight and quantify the performance of a given purification step and could be used as the basis for characterising a chromatographic design space.

As mentioned above, the use of small scale high throughput experimentation and empirical modelling was considered the most suitable approach to characterising chromatographic separations during the early phases of process development. The typical method used to derive these empirical models is response surface methodology (RSM) but this approach can struggle to cope with non-linear relationships between the process variables and the response which sometimes occur in the experimental spaces of chromatographic purifications. Kriging is a non-parametric method which produces predictions from a weighted interpolation of the available data and was therefore considered a potential alternative to RSM for modelling these non-linear relationships. Kriging was explored as an alternative to RSM in **Chapter 5** using a chromatographic dataset which had a non-linear relationship between a single process variable and the response. This dataset was produced by using cation exchange chromatography to purify myoglobin from a mixture of myoglobin and egg white proteins across a range of elution salt concentrations. In this dataset the process variable was the elution salt concentration and the response was the maximum purification factor and their was relationship was found to have non-linear artifacts. Using this dataset it was shown that Kriging was able to characterise these non-linear artifacts while RSM was not capable.

Another issue that may affect the choice of modelling approach is that scale-down experimentation is particularly susceptible to variability which affects the results of these experiments. In **Chapter 6** Monte Carlo simulations coupled to a general rate model

of a chromatographic separation were used to simulate the effect of various sources of variability and investigate the capability of three modelling approaches to produce accurate process models from noisy data. In this study two sources of variability were modelled and the magnitude of each source of variability was varied. Response surface methodology, Kriging and partial least squares regression were the modelling approaches tested in this study. For each method the average error and the error distributions were determined. While the average error was similar for all three methods, the error distributions showed that Kriging could better approximate the underlying trends in the experimental space of the process and was therefore the least susceptible to the simulated effects of variability in scale-down experimentation.

A complication that may arise through the use of scale-down experimentation is that the results may not represent the actual large scale process due to the influence of various scaling effects. These scaling effects cause the results of scale-down experiments to deviate from those of the large scale process. However, using large scale experiments to characterise the process would result in a larger experimental burden. In **Chapter 5** it was demonstrated that cokriging could be used to reduce the burden of characterising the large scale process by using a limited amount of large scale data augmented with a comprehensive small scale dataset. This was demonstrated using the cation exchange chromatographic separation of myoglobin from egg white proteins that was previously used to demonstrate Kriging. In this study the separation was performed at three different scales using columns with 1 mL, 5 mL and 10 mL column volumes where the 1 mL column was considered small scale and the 5 mL and 10 mL columns were considered large scale. A comprehensive dataset was produced at small scale consisting of 13 runs while only 3 large scale experiments were performed. The cokriging model produced using this augmented dataset was compared to a quadratic RSM model fitted to the 3 large scale experiments and the cokriging model was found to provide a better understanding of the relationship between the process variable and the response.

In **Chapter 7** another method for using data from scale down experiments to characterise large scale separations was developed. This method involved the derivation of a transformation function which was used to transform the scale-down data into the large scale design space. Models describing the large scale design space were then produced

by fitting response surfaces to the transformed data. The cation exchange purification of myoglobin from egg white proteins was used to test the transformation function and cokriging methods. The experimental space was enlarged to include 4 process variables to further challenge these approaches. The predictions of these methods were compared to the typical approach of a response surface fitted to data from a fractional factorial study carried out at large scale. The root mean squared error of prediction (RMSEP) was calculated for each approach and the RMSEPs of the methods using small scale data were found to be larger but of a similar magnitude to RMSEP of the model fitted directly to large scale data. However, the methods using the small scale data provided a significant saving in large scale experimentation and therefore the reduced accuracy could be considered acceptable.

These approaches for using scale-down experimentation were further tested in **Chapter 8** using a more complex two step sequence for the purification of an antibody fragment from *E.coli* lysate. The purification sequence consisted of a heat treatment step followed by a cation exchange chromatography step. The objective was to produce a model that could be used to optimise the yield, the purity, and the HCP and DNA clearance of the process sequence which required the modelling of four different process responses. This was achieved by modifying fractionation diagrams to describe the elution profiles of the product and the specific impurities for each of the experiments. The cokriging and transformation methods were adapted to model these diagrams and the predictions of these approaches were compared by predicting the results of a validation set and also by cross-validation. The results of the cokriging and transformation methods were found to be comparable or better than the predictions of RSM models fitted directly to the large scale data.

In this thesis fractionation diagrams and PFY diagrams were used to simplify the output of chromatographic experiments to facilitate the creation of empirical models that described the chromatography process. Alternative methods of creating empirical models were explored and two new approaches were established; cokriging and transformation functions. It was demonstrated that these approaches could be used to reduce the experimental burden of characterising chromatographic separations without compromising accuracy.

Chapter 10

Future Work

It was demonstrated in Chapter 5 that Kriging could be used to model the non-linear relationship between the response and process variable that was observed in the chromatographic separation used in that study. As the Kriging model is non-parametric and does not assume a form or function, it has a greater potential than response surface methods to model design spaces with complex non-linear interactions. This potential could be further challeneged by modelling the experimental space of a chromatographic process which is likely to have complex interactions such as a mixed mode chromatography step where the type of interaction between the molecules and the resin changes according to the pH and salt concentration of the solution. The Kriging models could also be used to model other biopharmaceutical processes with complex experimental spaces such as centrifugation, tangential flow filtration and even bioreactors.

In Chapter 6 Monte Carlo simulations were carried out in conjunction with a general rate model of a cation exchange chromatography step to investigate the effects of variability on scale-down experimentation. These simulations were used to test the capability of response surface methods, Kriging and partial least squares regression to mitigate the effects of variability on the accuracy of the process characterisation. This study could also be further extended by replacing the cation exchange chromatography model with a model of a more complex chromatographic process such as a mixed mode chromatography step. Such a process is likely to have more complex interactions between the process variables and the performance of the process and therefore the effects of variability could have a greater detrimental effect on the resulting process model.

In Chapter 7 two methodologies were developed to circumvent scaling effects and enable the use of scale-down data to characterise large scale processes. One approach involved the use of transformation functions to transform small scale experimental data into the large scale design space while the other approach used cokriging to augment a small amount of large scale data with a comprehensive scale down dataset to create process models. In the study described in Chapter 7 these methods were tested using bench scale columns where the small scale column had a volume of 1 mL and the large scale columns had volumes of 5 mL and 10 mL. Further investigations could be carried out to determine whether these methods could be used with data produced using scale down devices such as Robocolumns or Phynexus tips which have even smaller packed bed volumes. In addition to requiring a smaller volume of feedstock, a further benefit of these devices is that they can be operated in parallel which increases the throughput of the experimentation and enables a more detailed characterisation of the experimental space.

In this study a degree of equivalence was maintained between the scale down experiments and the large scale process by maintaining the same residence time throughout all of the experiments. While there was a significant saving in the material requirement, the constant residence time meant that performing these experiments took the same amount of time regardless of scale. The methods for using scale down data developed in this study could be further tested to establish whether scale-down experiments with a shorter residence time can be used to predict the performance of the large scale process. This would serve to further increase the throughput of the small scale experiments.

These methods for using scale down data could be further extended to an even smaller scale by linking batch experiments performed in microwell plates to the large scale process. The major benefit of these experiments is that the volumes involved are very small ($<$100 μL). Howevere, these experiments can only approximate the adsorption/desorption kinetics of a resin and are unable to mimic the mass transfer dynamics in a chromatography column. Therefore relating the resulting data to the large scale process will be more complicated. However, the ability to link batch binding characteristics such as static binding capacities and partition coefficients to the performance of large scale processes would be a major benefit as these experiments can be carried out very

cheaply and rapidly using automated liquid handlers.

Using the above mentioned scale down methods to improve the throughput of the experiments will transfer the burden to sample analysis. However, as shown in Chapter 6 the effects of variability introduced in scale down experimentation can be mitigated by selecting an appropriate modelling approach. Therefore, a review of analytical methods could be performed to identify less precise but high throughput analytical methods that could be used to alleviate the analytical burden. The use of spectroscopic methods would be particularly useful as the short amount of time required to produce results would enable rapid iterative experimentation where the results of the previous round of experiments informs the experimental design of the next round of experiments. This iterative platform could then be used to rapidly identify the optimum of a process.

The scale-down methods established in this study could be augmented with an appropriate method for calculating confidence intervals for the predictions of the large scale design space. The ability to calculate confidence intervals would be beneficial to understanding the quality of the predictions and directing further experimentation.

These methodologies could also be tested for use with other unit processes. Scaling effects also hinder the use of data from scale-down methods for the characterisation of other upstream and downstream unit processes such bioreactors, centrifuges and tangential flow filtration. As the developed methods were generic and not specific to chromatographic process they have the potential to be applied to these unit operations.

Appendix A

MATLAB code

A.1 Function for calculating the fractionation diagrams

```
function [fracProduct,fracTotal]=fractionationDiagram(concProduct,...
concImpurities)

% Function to calculate the fractionation diagram from a chromatogram

% The inputs 'concProduct' and 'concImpurities' are respectively the
% concentration profiles of the product and the impurities. The outputs
% 'fracProduct' and 'fracTotal' are the fraction of the product and the
% fraction of total protein in the calculated fractionation diagram.

%Set all negative values to zero
concImpurities(concImpurities<=0)=0;
concProduct(concProduct<=0)=0;

%Calculate vector for the concentration profile of the total proteins
concTotalProtein=concProduct+concImpurities;

%Cumulative of target protein
sumConcProduct=cumsum(concProduct);

```

```
%Cumulative of total protein
sumConcTotal=cumsum(concTotalProtein);

%Calculating the fraction of the target protein
fracProduct=sumConcProduct/sumConcProduct(end);

%Calculating the fraction for the total protein
fracTotal=sumConcTotal/sumConcTotal(end);
```

A.2 Function for calculating the maximum purity vs. yield diagrams

```
function [PF,Y,cut1,cut2]=maxPY(fracProduct,fracTotal)

% Script to calculate the maximum purification factor vs. yield diagram
% from a fractionation diagram.

% The inputs 'fracProduct' and 'fracTotal' are fractions of product and
% total protein calculated using a fractionation diagram.
% The outputs 'PF' and 'Y' are the calculated maximum purification factors
% and the corresponsing yield values. 'cut1' and 'cut2' are the
% corresponding cuts that provide the calculated purification factor and
% yield.

% Number of fractions
n=size(fracProduct,1);

%Create vector for the purification factors
purifFact=zeros(sum(1:n),1);

%Create vector for the yield
yield=zeros(sum(1:n),1);

%Create vector for the first cut
PFcut1=zeros(sum(1:n),1);

```

```
%Create vector for the second cut
PFcut2=zeros(sum(1:n),1);

%Create count for the number of calculated purification factors
count1=0;

%Loop to calculate the gradient between two points on the fractionation
%diagram, i.e. the purification factor --> (y2-y1)/(x2-x1)
%First loop through point 1 or the first cut
for a=1:n-1

%Second loop through point 2 or the second cut
for b=a+1:n

%Check that x2>x1
if fracTotal(b)>fracTotal(a)

%Check that y2>y1
if fracProduct(b)>fracProduct(a)

%Calculate the purification factor
gradient=(fracProduct(b)-fracProduct(a))/...
(fracTotal(b)-fracTotal(a));

%Update the count of PFs calculated
count1=count1+1;

%Add the PF to the vector
purifFact(count1)=gradient;

%Add the yield to the vector
yield(count1)=fracProduct(b)-fracProduct(a);

%Add the first cut to the vector
PFcut1(count1)=a;

%Add the second cut to the vector;
PFcut2(count1)=b;
```

```
63
64 end
65 end
66 end
67 end
68
69 %Set initial value of 'n' or yield
70 n=0.001;
71
72 % Number of purification factor points
73 nPF=size(purifFact,1);
74
75 %Create 'q' which will take value of the yield at the maxima
76 q=[];
77
78 %Create 'r' which will take the valued of the cuts at the maxima
79 r=[];
80
81 %Create vector for the values of the max PF
82 maxPF=zeros(1,nPF);
83
84 %Create vector for the values of the yield at the max PFs
85 maxPFYields=zeros(1,nPF);
86
87 %Create matrix for the values of the cuts at the max PFs
88 maxPFCuts=zeros(2,nPF);
89
90 %Create count for the number of max PFs found
91 count2=1;
92
93 %Search is carried out starting at the initial value of 'n' until 'n'
94 %reaches 1.001
95 while n<=1.001
96
97 %Resetting the value of 'p' after a maximum is found
98 p=1;
99
100 %Loop through the calculated values of PF
```

```
for vi=1:nPF

%Check if this value of yield is greater than value of 'n'
if yield(vi)>n;

%and value of PF is greater than the value of 'p'
if purifFact(vi)>p;

%Then set value of 'q' to this value of yield
q=yield(vi);

%and set value of 'p' to this value of PF
p=purifFact(vi);

%'r' takes the values of the cuts
r=[PFcut1(vi),PFcut2(vi)];

end
end
end

%If the value of PF for this max. is not equal to the previous max.
if maxPF(count2)~=p;

%and the value of yield for this max. is not equal to the previous
if maxPFYields(count2)~=q;

%then update the count of the maxPFs
count2=count2+1;

%and save the PF of this new maximum
maxPF(count2)=p;

%and the yield of this maximum
maxPFYields(count2)=q;

%and the cuts at this maximum
maxPFCuts(:,count2)=r;
```

```
139
140 end
141 end
142
143 %Increase value of 'n' to restart search
144 n=n+0.001;
145
146 end
147
148
149 %Remove excess from vectors
150 maxPF=maxPF(2:count2);
151 maxPFYields=maxPFYields(2:count2);
152 maxPFCuts=maxPFCuts(:,2:count2);
153
154 PF=maxPF';
155 Y=maxPFYields';
156 cut1=maxPFCuts(1,:)';
157 cut2=maxPFCuts(2,:)';
```

A.3 Function for calculating the variogram

```
1 function [gamma,h,gammaBin,hBin] = semivariogram(inputMatrix,nBins)
2
3
4 % Script to calculate the raw variogram data and average at each unique
5 % location. The data is not normalised and the locations should be provided
6 % in coded form.
7
8 % Semivariogram model functions for curve fitting tool box
9
10 % Spherical - a*(1.5*x/b-0.5*(x/b)^3)
11 % Gaussian - a*(1-exp(-3*(x^2)/(b^2)))
12 % Exponential - a*(1-exp(-3*x/b))
13 % Linear - a*x
14 % Power - a*x^b
15
```

```
% Determine column containing max PF values
outputCol=size(inputMatrix,2);

% Determine the number of datapoints in the matrix
n=size(inputMatrix,1);

% Allocate blank vectors for the calculated gamma and h
gamma=zeros((sum(1:1:n-1)),1);
h=zeros((sum(1:1:n-1)),1);

% Calculate gamma and h
i=0;
for ii=1:(n-1)
for iii=(ii+1):n
i=i+1;
h(i)=sqrt(sum((inputMatrix(ii,1:(outputCol-1))-...
inputMatrix(iii,1:(outputCol-1))).^2));
gamma(i)=((inputMatrix(ii,outputCol)-...
inputMatrix(iii,outputCol))^2)/2;
end
end

if nargin==2
[~,edges,bin] = histcounts(h,nBins);
gammaBin=zeros(nBins,1);

for i=1:nBins
gammaBin(i)=mean(gamma(bin==i));
end

edges=edges';
hBin=(edges(1:end-1)+edges(2:end))./2;

hBin(isnan(gammaBin))=[];
gammaBin(isnan(gammaBin))=[];


else
```

```
hBin=unique(h);

nBin=size(hBin,1);
gammaBin=zeros(nBin,1);

for i=1:nBin
gammaBin(i)=mean(gamma(h==hBin(i)));
end
end
```

A.4 Function for calculating the cross-variogram

```
function [gamma,h,gammaBin,hBin] = crossvariogram(inputMatrix1,...
inputMatrix2,nBins)


% Script to calculate the raw cross-variogram data and average at each unique
% location. The data is not normalised and the locations should be provided
% in coded form.

% 'inputMatrix1' should contain the primary variable data and
% 'inputMatrix2' should contain the secondary variable data

% Check that inputMatrix1 and inputMatrix2 have the same number of columns
if size(inputMatrix1,2)~=size(inputMatrix2,2)
error('Primary and secondary variable matrices do not have the same number of columns')
end

% Determine the number of datapoints in the primary and secondary matrix
n1=size(inputMatrix1,1);
n2=size(inputMatrix2,1);

% Allocate blank vectors for the calculated gamma and h
gamma=zeros(n1,n2);
h=zeros(n1,n2);

% Calculate gamma and h
```

```
26
27 for i=1:n1
28 for ii=1:n2
29 h(i,ii)=sqrt(sum((inputMatrix1(i,1:(end-1))...
30 -inputMatrix2(ii,1:(end-1))).^2));
31 gamma(i,ii)=((inputMatrix1(i,end)-inputMatrix2(ii,end))^2)/2;
32 end
33 end
34
35 gamma=reshape(gamma,[],1);
36 h=reshape(h,[],1);
37
38
39 if nargin==3
40 [~,edges,bin] = histcounts(h,nBins);
41 gammaBin=zeros(nBins,1);
42
43 for i=1:nBins
44 gammaBin(i)=mean(gamma(bin==i));
45 end
46
47 edges=edges';
48 hBin=(edges(1:end-1)+edges(2:end))./2;
49
50 hBin(isnan(gammaBin))=[];
51 gammaBin(isnan(gammaBin))=[];
52
53
54 else
55
56 hBin=unique(h);
57
58 nBin=size(hBin,1);
59 gammaBin=zeros(nBin,1);
60
61 for i=1:nBin
62 gammaBin(i)=mean(gamma(h==hBin(i)));
63 end
```

```
64
65 end
```

A.5 Function for carrying out the ordinary Kriging algorithm

```
1  function [predValues,predVariance]=ordKriging(sampleLocations,...
2  sampleValues,predLocations,model)
3
4
5
6  % Determine the number of datapoints in the matrix
7  nSamples=size(sampleLocations,1);
8
9  % Create d2d matrix
10 d2d=zeros(nSamples,nSamples);
11
12 for i=1:nSamples;
13 for j=1:nSamples;
14 d2d(i,j)=sqrt(sum((sampleLocations(i,:)-sampleLocations(j,:)).^2));
15 end
16 end
17
18 gammad2d=model(d2d);
19 gammad2d=reshape(gammad2d,size(d2d));
20
21 gammad2d(1:nSamples,nSamples+1)=1;
22 gammad2d(nSamples+1,1:nSamples)=1;
23 gammad2d(nSamples+1,nSamples+1)=0;
24
25 % Number of points to be predicted
26 nPred=size(predLocations,1);
27
28 % Matrix between unknown points and known data points and sorted index
29 d2u=zeros(nSamples,nPred);
30
```

```
for i=1:nSamples;
for j=1:nPred;
d2u(i,j)=sqrt(sum((sampleLocations(i,:)-predLocations(j,:)).^2));
end
end

gammad2u=model(d2u);
gammad2u=reshape(gammad2u,size(d2u));

gammad2u(nSamples+1,:)=1;

predValues=zeros(nPred,1);
predVariance=zeros(nPred,1);

h=waitbar(0,'Kriging');

for i=1:nPred;
w=gammad2d\gammad2u(:,i);
predValues(i)=sum(sampleValues.*w(1:nSamples));
predVariance(i)=model.a-sum(w.*gammad2u(:,i));
waitbar(i/nPred,h);
end

close(h)

end
```

A.6 Function for carrying out the Cokriging algorithm

```
function [predValues,predVariance]=coKriging(inputMatrix1,...
inputMatrix2,predLocations,model)

% Function to carry out coKriging.
% inputMatrix1 - Matrix including the primary sample locations and values
% inputMatrix2 - Matrix including the secondary sample locations and values
% predLocations - Locations of the points to be predicted
% model - Cell array containing the primary(.pri), secondary(.sec) and cross model
```

```
9
10
11
12 % Determine the number of datapoints in the primary and secondary matrix
13 nPri=size(inputMatrix1,1);
14 nSec=size(inputMatrix2,1);
15
16 % Determine the mean of the primary and secondary matrices
17 meanPri=mean(inputMatrix1(:,end));
18 meanSec=mean(inputMatrix2(:,end));
19
20 % Number of points to be predicted
21 nPred=size(predLocations,1);
22
23 % Create primary d2d matrix
24 d2dPri=zeros(nPri,nPri);
25
26 for j=1:nPri;
27 for k=1:nPri;
28 d2dPri(j,k)=sqrt(sum((inputMatrix1(j,1:end-1)...
29 -inputMatrix1(k,1:end-1)).^2));
30 end
31 end
32
33 gammad2dPri=model.pri(d2dPri);
34 gammad2dPri=reshape(gammad2dPri,size(d2dPri));
35
36 % Create secondary d2d matrix
37 d2dSec=zeros(nSec,nSec);
38
39 for j=1:nSec;
40 for k=1:nSec;
41 d2dSec(j,k)=sqrt(sum((inputMatrix2(j,1:end-1)...
42 -inputMatrix2(k,1:end-1)).^2));
43 end
44 end
45
46 gammad2dSec=model.sec(d2dSec);
```

```
47 gammad2dSec=reshape(gammad2dSec,size(d2dSec));
48
49 % Create cross d2d matrix
50 d2dx=zeros(nPri,nSec);
51
52 for j=1:nPri;
53 for k=1:nSec;
54 d2dx(j,k)=sqrt(sum((inputMatrix1(j,1:end-1)-...
55 inputMatrix2(k,1:end-1)).^2));
56 end
57 end
58
59 gammad2dx=model.x(d2dx);
60 gammad2dx=reshape(gammad2dx,size(d2dx));
61
62
63 % Create complete coKriging d2d matrix
64 gammad2d=[gammad2dPri,gammad2dx;gammad2dx',gammad2dSec];
65
66 gammad2d(1:nPri+nSec,nPri+nSec+1)=1;
67 gammad2d(nPri+nSec+1,1:nPri+nSec)=1;
68 gammad2d(nPri+nSec+1,nPri+nSec+1)=0;
69
70 % Create primary d2u matrix
71 d2uPri=zeros(nPri,nPred);
72
73 for j=1:nPri;
74 for k=1:nPred;
75 d2uPri(j,k)=sqrt(sum((inputMatrix1(j,1:end-1)-...
76 predLocations(k,:)).^2));
77 end
78 end
79
80 gammad2uPri=model.pri(d2uPri);
81 gammad2uPri=reshape(gammad2uPri,size(d2uPri));
82
83
84 % Create secondary d2u matrix
```

```
d2uSec=zeros(nSec,nPred);

for j=1:nSec;
for k=1:nPred;
d2uSec(j,k)=sqrt(sum((inputMatrix2(j,1:end-1)-...
predLocations(k,:)).^2));
end
end

gammad2uSec=model.sec(d2uSec);
gammad2uSec=reshape(gammad2uSec,size(d2uSec));

% Create complete coKriging d2u matrix
gammad2u=[gammad2uPri;gammad2uSec];
gammad2u(nPri+nSec+1,:)=1;

% Vector for predictions
predValues=zeros(nPred,1);
predVariance=zeros(nPred,1);

% h=waitbar(0,'coKriging');

for j=1:nPred;
% w=mldivide(gammad2d,gammad2u(:,j));
w=gammad2d\gammad2u(:,j);
% w=inv(gammad2d)*gammad2u(:,j);
predValues(j)=sum(inputMatrix1(:,end).*w(1:nPri))+...
sum((inputMatrix2(:,end)-meanSec+meanPri).*w(nPri+1:nPri+nSec));
predVariance(j)=model.pri.a-sum(w.*gammad2u(:,j));
%     waitbar(j/nPred,h);
end

% close(h)

end
```

A.7 Function for carrying out the Monte Carlo simulation for process variability

```
function [errors]=procVarMonteCarloSim


% Script to carry out a Monte Carlo simulation to compare the performance
% of Kriging, RSM and PLS to accurately characterise a process using noisy
% input data. The noise in this data is due to the variations in the
% set points of the process. The input data for this simulation is found in the
% procVarResults folder and the resulting models are validated against the
% data found in valData.

% Define intial purity
initialPurity=5/7;

% Define minimum purity
minYield=0.9;

% Define elution fraction size
poolSize=0.25;

% Load validation dataset
load(fullfile('Chpt 1','Variability - process','valData'))

% Number of validation datapoints
nVal=size(valMatrix,1);

% Code the matrix
valMatrix=[(valMatrix(:,1)-250)./25,(valMatrix(:,2)-0.5)/0.05,...
(valMatrix(:,3)-0.1)/0.01,(valMatrix(:,4)-0.2)/0.01];

% Convert the valPurity values to percentages
valPurity=valPurity*100;


```

```
% Get list of simulations
fileList=dir(fullfile('Chpt 1','Variability - process','procVarResults','*.mat'));

% Number of simulations
nSim=size(fileList,1);

errors.allRSMSWerrs=zeros(nVal*nSim,1);
errors.allRSMerrs=zeros(nVal*nSim,1);
errors.allKrigerrs=zeros(nVal*nSim,1);
errors.allUnivKrigerrs=zeros(nVal*nSim,1);
errors.allPLSerrs=zeros(nVal*nSim,1);



% Create progress bar
h=waitbar(0);

for i=1:nSim
% Load list of runs that make up the DOE
runList=whos('-file',fullfile('Chpt 1','Variability - process','procVarResults',...
fileList(i).name));

% Load the experimental design
load(fullfile('Chpt 1','Variability - process','procVarPar.mat'),...
'u','vf','M1','M2')

% Number of runs
nRun=size(runList,1);

purity=zeros(nRun,1);

% Cycle through and process each chromatogram in the simulation
for ii=1:nRun


% Load the chromatogram
load(fullfile('Chpt 1','Variability - process','procVarResults',...
```

```
72 fileList(i).name),runList(ii).name)
73
74 % Create variables from the loaded structure
75 t=eval([runList(ii).name,'.t(:,end)']);
76 cb_Aout=eval([runList(ii).name,'.cb_A(:,end)']);
77 cb_Bout=eval([runList(ii).name,'.cb_B(:,end)']);
78 cb_Cout=eval([runList(ii).name,'.cb_C(:,end)']);
79
80 % Number of pools
81 numPools=ceil(t(end)/poolSize);
82
83 % Sort the fractions
84 [~,I]=histc(t,0:poolSize:numPools*poolSize);
85
86 % % The midpoints of the fractions
87 % t=(linspace(poolSize/2,numPools*poolSize-poolSize/2,numPools))';
88
89 cb_A=zeros(numPools,1);
90 cb_B=zeros(numPools,1);
91 cb_C=zeros(numPools,1);
92
93 % Mean concentration in each fraction
94 for iii=1:numPools
95 cb_A(iii)=mean(cb_Aout(I==iii));
96 cb_B(iii)=mean(cb_Bout(I==iii));
97 cb_C(iii)=mean(cb_Cout(I==iii));
98 end
99
100 % Calculate the fractionation diagram
101 [fracProduct,fracTotal]=fractionationDiagram(cb_B,cb_A+cb_C);
102
103 % Calculate the max PFs and corresponding yields
104 [maxPFVals,yieldVals]=maxPY(fracProduct,fracTotal);
105
106 % Convert the max PFs to purities
107 purityVals=maxPFVals*initialPurity;
108
109 % Record the optimal purity
```

```
110
111 if isempty(purityVals(yieldVals>=minYield))==1
112 purity(sscanf(runList(ii).name,'Run_%f'))=0;
113 else
114 purity(sscanf(runList(ii).name,'Run_%f'))=...
115 max(purityVals(yieldVals>=minYield))*100;
116 end
117
118 end
119
120 % Create matrix containing DOE results
121 DOEMatrix=[ccdesign(4,'center',1),purity];
122
123 %%% RSM SW
124
125 % Fit RSM model by stepwise regression
126 rsmModelSW = stepwiselm(DOEMatrix(:,1:end-1),DOEMatrix(:,end),...
127 'quadratic','verbose',0);
128
129 % Calculate and record RSM using stepwise regression errors
130 [rsmSWPred] = predict(rsmModelSW,valMatrix);
131 rsmSWErrs=sqrt((valPurity-rsmSWPred).^2);
132 errors.allRSMSWerrs((i-1)*nVal+1:(i-1)*nVal+nVal)=rsmSWErrs;
133
134
135
136 %%% RSM
137
138 % Fit RSM model
139 rsmModel = fitlm(DOEMatrix(:,1:end-1),DOEMatrix(:,end),'quadratic');
140 %rsmModel = fitlm(DOEMatrix(:,1:end-1),DOEMatrix(:,end),'y ~ 1 + x2*x3 + x2*x4 + x3*x4 +
141
142 % Calculate and record RSM errors
143 [rsmPred] = predict(rsmModel,valMatrix);
144 rsmErrs=sqrt((valPurity-rsmPred).^2);
145 errors.allRSMerrs((i-1)*nVal+1:(i-1)*nVal+nVal)=rsmErrs;
146
147
```

```
148 %%% Kriging
149
150
151 % Fit Kriging model
152 %krigingModel = oodacefit(DOEMatrix(:,1:end-1),DOEMatrix(:,end));
153
154 % Calculate semivariogram model
155 [~,~,gammaBin,hBin] = semivariogram(DOEMatrix);
156 [semivarModel]=semivariogramModel(hBin,gammaBin);
157
158 % Calculate and record Kriging errors
159 [krigingPred]=ordKriging(DOEMatrix(:,1:end-1),DOEMatrix(:,end),valMatrix,...
160 semivarModel);
161 %[krigingPred] = krigingModel.predict(valMatrix);
162 krigingErrs=sqrt((valPurity-krigingPred).^2);
163 errors.allKrigerrs((i-1)*nVal+1:(i-1)*nVal+nVal)=krigingErrs;
164
165
166 %%% Universal Kriging
167
168
169
170 % Use above RSM to detrend the DOE data
171 [detrendPurity] = purity-predict(rsmModel,DOEMatrix(:,1:end-1));
172
173
174 % Fit Kriging model
175 %krigingModel = oodacefit(DOEMatrix(:,1:end-1),DOEMatrix(:,end));
176
177 % Calculate semivariogram model
178 [~,~,gammaBin,hBin] = semivariogram([DOEMatrix(:,1:end-1),detrendPurity]);
179 [semivarModel]=semivariogramModel(hBin,gammaBin);
180
181 % Calculate and record Kriging errors
182 [krigingUnivPred]=ordKriging(DOEMatrix(:,1:end-1),detrendPurity,valMatrix,...
183 semivarModel);
184
185 % Add the trend back into the predictions
```

```
186 krigingPredTrend=krigingUnivPred+predict(rsmModel,valMatrix);
187
188 %[krigingPred] = krigingModel.predict(valMatrix);
189 krigingUnivErrs=sqrt((valPurity-krigingPredTrend).^2);
190 errors.allUnivKrigerrs((i-1)*nVal+1:(i-1)*nVal+nVal)=krigingUnivErrs;
191
192
193 %%% PLS
194
195
196 % Fit PLS model
197 [~,~,~,~,BETA] = plsregress(DOEMatrix(:,1:end-1),DOEMatrix(:,end));
198 %[~,~,~,~,BETA] = plsregress(DOEMatrix(:,1:end-1),DOEMatrix(:,end),1);
199
200 % Calculate and record PLS errors
201 plsPred = [ones(size(valMatrix,1),1),valMatrix]*BETA;
202 plsErrs=sqrt((valPurity-plsPred).^2);
203 errors.allPLSerrs((i-1)*nVal+1:(i-1)*nVal+nVal)=plsErrs;
204
205
206
207
208 %
209 %
210 %
211 %
212 %
213 %     % Fit RSM model
214 %     rsmModel = fitlm(DOEMatrix(:,1:end-1),DOEMatrix(:,end),'quadratic');
215 %
216 %     % Fit Kriging model
217 %     krigingModel = oodacefit(DOEMatrix(:,1:end-1),DOEMatrix(:,end));
218 %
219 %     % Fit PLS model
220 %     [~,~,~,~,BETA] = plsregress(DOEMatrix(:,1:end-1),DOEMatrix(:,end));
221 %
222 %     % Calculate and record RSM errors
223 %     [rsmPred] = predict(rsmModel,valMatrix);
```

```
%     rsmErrs=sqrt((valPurity-rsmPred).^2);
%     allRSMerrs((i-1)*nVal+1:(i-1)*nVal+nVal)=rsmErrs;
%
%     % Calculate and record Kriging errors
%     [krigingPred] = krigingModel.predict(valMatrix);
%     krigingErrs=sqrt((valPurity-krigingPred).^2);
%     allKrigerrs((i-1)*nVal+1:(i-1)*nVal+nVal)=krigingErrs;
%
%     % Calculate and record PLS errors
%     plsPred = [ones(size(valMatrix,1),1),valMatrix]*BETA;
%     plsErrs=sqrt((valPurity-plsPred).^2);
%     allPLSerrs((i-1)*nVal+1:(i-1)*nVal+nVal)=plsErrs;
%
% Update progress bar
waitbar(i/nSim,h);
end

% Close progress bar
close(h)
```

A.8 Function for carrying out the Monte Carlo simulation for experimental error in the assay

```
function [errors]=ExptErrMonteCarloSimV2

% Function carries out a Monte Carlo simulation to compare the performance
% of Kriging to that of a RSM when presented with noisy data. The noise in
% this data is due to the variations introduced by normally distributed
% experimental error.
% The input data for this simulation is found in the
% results folder and the resulting models are validated against the data
% found in valData.


tic

```

```
% Define elution fraction size
poolSize=0.25;

% Define intial purity
initialPurity=5/7;

% Define minimum purity
minYield=0.9;

% Define measurement error relative standard deviation
errRSD=10;

% Load validation dataset
load(fullfile('Chpt 1','Experimental error','valData'))

% Number of validation datapoints
nVal=size(valMatrix,1);

% Code the matrix
valMatrix=[(valMatrix(:,1)-250)./25,(valMatrix(:,2)-0.5)/0.05,...
(valMatrix(:,3)-0.1)/0.01,(valMatrix(:,4)-0.2)/0.01];

% Convert the valPurity values to percentages
valPurity=valPurity*100;

% Number of cycles
nCycles=100;

errors.allRSMSWerrs=zeros(nVal*nCycles,1);
errors.allRSMerrs=zeros(nVal*nCycles,1);
errors.allKrigerrs=zeros(nVal*nCycles,1);
errors.allUnivKrigerrs=zeros(nVal*nCycles,1);
errors.allPLSerrs=zeros(nVal*nCycles,1);


% Create progress bar
h=waitbar(0);

```

```
52 for iii=1:nCycles
53
54 % Load DOE chromatograms
55 fileList=dir(fullfile('Chpt 1','Experimental error',...
56 'DOE chromatograms','*.mat'));
57
58
59 % Number of DOE chromatograms
60 n=size(fileList,1);
61
62 purity=zeros(n,1);
63
64
65 % Loop to load and process chromatograms
66 for i=1:n
67 % Load chromatograms
68 load(fullfile('Chpt 1','Experimental error',...
69 'DOE chromatograms',fileList(i).name))
70
71 % Number of pools
72 numPools=ceil(t(end)/poolSize);
73
74 % Sort the fractions
75 [~,I]=histc(t,0:poolSize:numPools*poolSize);
76
77 % The midpoints of the fractions
78 t=(linspace(poolSize/2,numPools*poolSize-poolSize/2,numPools))';
79
80 cb_A=zeros(numPools,1);
81 cb_B=zeros(numPools,1);
82 cb_C=zeros(numPools,1);
83
84 % Mean concentration in each fraction
85 for ii=1:numPools
86 cb_A(ii)=mean(cb_Aout(I==ii));
87 cb_B(ii)=mean(cb_Bout(I==ii));
88 cb_C(ii)=mean(cb_Cout(I==ii));
89 end
```

```
90
91  % Apply normally distributed measurement error
92  cb_Aerr=normrnd(cb_A,sqrt((errRSD*cb_A/100).^2));
93  cb_Berr=normrnd(cb_B,sqrt((errRSD*cb_B/100).^2));
94  cb_Cerr=normrnd(cb_C,sqrt((errRSD*cb_C/100).^2));
95
96  % Calculate the fractionation diagram
97  [fracProduct,fracTotal]=fractionationDiagram(cb_Berr,...
98  cb_Aerr+cb_Cerr);
99
100 % Calculate the max PFs and corresponding yields
101 [maxPFVals,yieldVals]=maxPY(fracProduct,fracTotal);
102
103 % Convert the max PFs to purities
104 purityVals=maxPFVals*initialPurity;
105
106 % Record the optimal purity
107 if isempty(purityVals(yieldVals>=minYield))==1
108 purity(sscanf(fileList(i).name,'run%f'))=0;
109 else
110 purity(sscanf(fileList(i).name,'run%f'))=...
111 max(purityVals(yieldVals>=minYield))*100;
112 end
113 end
114
115 % Create matrix containing DOE results
116 DOEMatrix=[ccdesign(4,'center',1),purity];
117
118
119 %%% RSM SW
120
121 % Fit RSM model by stepwise regression
122 rsmModelSW = stepwiselm(DOEMatrix(:,1:end-1),DOEMatrix(:,end),...
123 'quadratic','verbose',0);
124
125 % Calculate and record RSM using stepwise regression errors
126 [rsmSWPred] = predict(rsmModelSW,valMatrix);
127 rsmSWErrs=sqrt((valPurity-rsmSWPred).^2);
```

```
128 errors.allRSMSWerrs((iii-1)*nVal+1:(iii-1)*nVal+nVal)=rsmSWErrs;
129
130
131
132 %%% RSM
133
134 % Fit RSM model
135 rsmModel = fitlm(DOEMatrix(:,1:end-1),DOEMatrix(:,end),'quadratic');
136 %rsmModel = fitlm(DOEMatrix(:,1:end-1),DOEMatrix(:,end),'y ~ 1 + x2*x3 + x2*x4 + x
137
138 % Calculate and record RSM errors
139 [rsmPred] = predict(rsmModel,valMatrix);
140 rsmErrs=sqrt((valPurity-rsmPred).^2);
141 errors.allRSMerrs((iii-1)*nVal+1:(iii-1)*nVal+nVal)=rsmErrs;
142
143
144 %%% Kriging
145
146
147 % Fit Kriging model
148 %krigingModel = oodacefit(DOEMatrix(:,1:end-1),DOEMatrix(:,end));
149
150 % Calculate semivariogram model
151 [~,~,gammaBin,hBin] = semivariogram(DOEMatrix);
152 [semivarModel]=semivariogramModel(hBin,gammaBin);
153
154 % Calculate and record Kriging errors
155 [krigingPred]=ordKriging(DOEMatrix(:,1:end-1),DOEMatrix(:,end),valMatrix,...
156 semivarModel);
157 %[krigingPred] = krigingModel.predict(valMatrix);
158 krigingErrs=sqrt((valPurity-krigingPred).^2);
159 errors.allKrigerrs((iii-1)*nVal+1:(iii-1)*nVal+nVal)=krigingErrs;
160
161
162 %%% Universal Kriging
163
164
165
```

```
% Use above RSM to detrend the DOE data
[detrendPurity] = purity-predict(rsmModel,DOEMatrix(:,1:end-1));


% Fit Kriging model
%krigingModel = oodacefit(DOEMatrix(:,1:end-1),DOEMatrix(:,end));

% Calculate semivariogram model
[~,~,gammaBin,hBin] = semivariogram([DOEMatrix(:,1:end-1),detrendPurity]);
[semivarModel]=semivariogramModel(hBin,gammaBin);

% Calculate and record Kriging errors
[krigingUnivPred]=ordKriging(DOEMatrix(:,1:end-1),detrendPurity,valMatrix,...
semivarModel);

% Add the trend back into the predictions
krigingPredTrend=krigingUnivPred+predict(rsmModel,valMatrix);

%[krigingPred] = krigingModel.predict(valMatrix);
krigingUnivErrs=sqrt((valPurity-krigingPredTrend).^2);
errors.allUnivKrigerrs((iii-1)*nVal+1:(iii-1)*nVal+nVal)=krigingUnivErrs;


%%% PLS


% Fit PLS model
[~,~,~,~,BETA] = plsregress(DOEMatrix(:,1:end-1),DOEMatrix(:,end));
%[~,~,~,~,BETA] = plsregress(DOEMatrix(:,1:end-1),DOEMatrix(:,end),1);

% Calculate and record PLS errors
plsPred = [ones(size(valMatrix,1),1),valMatrix]*BETA;
plsErrs=sqrt((valPurity-plsPred).^2);
errors.allPLSerrs((iii-1)*nVal+1:(iii-1)*nVal+nVal)=plsErrs;

% Update progress bar
waitbar(iii/nCycles,h);
end
```

```
204
205 % Close progress bar
206 close(h)
207
208 toc
209 end
```

Bibliography

Alastair Aitken and Michele Learmonth. Protein Determination by UV Absorption. *The Protein Protocols Handbook*, pages 3–6, 1996.

Sattar Al-Jibbouri. Scale-up of chromatographic ion-exchange processes in biotechnology. *Journal of Chromatography A*, 1116(1-2):135–142, 2006.

Suzanne Aldington and Julian Bonnerjea. Scale-up of monoclonal antibody purification processes. *Journal of Chromatography B*, 848(1):64–78, 2007.

Dorota Antos, Krzysztof Kaczmarski, Piatkowski Wojciech, and Andreas Seidel-Morgenstern. Concentration dependence of lumped mass transfer coefficients: Linear versus non-linear chromatography and isocratic versus gradient operation. *Journal of Chromatography A*, 1006(1-2):61–76, 2003. ISSN 00219673.

John M.S. Bartlett and David Stirling. *PCR Protocols*, volume 226. Humana Press, New Jersey, aug 2003. ISBN 1-59259-384-4.

M. Bensch, P. Schulze Wierling, E. von Lieres, and J. Hubbuch. High Throughput Screening of Chromatographic Phases for Rapid Process Development. *Chemical Engineering & Technology*, 28(11):1274–1284, nov 2005. ISSN 0930-7516.

R. Bhambure and a. S. Rathore. Chromatography process development in the quality by design paradigm I: Establishing a high-throughput process development platform as a tool for estimating "characterization space" for an ion exchange chromatography step. *Biotechnology Progress*, 29:403–414, 2013. ISSN 87567938.

Niklas Borg, Yan Brodsky, John Moscariello, Suresh Vunnum, Ganesh Vedantham, Karin Westerberg, and Bernt Nilsson. Modeling and robust pooling design of a

preparative cation-exchange chromatography step for purification of monoclonal antibody monomer from aggregates. *Journal of Chromatography A*, 1359:170–181, 2014. ISSN 18733778.

Fani Boukouvala, FernandoJ Muzzio, and MarianthiG Ierapetritou. Design Space of Pharmaceutical Processes Using Data-Driven-Based Methods. *Journal of Pharmaceutical Innovation*, 5(3):119–137, 2010.

Timothy N Breece, Ellen Gilkerson, and Charles Schmelzer. Validation of large scale chromatographic processes, part 1. *BioPharm*, (15):16–20, 2002.

Giorgio Carta. Predicting protein dynamic binding capacity from batch adsorption tests. *Biotechnology journal*, 7(10):1216–20, oct 2012. ISSN 1860-7314.

Alex Chatel, Peter Kumpalume, and Mike Hoare. Ultra scale-down characterization of the impact of conditioning methods for harvested cell broths on clarification by continuous centrifugation-Recovery of domain antibodies from rec E. coli. *Biotechnology and Bioengineering*, 111(5):913–924, 2014. ISSN 00063592.

Sunil Chhatre and Nigel J Titchener-Hooker. Review: Microscale methods for high-throughput chromatography development in the pharmaceutical industry. *Journal of Chemical Technology & Biotechnology*, 84(7):927–940, 2009.

Sunil Chhatre, Suzanne S. Farid, Jonathan Coffman, Paul Bird, Anthony R. Newcombe, and Nigel J. Titchener-Hooker. How implementation of quality by design and advances in biochemical engineering are enabling efficient bioprocess development and manufacture. *Journal of Chemical Technology and Biotechnology*, 86(9): 1125–1129, 2011. ISSN 02682575.

Edward J. Close, Jeffrey R. Salm, Daniel G. Bracewell, and Eva Sorensen. A model based approach for identifying robust operating conditions for industrial chromatography with process variability. *Chemical Engineering Science*, 116:284–295, 2014. ISSN 00092509.

Jonathan L Coffman, Jack F Kramarczyk, and Brian D Kelley. High-throughput screening of chromatographic separations: I. Method development and column modeling. *Biotechnology and Bioengineering*, 100(4):605–618, 2008.

Lisa Connell-Crowley, Elizabeth a. Larimore, and Ron Gillespie. Using high throughput screening to define virus clearance by chromatography resins. *Biotechnology and Bioengineering*, 110(7):1984–1994, 2013. ISSN 00063592.

Steven M Cramer and Guhan Jayaraman. Preparative chromatography in biotechnology. *Current Opinion in Biotechnology*, 4(2):217–225, 1993.

Eddie Davis and Marianthi Ierapetritou. A centroid-based sampling strategy for kriging global modeling and optimization. *AIChE Journal*, 56(1):220–240, 2010.

Clayton V. Deutsch. Correcting for negative weights in ordinary kriging. *Computers and Geosciences*, 22(7):765–773, 1996. ISSN 00983004.

Wolfgang Dietrich, Christian H Rüdel, and Markus Neumann. Fast and precise automatic baseline correction of one- and two-dimensional nmr spectra. *Journal of Magnetic Resonance (1969)*, 91(1):1–11, jan 1991. ISSN 00222364.

Pauline M. Doran. *Bioprocess Engineering Principles*. Academic Press, San Diego; London, 1995. ISBN 0-12-220855-2.

S Edwards-Parton, N F Thornhill, D G Bracewell, J M Liddell, and N J Titchener-Hooker. Principal Component Score Modeling for the Rapid Description of Chromatographic Separations. *Biotechnology Progress*, 24(1):202–208, 2008.

Georgina Espuny Garcia Del Real, Jim Davies, and Daniel G Bracewell. Scale-down characterization of post-centrifuge flocculation processes for high-throughput process development. *Biotechnology and bioengineering*, 111(12):2486–98, dec 2014. ISSN 1097-0290.

Jace Fogle, Nina Mohan, Eric Cheung, and Josefine Persson. Effects of resin ligand density on yield and impurity clearance in preparative cation exchange chromatography. I. Mechanistic evaluation. *Journal of Chromatography A*, 1225:62–69, 2012. ISSN 00219673.

Food and Drug Administration. Guidance for Industry Guidance for Industry. Technical Report November, Food and drug administration, 2009.

Food and Drug Administration. Guidance for Industry Process Validation : General Principles and Practices Guidance for Industry Process Validation : General Principles and Practices. Technical Report January, Food and Drug Administration, 2011.

Pete Gagnon. Purification of monoclonal antibodies by mixed-mode chromatography. In Uwe Gottschalk, editor, *Process scale purification of antibodies*. Wiley, Hoboken, N.J., 2009.

P. H. Garthwaite. An interpretation of partial least squares. *Journal of the American Statistical Association*, 89(425):122–127, 1994. ISSN 01621459.

Spyridon Gerontas, Magnus Asplund, Rolf Hjorth, and Daniel G. Bracewell. Integration of scale-down experimentation and general rate modelling to predict manufacturing scale chromatographic separations. *Journal of Chromatography A*, 1217(44): 6917–6926, 2010. ISSN 00219673.

Raja Ghosh. Protein separation using membrane chromatography: opportunities and challenges. *Journal of Chromatography A*, 952(1-2):13–27, 2002.

J Calvin Giddings and Henry Byring. A Molecular Dynamic Theory of Chromatography. *The Journal of Physical Chemistry*, 59(5):416–421, 1955.

Tingyue Gu, Yung-Huoy Truei, Gow-Jen Tsai, and George T. Tsao. Modeling of gradient elution in multicomponent nonlinear chromatography. *Chemical Engineering Science*, 47(1):253–262, 1992. ISSN 00092509.

Tingyue Gu, Kuang-Hsin Hsu, and Mei-Jywan Syu. Scale-up of affinity chromatography for purification of enzymes and other proteins. *Enzyme and Microbial Technology*, 33(4):430–437, sep 2003. ISSN 01410229.

Tingyue Gu, Ganesh Iyer, and Kwok Shun C Cheng. Parameter estimation and rate model simulation of partial breakthrough of bovine serum albumin on a column packed with large Q Sepharose anion-exchange particles. *Separation and Purification Technology*, 116:319–326, 2013. ISSN 13835866.

Georges Guiochon. Preparative liquid chromatography. *Journal of Chromatography A*, 965(1-2):129–161, 2002.

Alexander T. Hanke and Marcel Ottens. Purifying biopharmaceuticals: knowledge-based chromatographic process development. *Trends in Biotechnology*, 32(4): 210–220, 2014. ISSN 01677799.

Ernst Hansen and Jørgen M Mollerup. The Influence of Retention on the Plate Height in Ion-Exchange Chromatography. *Separation Science and Technology*, 39 (9):2011–2030, 2005.

Roger Harrison, Paul Todd, Scott R Rudge, and Demetri P Pterides. *Bioseparations science and engineering*. Oxford University Press, Oxford, 2003. ISBN 0-19-512340-9.

Christian Heuer, Peter Hugo, Gregor Mann, and Andreas Seidel-Morgenstern. Scale up in preparative chromatography. *Journal of Chromatography A*, 752(1-2):19–29, 1996.

N Hutchinson, S Chhatre, H Baldascini, J L Davies, D G Bracewell, and M Hoare. Ultra scale-down approach to correct dispersive and retentive effects in small-scale columns when predicting larger scale elution profiles. *Biotechnology Progress*, 25 (4):1103–1110, 2009.

ICH. Pharmaceutical Development Q8(R2). Technical report, 2009.

Zhenya Jia, Eddie Davis, Fernando Muzzio, and Marianthi Ierapetritou. Predictive Modeling for Pharmaceutical Processes Using Kriging and Response Surface. *Journal of Pharmaceutical Innovation*, 4(4):174–186, 2009.

Oliver Kaltenbrunner, Alois Jungbauer, and Shuichi Yamamoto. Prediction of the preparative chromatography performance with a very small column. *Journal of Chromatography A*, 760(1):41–53, 1997.

Amir S. Kazemi and David R. Latulippe. Stirred well filtration (SWF) A high-throughput technique for downstream bio-processing. *Journal of Membrane Science*, 470:30–39, 2014. ISSN 03767388.

Vijesh Kumar, Akriti Bhalla, and Anurag S. Rathore. Design of experiments applications in bioprocessing: Concepts and approach. *Biotechnology Progress*, 30(1): 86–99, 2014. ISSN 87567938.

Vijesh Kumar, Samuel Leweke, Eric von Lieres, and Anurag S Rathore. Mechanistic modeling of ion-exchange process chromatography of charge variants of monoclonal antibody products. *Journal of Chromatography A*, 1426:140–153, dec 2015. ISSN 00219673.

Karol M Lacki. High-throughput process development of chromatography steps: advantages and limitations of different formats used. *Biotechnology journal*, 7(10): 1192–202, oct 2012. ISSN 1860-7314.

Karol M Lacki. High throughput process development in biomanufacturing. *Current Opinion in Chemical Engineering*, 6:25–32, 2014. ISSN 22113398.

Seungwoon Lee, Kyoung-Hwa Ryu, Yeon-Gu Kim, Jung Oh Ahn, Hongweon Lee, Joon-Ki Jung, and Eun Gyo Lee. Radial scale-down of packed bed chromatography in a thin cylindrical tube for preparative media. *Process Biochemistry*, 50(5): 839–845, 2015. ISSN 13595113.

Qiang Li, Gareth J Mannall, Shaukat Ali, and Mike Hoare. An ultra scale-down approach to study the interaction of fermentation, homogenization, and centrifugation for antibody fragment recovery from rec E. coli. *Biotechnology and bioengineering*, 110(8):2150–60, aug 2013. ISSN 1097-0290.

Xiaonan Li, Guy de Roo, Kim Burgers, Marcel Ottens, and Michel H M Eppink. Self-packed filter plates: A good alternative for pre-packed filter plates for developing purification processes for therapeutic proteins. *Biotechnology Journal*, 7(10): 1269–1276, 2012. ISSN 18606768.

Zhiguo Li, Yesong Gu, and Tingyue Gu. Mathematical modeling and scale-up of size-exclusion chromatography. *Biochemical Engineering Journal*, 2(2):145–155, 1998.

J M Liddell. Introduction to downstream processing. In Laurence R Weatherley, editor, *Engineering processes for bioseparations*. Butterworth-Heinemann, Oxford; Boston, 1994.

F G Lode, A Rosenfeld, Q S Yuan, T W Root, and E N Lightfoot. Refining the scale-up of chromatographic separations. *Journal of Chromatography A*, 796(1):3–14, 1998.

Georges Matheron. Principles of geostatistics. *Economic Geology*, 58(8):1246–1266, 1963.

Abdul W. Mohammad, Donna G. Stevenson, and Phillip C. Wankat. Pressure drop correlations and scale-up of size exclusion chromatography with compressible packings. *Industrial & Engineering Chemistry Research*, 31(2):549–561, 1992. ISSN 0888-5885.

Jørgen M Mollerup, Thomas Budde Hansen, Steffen Kidal, Lars Sejergaard, and Arne Staby. Development, modelling, optimisation and scale-up of chromatographic purification of a therapeutic protein. *Fluid Phase Equilibria*, 261(1-2):133–139, 2007.

Beckley K. Nfor, Jovana Ripić, Albert van der Padt, Marc Jacobs, and Marcel Ottens. Model-based high-throughput process development for chromatographic whey proteins separation. *Biotechnology Journal*, 7(10):1221–1232, 2012. ISSN 18606768.

S H Ngiam, Y H Zhou, M K Turner, and N J Titchener-Hooker. Graphical method for the calculation of chromatographic performance in representing the trade-off between purity and recovery. *Journal of Chromatography A*, 937(1-2):1–11, 2001.

Sheau-Huey Ngiam, Daniel G Bracewell, Yuhong Zhou, and Nigel J Titchener-Hooker. Quantifying Process Tradeoffs in the Operation of Chromatographic Sequences. *Biotechnology Progress*, 19(4):1315–1322, 2003.

Aaron Noyes, Ranga Godavarti, Nigel Titchener-Hooker, Jonathan Coffman, and Tarit Mukhopadhyay. Quantitative high throughput analytics to support polysaccharide production process development. *Vaccine*, 32(24):2819–28, may 2014. ISSN 1873-2518.

Aaron Noyes, Jonida Basha, John Frostad, Scott Cook, Doug Millard, Jim Mullin, Daniel LaCasse, Richard S. Wright, Benjamin Huffman, Robert Fahrner, Ranga Godavarti, Nigel Titchener-Hooker, Khurram Sunasara, and Tarit Mukhopadhyay. A modular approach for the ultra-scale-down of depth filtration. *Journal of Membrane Science*, 496:199–210, 2015. ISSN 03767388.

C A Orellana, C Shene, and J A Asenjo. Mathematical modeling of elution curves for

a protein mixture in ion exchange chromatography applied to high protein concentration. *Biotechnology and Bioengineering*, 104(3):572–581, 2009.

A. Osberghaus, K. Drechsel, S. Hansen, S.K. Hepbildikler, S. Nath, M. Haindl, E. von Lieres, and J. Hubbuch. Model-integrated process development demonstrated on the optimization of a robotic cation exchange step. *Chemical Engineering Science*, 76: 129–139, 2012. ISSN 00092509.

Steven M Paul, Daniel S Mytelka, Christopher T Dunwiddie, Charles C Persinger, Bernard H Munos, Stacy R Lindborg, and Aaron L Schacht. How to improve R&D productivity: the pharmaceutical industry's grand challenge. *Nature reviews. Drug discovery*, 9(3):203–14, 2010. ISSN 1474-1784.

Ernie X Perez-Almodovar and Giorgio Carta. IgG adsorption on a new protein A adsorbent based on macroporous hydrophilic polymers. II. Pressure-flow curves and optimization for capture. *Journal of Chromatography A*, 1216(47):8348–8354, 2009. ISSN 00219673.

Anurag S. Rathore. Roadmap for implementation of quality by design (QbD) for biotechnology products. *Trends in Biotechnology*, 27(9):546–553, 2009. ISSN 01677799.

Anurag S. Rathore. QbD/PAT for bioprocessing: Moving from theory to implementation. *Current Opinion in Chemical Engineering*, 6:1–8, 2014. ISSN 22113398.

Anurag S Rathore and Ajoy Velayudhan. An Overview of Scale-Up in Preparative Chromatography. In Anurag S Rathore and Ajoy Velayudhan, editors, *Scale-Up and Optimization in Preparative Chromatography*. Marcel Dekker, Inc., New York, 2003.

Anurag S Rathore, Gary V Johnson, John J Buckley, Denis M Boyle, and Mark E Gustafson. Process characterization of the chromatographic steps in the purification process of a recombinant Escherichia coli-expressed protein. *Biotechnology and Applied Biochemistry*, 37(1):51–61, 2003.

Andrea C M E Rayat, Gary J. Lye, and Martina Micheletti. A novel microscale cross-flow device for the rapid evaluation of microfiltration processes. *Journal of Membrane Science*, 452:284–293, 2014. ISSN 03767388.

Kaushal Rege, Mike Pepsin, Brandy Falcon, Landon Steele, and Meng Heng. High-throughput process development for recombinant protein purification. *Biotechnology and Bioengineering*, 93(4):618–630, 2006. ISSN 00063592.

P Richardson, M Hoare, and P Dunnill. A new biochemical engineering approach to the fractional precipitation of proteins. *Biotechnology and Bioengineering*, 36(4): 354–366, 1990.

Rebecca S. Salisbury, Daniel G Bracewell, and Nigel J Titchener-Hooker. A methodology for the graphical determination of operating conditions of chromatographic sequences incorporating the trade-offs between purity and yield. *Journal of Chemical Technology & Biotechnology*, 81(11):1803–1813, nov 2006. ISSN 02682575.

Nooshafarin Sanaie, Douglas Cecchini, and John Pieracci. Applying high-throughput methods to develop a purification process for a highly glycosylated protein. *Biotechnology journal*, 7(10):1242–55, oct 2012. ISSN 1860-7314.

Abhinav A Shukla and Yinges Yigzaw. Modes of preparative chromatography. In Abhinav A Shukla, Mark R Etzel, and Shishir Gadam, editors, *Process scale bioseparations for the biopharmaceutical industry*. Taylor & Francis, Boca Raton; London, 2007.

Abhinav A Shukla, Brian Hubbard, Tim Tressel, Sam Guhan, and Duncan Low. Downstream processing of monoclonal antibodies–Application of platform approaches. *Journal of Chromatography B*, 848(1):28–39, 2007.

Sun Chau Siu, Celeste Chia, Yanglin Mok, and Priyabrata Pattnaik. Packing of large-scale chromatography columns with irregularly shaped glass based resins using a stop-flow method. *Biotechnology Progress*, 30(6):1319–1325, 2014. ISSN 15206033.

Gail Sofer and Lars Hagel. *Handbook of process chromatography: a guide to optimization, scale-up and validation*. Academic Press, San Diego; London, 1997.

E Sorensen, S Chan, and N Titchener-Hooker. Optimal economic design and operation of single- and multi-column chromatographic processes. *Biotechnology Progress*, 24 (2):389–401, 2008.

J. J. Stickel and A. Fotopoulos. Pressure-flow relationships for packed beds of compressible chromatography media at laboratory and production scale. *Biotechnology Progress*, 17(4):744–751, 2001. ISSN 87567938.

Magali Toueille, Audrey Uzel, Jean-François Depoisier, and René Gantier. Designing new monoclonal antibody purification processes using mixed-mode chromatography sorbents. *Journal of Chromatography B*, 879(13-14):836–843, 2011. ISSN 15700232.

Steven J Traylor, Xuankuo Xu, Yi Li, Mi Jin, and Zheng Jian Li. Adaptation of the pore diffusion model to describe multi-addition batch uptake high-throughput screening experiments. *Journal of chromatography. A*, 1368:100–6, 2014. ISSN 1873-3778.

Katrin Treier, Sigrid Hansen, Carolin Richter, Patrick Diederich, Jürgen Hubbuch, and Philip Lester. High-throughput methods for miniaturization and automation of monoclonal antibody purification processes. *Biotechnology Progress*, 28:723–732, 2012. ISSN 87567938.

J J van Deemter, F J Zuiderweg, and A Klinkenberg. Longitudinal diffusion and resistance to mass transfer as causes of nonideality in chromatography. *Chemical Engineering Science*, 5(6):271–289, 1956.

Gary Walsh. *Proteins: biochemistry and biotechnology*. Wiley, Chichester, 2nd edition, 2002.

Fengqiang Wang and Daisy Richardson. Host-Cell Protein Measurement and Control. *BioPharm International*, (6):32–38, 2015.

John P. Welsh, Matthew G. Petroff, Patricia Rowicki, Haiying Bao, Thomas Linden, David J. Roush, and Jennifer M. Pollard. A practical strategy for using miniature chromatography columns in a standardized high-throughput workflow for purification development of monoclonal antibodies. *Biotechnology Progress*, 30(3):626–35, 2014. ISSN 87567938.

Scott M Wheelwright. *Protein purification: design and scale up of downstream processing*. Wiley, New York, 1991. ISBN 0471037230 9780471037231.

Andreas Wieser, Andreas Berting, Christian Medek, Gerhard Poelsler, and Thomas R Kreil. The evolution of down-scale virus filtration equipment for virus clearance studies. *Biotechnology and bioengineering*, 112(3):633–7, mar 2015. ISSN 1097-0290.

Svante Wold, Michael Sjöström, and Lennart Eriksson. PLS-regression: a basic tool of chemometrics. *Chemometrics and Intelligent Laboratory Systems*, 58(2):109–130, 2001.

Tanja Wolter and Andreas Richter. Assays for controlling host-cell impurities in biopharmaceuticals. *BioProcess Int*, 3:40–46, 2005.

Shuichi Yamamoto, Masaki Nomura, and Yuji Sano. Resolution of proteins in linear gradient elution ion-exchange and hydrophobic interaction chromatography. *Journal of Chromatography A*, 409:101–110, 1987.

Noriko Yoshimoto, Kazunobu Minakuchi, Daisuke Itoh, Yu Isakari, and Shuichi Yamamoto. High-throughput process development methods for chromatography and precipitation of proteins: Advantages and precautions. *Engineering in Life Sciences*, 13:446–455, 2013. ISSN 16180240.